

Late-Holocene Climate Variability in Southern New Zealand:
A reconstruction of regional climate from an annually laminated sediment sequence
from Lake Ohau

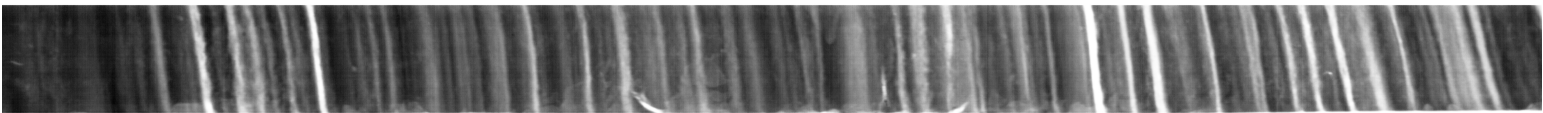
BY

HEIDI ANNE ROOP

A thesis

Submitted to the Victoria University of Wellington
in fulfillment of the requirements for the degree of
Doctor of Philosophy
in Geology

Victoria University of Wellington
(2015)



ABSTRACT

This research aims to improve understanding of synoptic climate systems influencing southern New Zealand and document changes in the intensity and frequency of these systems beyond the historical record by analyzing a 1,350-year annually laminated sediment sequence recovered from Lake Ohau, South Island, New Zealand (44.234°S, 169.854°E). Climatological patterns originating in both the tropics (El-Niño-Southern Oscillation (ENSO), Interdecadal Pacific Oscillation (IPO)) and in the Antarctic (Southern Annular Mode (SAM)) influence year-to-year variability in New Zealand's climate (e.g. temperature and precipitation). However, the range of natural variability of these systems in the southwest Pacific over time is poorly known because the instrumental record is short (~100 years). The high-resolution record from Lake Ohau offers a unique opportunity to investigate changes in regional hydrology and climate, and to also explore connections to large-scale climate patterns over the last millennium.

Hydrodynamic and hydroclimatic processes that influence and control the production, transport, and deposition of sediment within the Lake Ohau catchment are examined and constrained in order to develop a robust climate record. A key aim is to determine the role that meteorology and climate play in controlling sediment flux. The physical properties and facies of a 5.5-meter-long Lake Ohau sediment core are analyzed using thin-sections, high-resolution X-radiographs scans, and particle-size analyses. Time-series analysis is used to establish links between varve facies, hydroclimate variability and regional synoptic climate types over the instrumental record. Utilizing this climate-proxy relationship, inflow conditions are reconstructed over the last 1,350 years and compared with regional temperature reconstructions to generate a Western South Island paleo-atmospheric circulation index. Relationship between this paleocirculation index and other proxy reconstructions show significant variability in the relative forcing of tropical (ENSO) and Southern Hemisphere high-latitude (SAM) synoptic climate drivers on New Zealand and southwest Pacific climate.

Overall, this work demonstrates that: a) the laminated sediments from Lake Ohau are varves and the formation of the annual stratigraphy is strongly controlled by lake hydrodynamics, in particular, thermal lake stratification; b) sediment stratigraphy reflects changes in austral warm period (December-May) inflow, enabling a high-resolution reconstruction of hydroclimate over the last 1,350 years and; c) the generation of a paleocirculation index for the Western South Island points to significant changes between northerly or southerly dominated atmospheric conditions in southern New Zealand, particularly over the 'Little Ice Age' (1385-1710 AD). During this time, the strength of tropical teleconnections weakened and a strong negative phase SAM persisted. Comparison with high-resolution regional proxy records from Antarctica and the Central Pacific point to significant regional coherence with a strong negative phase SAM acting as a primary driver of the onset of Little Ice Age conditions across the South Pacific.

ACKNOWLEDGEMENTS

This work is the culmination of the efforts of a broad cast of characters. As with any scientific endeavor, this thesis only came to fruition through a significant amount of teamwork. Many thanks to Gavin Dunbar, Richard Levy, and Marcus Vandergoes for their dedication to the Lake Ohau project, and support throughout the thesis process. In addition to some good science, we have had some fun adventures together from swimming in freezing cold tarns in the name of science to ‘nerding out’ over a pint. A special thanks to Richard Levy for the plentiful chats about life and careers and for the encouragement to pursue my passion for science communication throughout the PhD process (despite the distraction!). I would not have had the skills to complete this work without the invaluable guidance from my previous scientific mentors, in particular, Darrell Kaufman, David Clow, and Al Werner. You all helped to build a solid foundation for my future while we worked at the Northern Arizona University, the USGS, and Mount Holyoke College. A sincere thanks to my new-found science mentors and colleagues, especially Andrew Lorrey, Rhian Salmon, James Renwick, Sharon Walker, Jamie Howarth, Warren Dickinson, Christian Ohlendorf, Catalina Gebhardt, Steven Phipps and Nerilie Abram. I extend my sincere appreciation to Lionel Carter, Christopher Moy, and Scott Lamoureux for their time and expertise in reviewing this thesis.

Financial support from the Sarah Beanland Memorial Scholarship, GNS Science, and the Antarctic Research Centre made this work possible. Emotional support and friendship from a large group of family and friends, both near and far, were critical to my sanity and perseverance during this process. A special shout out to Ben and Melanie Hodgman for all of the mail and mixed CD’s from Seattle! Peter Neff, thank you for all of your support and the many fun adventures during our time together in New Zealand. Kuna, you kept me healthy and happy. It is my parents, Peter and Connie Roop, who are responsible for inspiring and encouraging me to pursue science. My curiosity and inquiring mind stems directly from their example. The apple really does not fall far from the tree! I am eternally grateful for your love and continued, unflinching support.

Onward to the next adventure!

Table of Contents

Abstract	iii
Acknowledgements	iv
Table of Contents	vi
Chapter 1 Introduction	1
1.1 Context and Rationale	2
1.2 Climatic and Geographic Setting	4
1.2.1 Synoptic Climate Patterns	4
1.2.2 Geographic Setting	7
1.3 Varves as Climate Proxies	9
1.3.1 Varve Formation and Characteristics	9
1.3.2 Limnological Controls on Sedimentation	12
1.4 Research Questions and Thesis Outline	14
1.4.1 Research Questions	14
1.4.2 Thesis Outline	15
1.5 References	16
Chapter 2 Seasonal Controls on sediment transport and deposition in Lake Ohau, South Island, New Zealand: Implications for a high-resolution Holocene palaeoclimate reconstruction	23
2 Abstract	25
2.1 Introduction	26
2.1.1 Physical Setting	29
2.2 Materials and Methods	30
2.2.1 Limnological Monitoring	30
2.2.2 Water Temperature	30
2.2.3 Turbidity	30
2.2.4 Sediment Traps	31
2.2.5 Sediment Cores	33
2.3 Results	34
2.3.1 Hydrometeorology	34
2.3.2 Physical Limnology	36
2.3.3 Sedimentation	40
2.3.4 Sediment Cores	41
2.4 Discussion	42
2.4.1 Winter ‘Inflow’ and ‘Outflow’ Conditions	42
2.4.2 Summer ‘Inflow’ and ‘Outflow’ Conditions	44
2.4.3 Flood Conditions	46
2.4.4 Characteristics of the Longer Sediment Sequence	47
2.4.5 Primary Mechanisms of Varve Formation	48
2.5 Conclusions	49
2.6 Acknowledgements	50
2.7 References	51
Chapter 3 A hydroclimate-proxy model based on sedimentary facies in an annually laminated sequence from Lake Ohau, South Island, New Zealand	57
3 Abstract	59
3.1 Introduction	60

3.1.1	Study Site	61
3.2	Materials and Methods	63
3.2.1	Physical Properties	63
3.2.2	Chronology	64
3.2.3	Hydrometeorological Data	67
3.3	Results	68
3.3.1	X-ray Density and Particle Size	68
3.3.2	Varve Classification	68
3.3.3	Core Chronology	71
3.3.4	Hydroclimate-varve Relationships	71
3.4	Discussion	74
3.4.1	Varve Thickness and Hydroclimatic Variability	75
3.4.2	Lamination Stratigraphy	76
3.4.3	Towards a Hydroclimate-proxy Model for the Pre-Instrumental Era	79
3.5	Conclusions	80
3.6	Acknowledgements	81
3.7	References	82
	Supplementary Figures and Tables	86
Chapter 4	Hydroclimate variability and regional atmospheric circulation over the past 1,350 years reconstructed from Lake Ohau, New Zealand	91
4	Abstract	93
4.1	Introduction	94
4.1.1	Geographic and Climatic Setting	96
4.2	Analytical Approach and Results	98
4.2.1	Age Model Development	98
4.2.2	Varve Classification and Distribution	101
4.2.3	Regional Climate Regime Classification	102
4.2.4	Assigning Paleo-Regimes	104
4.3	Synthesis and Discussion	110
4.3.1	RCRC Regimes, Lake Ohau Inflow and WSI Climate	110
4.3.2	Paleocirculation History of the Western South Island	111
4.3.3	Regional to Hemispheric Scale Drivers of Paleocirculation	114
4.3.4	Future Directions	116
4.4	Conclusions	117
4.5	Acknowledgements	118
4.6	References	119
	Supplementary Figures and Methods	123
Chapter 5	Project Summary and Future Research	133
5.1	Research Motivations	134
5.2	Project Summary	134
5.3	Future Directions	137
5.4	References	141
Appendix A	Seasonal variability in turbidity currents in Lake Ohau, New Zealand and their influence on sedimentation	143
Appendix B	Project Datasets & X-ray Imagery	Attached Insert

CHAPTER 1

Introduction:

Southern Hemisphere Climate and the Importance of High-Resolution Paleoclimate
Records

1.1 CONTEXT AND RATIONALE

Annually- to decadal-resolved paleoclimate records extending beyond the instrumental period are key to understanding natural climate system dynamics. These high-resolution records can capture environmental change on sub-decadal timescales and serve as a bridge between short instrumental records and longer, lower resolution paleoclimate sequences (Zolitschka and Pike, 2014). Only a few types of records capture environmental change at such high resolution—these include tree rings, ice cores, varved sediments, corals and speleothems (Bradley, 1999; Zolitschka and Pike, 2014). A number of these records are documented across the Northern Hemisphere (Mann et al., 1998; Ojala et al., 2012), but there remains a need to develop comparable records from the Southern Hemisphere (SH; Fig. 1; Neukom and Gergis, 2012).

This is particularly true for the SH mid-latitudes which sit in the core of the westerlies winds, which are an important driver of hemispheric-wide climatic changes (Fig. 1; Marshall et al., 2003; Neukom and Gergis, 2012). New Zealand is one of the areas near the core of the zonal westerlies where high-resolution records can be recovered. A current SH synthesis of 2,000-year high-resolution paleoclimate reconstructions includes only tree-rings records for the New Zealand region (Fig. 1; Neukom and Gergis, 2012), highlighting the need for additional, diverse proxy records from the western Pacific sector and the broader SH mid-latitudes.

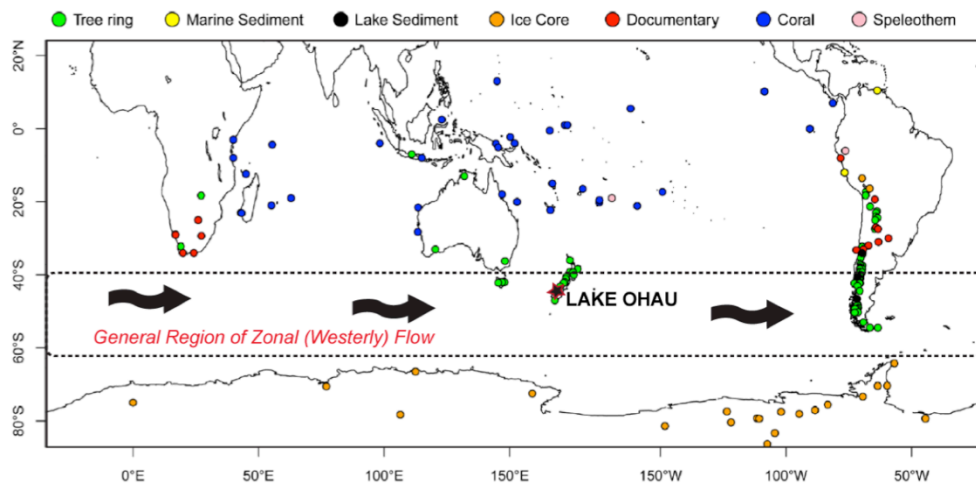


Fig. 1: Distribution of high-resolution climate proxies records from the SH spanning the last 2,000 years. Each circle represents a record from a different high-resolution archive. In New Zealand, records of sufficient quality for this composite were all derived from tree-rings, many of which are located in northern New Zealand. Proxy records from regions in the core of the circumpolar westerlies are even less common. This research aims to contribute a new lacustrine record from Lake Ohau, which is centrally located in this currently data-sparse region in the Southern Hemisphere. Figure modified from Neukom and Gergis (2012).

The combination of short instrumental records and the relative paucity of high-resolution SH records is particularly problematic as it limits understanding of ocean-atmosphere system dynamics on different spatial and temporal scales and hinders the ability to place modern observations in context with past climatic variability. Further, the limited data from this region limits the ability to resolve the drivers and temporal synchronicity of climate changes over the last 2,000 years like the Little Ice Age (LIA) and Medieval Climate Anomaly (MCA) between the Northern and Southern Hemispheres (Cook et al., 2002; Mann et al., 2009; Abram et al., 2013; Chambers et al., 2014; Lorrey et al., 2014). Without additional high-resolution records from this region, our understanding of past and potentially future climate variability will remain limited.

This research provides a new, highly resolved record from the SH mid-latitudes through the investigation of a 1,350-year varved sediment sequence recovered from Lake Ohau, Mackenzie Basin, New Zealand (Figs. 1 to 3; 44.234°S, 169.854°E). In New Zealand, a majority of high-resolution records spanning this time-period are derived from tree rings and speleothems, which generally show greater sensitivity to temperature (Cook et al., 2002; 2006; Lorrey et al., 2008; Fowler et al., 2012). Proxy records that reflect changes in precipitation and wind regimes or storm frequency are even more limited across New Zealand (Page et al., 1994; 2010; Pepper et al., 2004; Orpin et al., 2010).

The Lake Ohau sediments offer a unique opportunity to explore variability in precipitation as the Lake Ohau catchment is geographically positioned at the northern extent of the zonal westerly wind belt, which is highly-correlated with seasonal variability in South Island precipitation (Fig. 2; Ummenhofer et al., 2009; see Geographic and Climatic Setting). With a close correlation between precipitation, lake inflow and suspended sediment in the Lake Ohau catchment (Roop et al., 2015), it is expected that minor shifts in the intensity and latitudinal position of the circumpolar westerlies will influence the physical and/or geochemical character of the annual laminae. Central to this research is interrogating these potential relationships in order to develop a robust climate-proxy record from the Lake Ohau varved sediments. In a three-tiered approach, this project: 1) examines the contemporary processes that influence and control the production, transport, and deposition of laminated sediments in Lake Ohau; 2) utilizes instrumental records of air temperature, precipitation and lake inflow extending back to 1926 to develop a robust climate-proxy model which

links hydroclimatic variability to seasonal sediment flux into the lake; and 3) applies these relationships to down core variability in order to reconstruct regional climatic change over the last ~1,350 years.

1.2 CLIMATIC AND GEOGRAPHIC SETTING

1.2.1 Synoptic Climate Patterns

New Zealand's largely 'maritime' climate limits the number of continental feedbacks with temperature and precipitation anomalies resulting primarily from subtle changes in westerly airflow (Lorrey et al., 2014). This circulation pattern serves as the primary pathway by which changes in surrounding ocean waters are translated to land (Lorrey et al., 2014). This makes New Zealand an ideal laboratory for exploring variability in Southern Hemisphere atmospheric circulation and its drivers.

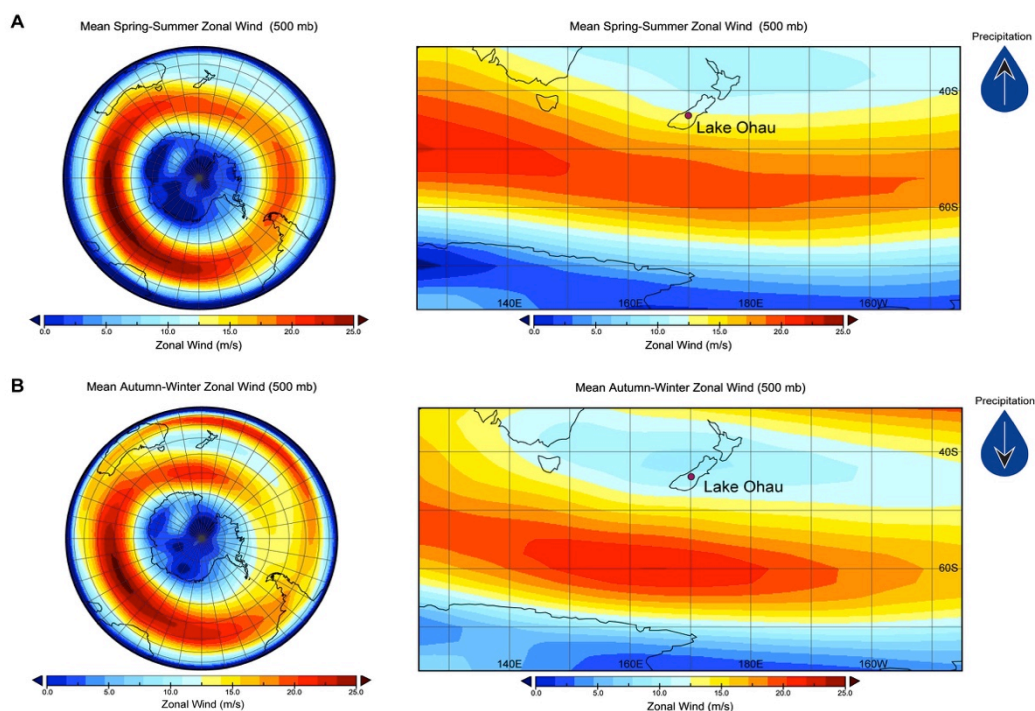


Fig. 2: The westerly winds are a dominant feature of Southern Hemisphere circulation. A) Mean austral spring and summer (September-February) and B) mean austral autumn and winter zonal wind (u-wind) over the reanalysis period of 1979-2014. Small latitudinal shifts in the westerly wind belt influence airflow over the South Island, including the Ohau catchment (Ummenhofer et al., 2009). At Lake Ohau, precipitation can vary by ~59% between summer and winter, in part, as a result of the position and intensity of the westerly wind belt. Data sourced from NOAA/ESRL Physical Sciences Division NCEP/NCAR Reanalysis datasets; <http://www.esrl.noaa.gov/psd/>.

The strength and position of the SH westerlies winds are linked to polar, tropical and subtropical modes of climate (Folland et al., 2002; Ummenhofer et al., 2009; Knudson et al., 2011). The main islands of New Zealand span a latitudinal range from 34°S to 47°S and has a climate influenced by circulation systems operating from the tropics to Antarctica. Observations show three of the most important synoptic climate features that influence this airflow across New Zealand on seasonal, inter-annual and decadal timescales include the Southern Annular Mode (SAM; also known as the Antarctic Oscillation (AAO)), El Niño-Southern Oscillation (ENSO), and the Interdecadal Pacific Oscillation (IPO; e.g. McKerchar and Henderson, 2003; Ummenhofer and England, 2007).

SAM is a leading mode of variability in the mid-latitudes, and accounts for 47% of the natural variability in SH zonal mean geopotential height (from 1000-50 hPa; Thompson and Wallace, 2000). Lake Ohau is potentially well situated to preserve fluctuations in the SAM, which has a zonal pressure anomaly centered at 45°S (Figs. 2 and 3; Thompson and Wallace, 2000; Kidston et al., 2009). The SAM index is defined as the difference in mean sea level pressure (MSLP) between 40°S and 65°S. The SAM is associated with seasonal and interannual variability in precipitation across New Zealand (Clare et al., 2002; Renwick and Thompson, 2006; Ummenhofer and England, 2007; Ummenhofer et al., 2009).

Positive phase SAM, characterized by below average atmospheric pressure over Antarctica and above average pressure over the mid-latitudes, results in a southward shift of the core of the sub-polar westerly flow and a decrease in precipitation over the South Island (Thompson and Solomon 2002; Renwick, 2004; Ummenhofer and England, 2007). The inverse occurs during negative phase SAM. Over the past thirty years there has been a trend towards a persistent positive phase SAM (Marshall, 2003; Renwick, 2004), which is associated with a 20-50% reduction in summer (December-February) precipitation (Ummenhofer and England, 2007), and increased maximum daily temperature anomalies (Renwick and Thompson, 2006) across the western South Island.

The El Niño-Southern Oscillation (ENSO) is another synoptic climate mode controlling precipitation patterns and surface air temperatures across New Zealand (Folland and Salinger 1995; Ummenhofer and England, 2007; Ummenhofer et al., 2009). ENSO is a coupled oceanic-atmospheric climate mode that oscillates in two to ten year cycles and is measured by the Southern Oscillation Index (SOI). The SOI is

the difference in MSLP anomalies between Tahiti and Darwin, Australia. In Chapter 4, the Niño 3.4 region sea surface temperature (SST) is discussed. This region spans 5°N-5°S and 170°W-120°W and SST anomalies from this region are typically used to describe the state of ENSO (positive anomaly = El Niño, negative anomaly = La Niña). In New Zealand, La Niña events increase the frequency of northerly to northeasterly winds, creating drier conditions in the south and southwest of the South Island (Mullan, 1995). During El Niño conditions, westerly to southwesterly airflow increases, creating wet conditions on the west coast of the South Island, and drought conditions on the leeward site of the Southern Alps.

The IPO is a ‘quasi-symmetric Pacific-wide manifestation of the Pacific Decadal Oscillation’ (Folland et al., 2002) and is defined by the 3rd Orthogonal Function of 13-year low-pass filtered global sea surface temperature (SST; Folland et al., 1999, 2002; Power et al., 1999). The IPO is linked to ENSO on decadal time scales. Over the 20th century, phase shifts have occurred in 1944 (shift to negative phase), in 1977/78 (shift to positive phase) and again in 1999 (McKerchar et al., 1996; Salinger et al., 2001; McKerchar and Henderson, 2003). Phase shifts influence the frequency and intensity of El Niño (increased during positive phase) and La Niña events (increased during negative phase; McKerchar and Henderson, 2003). Discharge records from the South Island increased by up to 14% following the 1978 IPO phase shift (McKerchar and Henderson, 2003). Further, precipitation in the Southern Alps region increased by 8% following the shift to a positive IPO in 1978 (Salinger et al., 2001). However, relative to ENSO and SAM, the IPO has a less pronounced influence on New Zealand’s surface climate particularly on annual to sub-decadal timescales (e.g. Renwick, 2011).

Overall, the interplay between synoptic climate modes such as SAM, ENSO, and the IPO and their relative influences on New Zealand’s climate are complex. While recent changes in extra-tropical atmospheric circulation are well-documented in the contemporary climate system (Fyfe, 2003; Renwick, 2004; Cai et al., 2006), our understanding of these systems is limited by the relatively short instrumental record and the additional influence of anthropogenic-driven changes such as ozone depletion and greenhouse gases emissions, which has a documented impact on circumpolar flow and synoptic climate patterns (e.g. Thompson and Solomon, 2002; Thompson et al., 2011). Highly resolved paleoclimate records like the Lake Ohau varved sediment sequence offer means to place presently observed changes in context within the range

of natural variability.

1.2.2 Geographic Setting

Lake Ohau (44.234°S, 169.854°E; Fig. 3) is a large glacial lake situated in a north-south trending catchment located to the east and in the lee of the Southern Alps. This makes the region characteristically dry and sensitive to fluctuations in the westerly wind flow impinging on the Alps, which in turn influences the amount of orographic precipitation that ‘spills’ over the mountains into the Lake Ohau catchment (Fig. 3; Chater and Sturman, 1998). Although the lake sits in the dry intermontane Mackenzie Basin (Garr and Fitzharris, 1991), the headwaters of Lake Ohau experiences overspill of precipitation from the wet West Coast, creating a significant gradient of decreasing rain from the mountains to the lake basin (Fig. 3; Table 1; Sinclair et al., 1997; Chater and Sturman, 1998; Roop et al., 2015 (Chapter 2)). Lake Ohau is considered part of the western South Island climate district (Kidson, 2000).

Table 1 Lake Ohau basin characteristics and seasonal mean climate conditions. Data summarized from Roop et al. (2015) and references therein.

Lake Ohau Basin Characteristics			
			Summer/Winter*
<i>Latitude, Longitude</i>	44.234°S 169.854°E	<i>Air Temperature (°C)</i>	14.3 / 6.2
<i>Catchment Area</i>	1135 km ²	<i>Headwater Precipitation (mm)</i>	2837 / 1537
<i>Lake Area</i>	54 km ²	<i>Precipitation at Lake (mm)</i>	625 / 444
<i>Maximum Depth</i>	129 m	<i>Inflow (m³/s)</i>	105 / 61
<i>Glacier Cover in catchment</i>	1.7%	<i>Surface Water Temperature (°C)[#]</i>	11.1 / 8.0
<i>Average Mean Accumulation (mm/year)[^]</i>	5.4	<i>Bottom Water Temperature (°C)[#]</i>	10.4 / 7.9

* Summer is defined as September-February; winter is defined as March-August (as in Chapter 2).

[^] Mean accumulation over the instrumental record (1926-2010).

[#] Water temperature as measured at the lake outflow

Discharge is controlled by seasonal meltwater (21% of total annual inflow (Kerr, 2013); September-November; Table 1) and summer (December-February) rainfall. Air temperature, lake inflow and precipitation vary seasonally in the catchment (Fig. 4; Table 1; Roop et al., 2015 (Chapter 2)). Long-term average headwater precipitation (measured at Elcho Flats; 1994 to 2013) indicates an average 20% (up to 50%) seasonal decrease in precipitation from summer to winter (Roop et

al., 2015 (Chapter 2)). Monthly total inflow at Lake Ohau correlates with total annual South Island precipitation ($r = 0.74$, $p = 0.0001$; Roop et al., accepted (Chapter 3)), which is controlled by the position and strength of westerly winds (Garreaud, 2007). The Lake Ohau region is, therefore, ideally located to investigate and reconstruct SH mid-latitude environmental response to regional and global climate variability (Chinn, 1999, Anderson and Mackintosh, 2006; Vandergoes et al., 2008).

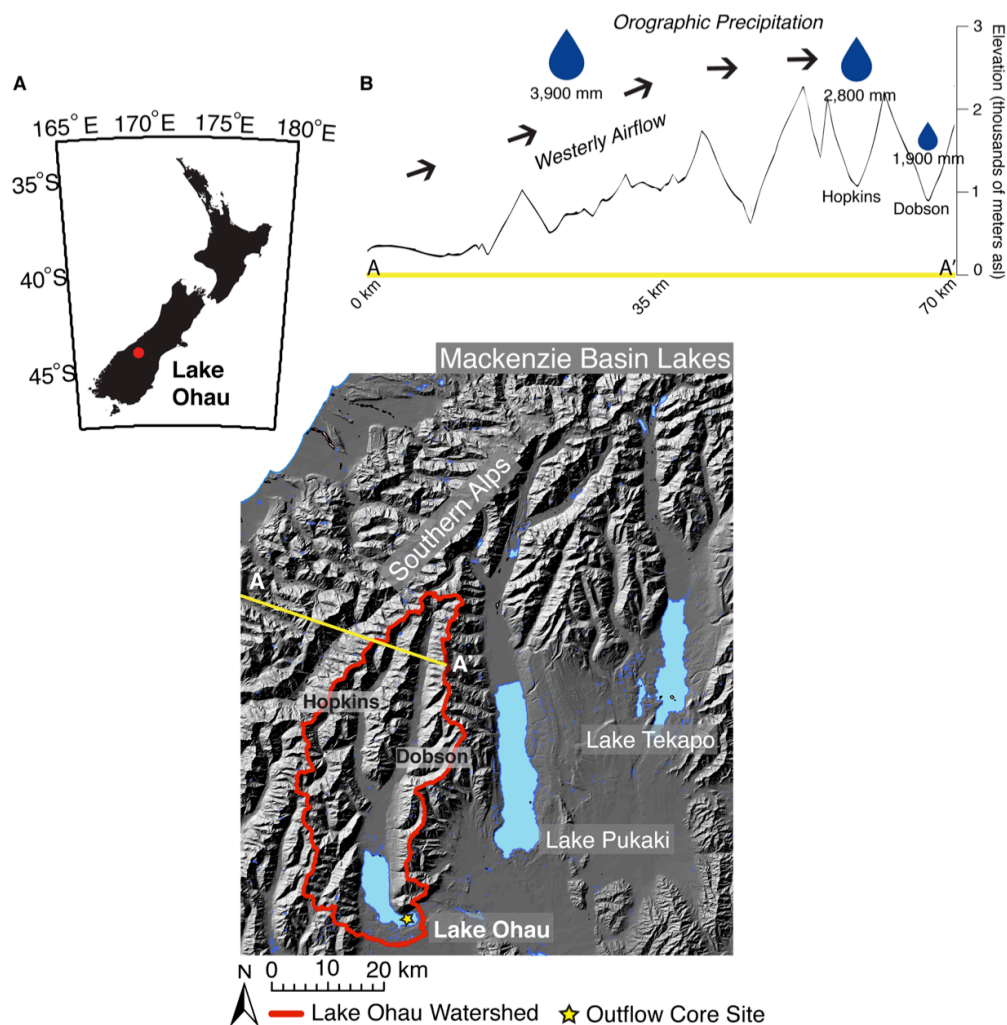


Fig. 3: A) Lake Ohau is the southernmost of three large glacial lakes in the Mackenzie Basin, South Island, New Zealand. Sediment cores collected from the lake outflow preserve fine, millimeter scale laminations. B) Elevation transect from the wet West Coast to the head of the Ohau catchment, demonstrating that westerly airflow results in significant overspill of orographic precipitation into the headwaters of the catchment. The southeast of the catchment experiences drier intermontane conditions. Changes in the position and intensity of the westerly jet influence this precipitation pattern, making the Ohau catchment potentially sensitive to the changes in the westerly winds. Precipitation values listed in mm/year are averaged over 1979-2014 (where available) and include data from east to west (locations not shown) from: Okarito (43.22°S, 170.16°E), Elcho Flats (43.92°S, 169.83°E) and Lake Tekapo (44.04°S, 170.38°E). Okarito and Lake Tekapo data were downloaded from <http://cliflo.niwa.co.nz/>; Elcho Flats data were provided by Meridian Energy Ltd.; 1900 mm is representative of lake outflow conditions.

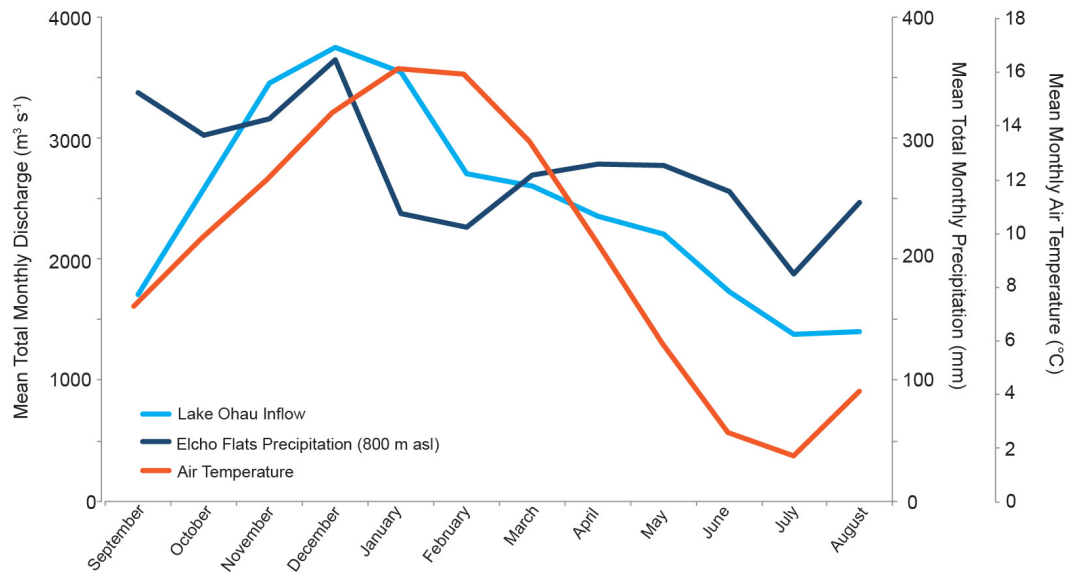


Fig. 4: Mean monthly lake inflow, headwater (Elcho Flats) precipitation and air temperature in the Lake Ohau catchment (1994-2012; data provided by Meridian Energy). These data highlight the average seasonality, particularly in lake inflow and air temperature, in the Lake Ohau catchment.

1.3 VARVES AS CLIMATE PROXIES

1.3.1 Varve Formation and Characteristics

With a potentially sensitive climatic setting, the Lake Ohau sediment record can provide a new perspective on past variability in circulation around the mid-latitudes. This is particularly true with a seasonally-resolved proxies including varve sequences. De Geer first used the term varve in 1912 as a way to describe annual cycles preserved in marine and lacustrine sediment sequences collected in Northern Europe (de Geer, 1912). These cyclic clay/silt couplets were observed in glaciated catchments across northern Europe and North America and were interpreted to represent the differing depositional environments between winter sedimentation, dominated by settling of fine clay particles, and coarser silts deposited during spring and summer when meltwater fluxes increase (de Geer, 1912; 1921).

Varves can provide high-resolution, annually resolved paleoclimate archives that extend beyond observational records, making them important paleoenvironmental tools (Zolitschka and Pike, 2014). Varves are rhythmically deposited couplets that

systems, the local features of climate (e.g. temperature, precipitation), and other factors that influence sedimentation (glaciers, vegetation, lithology, basin morphology, etc.) must be considered (Fig. 6; Bradley, 1999; Hodder et al., 2007).

Geologic processes such as earthquakes and slope failure can, in geologic time, instantly alter a basin's sediment availability. The climate system itself operates on various temporal and spatial scales and can be complicated in mountainous terrain by microclimates, which can be poorly resolved in modeled data and are generally underrepresented in meteorological time-series (Hannah et al., 2000). Additionally, complex hydrologic systems can influence sediment transport and internal lake dynamics, which can attenuate the dispersal and accumulation patterns of sediments once they enter the lacustrine system (Desloges and Gilbert, 1994, Hodder et al., 2007). The schematic in Figure 6 highlights some of the geological and climatological processes that may influence the deposition of laminae in Lake Ohau.

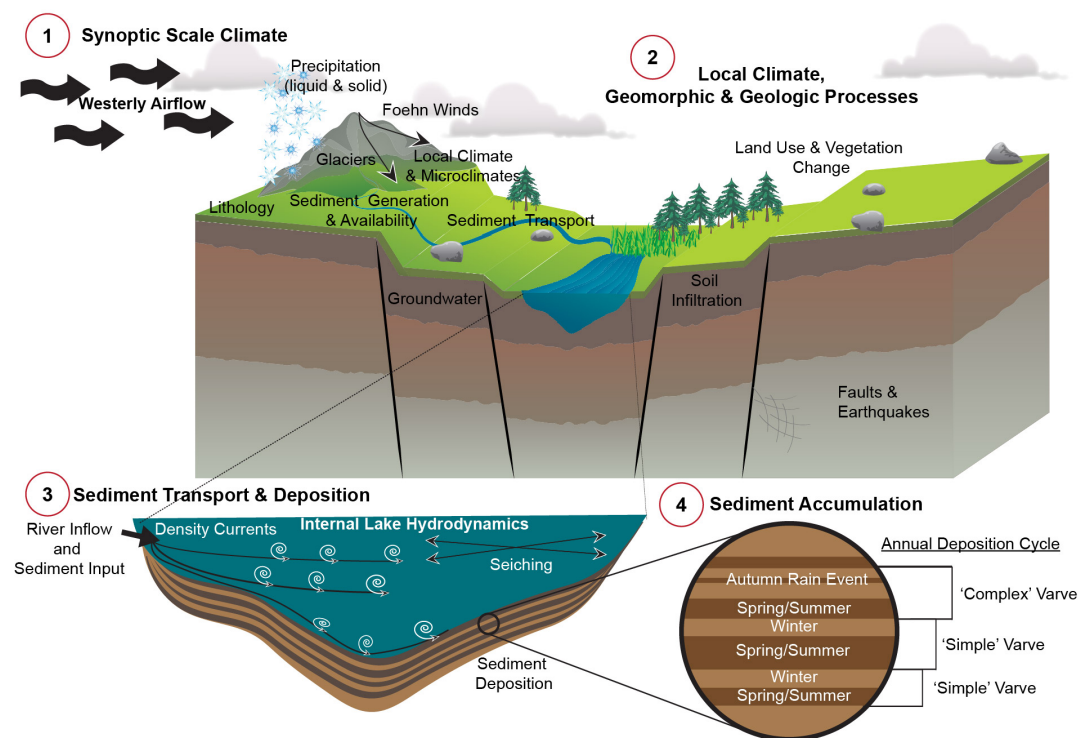


Fig. 6: Several climatic (1), geomorphic (2), and lacustrine processes (3) operating on different temporal and spatial scales can influence the physical and geochemical character of varved sequences (4). A paleoclimate record ultimately aims to link climate (1) to sedimentary changes (4). This research is structured to better understand synoptic scale climate (1), local climate variability (2), and mechanisms of sediment transport and deposition (3) in order to generate a robust paleoclimate reconstruction for the Lake Ohau region.

As outlined in Figure 6, process-network and hydrolimnological monitoring provide observations that yield important details about the contemporary interplay

between synoptic climate (1), local climate and geomorphic processes (2), hydrolimnological changes (3) and the sedimentary record (4). This type of climate-proxy work ultimately improves the paleoclimate interpretations derived from records such as the Lake Ohau varves.

Determining the relationship between climate and sedimentation patterns requires a detailed comparison of the stratigraphy with instrumental climate records. The annual Lake Ohau hydrograph is the product of seasonal snowmelt and sporadic rain events throughout the annual cycle, which can result in the creation of complex laminae (Figs. 5 and 6). Meltwater accounts for 21% of the total annual inflow into Lake Ohau (Kerr et al., 2013) creating a notable increase in discharge in spring and early summer. Inflow remains elevated throughout the summer due to seasonally elevated rainfall.

Therefore, utilizing varves as proxies requires an understanding of the nival pulse (spring melt) conditions, in addition to any year-round sediment-producing inflow events, as both have a pronounced impact on lacustrine thermal regimes and the subsequent dispersal and deposition of sediments (Østrem et al., 1967; Weirich, 1985). The timing and duration of inflow events, and the processes that occur as a result, can dramatically impact sediment thickness and stratigraphy, and thus, the climate-proxy relationship(s) preserved in laminated sequences.

1.3.2 Limnological Controls on Sedimentation

Sediment entering a lake from a point source such as a river is initially dispersed by under-, inter- and overflows throughout the lake in a manner determined by the relative densities of the inflow and lake water. Currents develop primarily due to differences in water temperature but also because of differences in suspended sediment load (Cohen, 2003). The timing and duration of these currents influences the distribution and pattern of deposition of sediment across lake basins (Pharo and Carmack, 1979; Braun et al., 2000; Lewis et al., 2002).

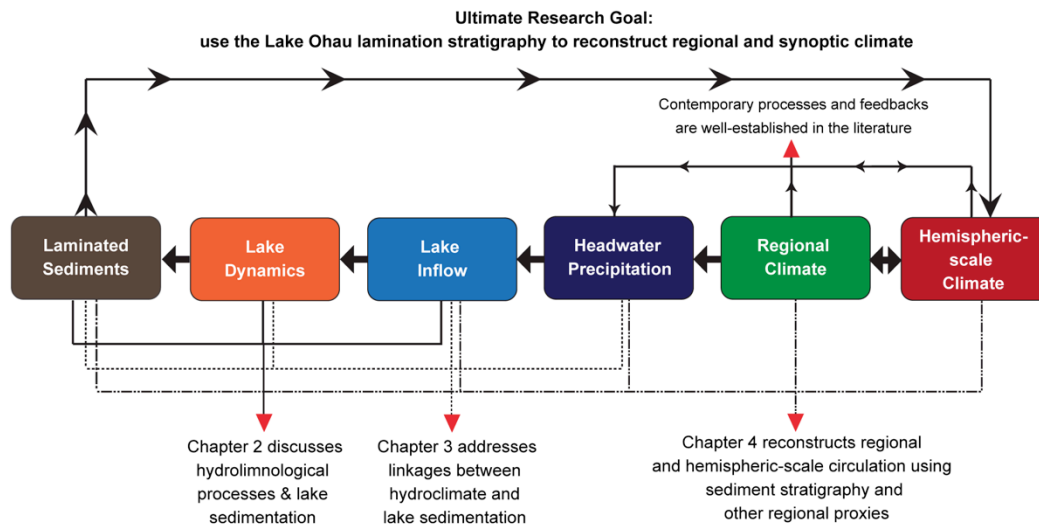
As demonstrated by Lamoureux and Gilbert (2004), current patterns within a lake can control the thickness of varve sediments on the lake floor and can also affect lateral continuity of sediment sequences. Underflows, which are the most typical and sustained form of sediment movement in lacustrine environments, appear to be the most effective at creating easily distinguishable varves (Leemann and Niessen, 1994;

Lewis et al., 2002; Sturm and Matter, 1978). Turbid under- or hyperpycnal-flows can travel long distances (10s of km) and typically transport coarser sediments relative to hypo- and homopycnal flows. Interflows, or hypopycnal and homopycnal flows tend to move finer sediments over and through the entire lake (Ashley et al., 1985). Forces such as wind stress generally disturb overflows, which often carry minimal sediment loads relative to the other flow types (Ashley et al., 1985). The density structure of lakes is further complicated by the interaction between the thermocline and lake inflow, which often show diurnal variability as the temperature of both lake and river water change throughout the day. These processes are further influenced by seiching and wind mixing (Carter and Lane, 1996; Cossu et al., in review).

Although one or two flow types may occur more frequently throughout a given season, on a daily or weekly basis, several flow types and additional hydrodynamic processes can influence sediment distribution and deposition in lacustrine environments. Understanding these shifts in these flow conditions with long-term monitoring including sediment traps, turbidity meters, acoustic Doppler current profilers (ADCP), and water temperature loggers often helps to elucidate the dynamics between the lacustrine and fluvial environments that operate on different temporal (seasonal to diurnal) and spatial scales, thereby helping to better interpret changes in sedimentation throughout the lake (Retelle and Child, 1996; Cockburn and Lamoureux, 2008; Cossu et al., in review). Paramount to developing the Lake Ohau record is documenting and generating a conceptual model that constrains the primary control(s) on sediment dispersal and deposition within this large, temperate lake.

Process-network monitoring at Lake Ohau commenced in 2012, and includes automated weather stations, thermistor strings, nephelometers, Acoustic Doppler Current Profilers (ADCP), and sediment traps. This monitoring equipment is used to document the hydrodynamic and hydroclimatic controls on annual sediment deposition (Chapter 2). These data, paired with a relatively long instrumental record (1926-2011) of air temperature, precipitation, lake inflow and modeled hydrometeorological data, are used to develop a sound climate-proxy model, which provides a means by which sedimentary characteristics can be linked to hydrometeorological variability (Chapter 3). Understanding these basin-wide processes provides the robust foundation required for interpreting down-core variability and for the development of a high-resolution record of paleoclimatic variability in the SH mid-latitudes (Chapter 4). Figure 7 outlines the overall structure of this thesis.

Fig. 7: The general thesis structure based on the overarching research goal of generating a robust paleoclimate reconstruction from Lake Ohau.



1.4 RESEARCH QUESTIONS AND THESIS OUTLINE

1.4.1 Research Questions

This thesis aims to improve our understanding of synoptic climate systems that determine precipitation and weather patterns in the SH mid-latitudes and how and why they have changed over the last ~1,350 years. Using the laminated sediments collected at Lake Ohau we aim to address the following questions:

- (1) How does sedimentation in Lake Ohau vary temporally and spatially, and how do the dark and light laminations preserved in the sediment cores relate to seasonal changes in terrigenous sediment input?
- (2) Over the instrumental period, what are the primary hydrological and meteorological drivers impact on the amount and timing of sediment discharge into Lake Ohau? Can we develop a reliable climate-proxy model for interpreting down-core variability in the physical character of the lamination stratigraphy?
- (3) Can the controls on sediment deposition into Lake Ohau and the resultant sedimentary sequence be reliably utilized to reconstruct climate over the past 1,350 years? If so, what climatic variations have occurred in the Lake Ohau catchment and, by extension, the South Island and Southern Hemisphere mid-latitudes over the late-Holocene?

1.4.2 Thesis Outline

This thesis is structured to answer the above questions through three separate research papers that include:

- Chapter 2: A modern catchment process study that demonstrates the hydroclimatic and hydrodynamic processes responsible for varve deposition in Lake Ohau. This chapter is published in the journal *Sedimentology*.
- Chapter 3: The development of a climate-proxy model for the Ohau catchment, which quantifies the relationship between climate and sedimentation over the instrumental record. This chapter is accepted for publication in the *Journal of Paleolimnology*.
- Chapter 4: The 1,350-year paleoclimate record developed from Lake Ohau. This chapter is in preparation for submission to *Quaternary Science Reviews*.

Chapter 5 provides a summary of the research findings and discusses future work. The anticipated collection of a ~17 ka sediment sequence from Lake Ohau in early 2016 provides additional scope for ongoing work. This research, therefore, provides a foundation onto which this larger project can build.

A note to the reader: One product of a thesis written as individual research papers is content repetition. Please be aware that introductory materials including geographic location and project motivations will be repeated at the commencement of each chapter. All chapters have references formatted to the individual journal requirements.

1.5 REFERENCES

- Abram, N.J., Mulvaney, R., Wolff, E.W., Triest, J., Kipfstuhl, S., Trusel, L., Vimeux, F., Fleet, L., and Arrowsmith, C., 2013. Acceleration of snowmelt in an Antarctic Peninsula ice core during the twentieth century. *Nature Geoscience* 6(5): 404-411.
- Ashley G.M., Shaw J., Smith N.D., 1985. Glacial sedimentary environments, SEPM Short Course 16. Tulsa (OK): *Society of Paleontologists and Mineralogist* 1-246.
- Anderson, B. and Mackintosh, A., 2006. Temperature change is the major driver of late-glacial and Holocene glacier fluctuations in New Zealand. *Geology* 34: 121-124.
- Bradley R.S., 1999. Paleoclimatology: Reconstructing Climates of the Quaternary. *International Geophysics Series* 68. Elsevier Academic Press, Amsterdam.
- Braun, C., Hardy, D.R., Bradley, R.S. and Retelle, M., 2000. Streamflow and Suspended Sediment Transfer to Lake Sophia, Cornwallis Island, Nunavut, Canada. *Arctic, Antarctic, and Alpine Research* 32: 456-465.
- Cai, W., 2006. Antarctic ozone depletion causes an intensification of the Southern Ocean super-gyre circulation. *Geophysical Research Letters* 33: L03712, doi:10.1029/2005GL024911
- Carter, G.S., and Lane, M.R., 1996. Modelling surface oscillations in New Zealand lakes. *New Zealand Journal of Marine and Freshwater Research* 30(3): 341-353.
- Chambers, F.M., Brain, S.A., Mauquoy, D., McCarroll, J., and Daley, T., 2014. The 'Little Ice Age' in the Southern Hemisphere in the context of the last 3000 years: Peat-based proxy-climate data from Tierra del Fuego. *The Holocene* 24: 1649-1656.
- Chater, A. M. and Sturman, A.P., 1998. Atmospheric conditions influencing the spillover of rainfall to lee of the Southern Alps, New Zealand. *International Journal of Climatology* 1: 77-92.
- Chinn, T.J., 1999. New Zealand glacier response to climate change of the past two decades. *Global and Planetary Change* 22: 155-168.
- Clare, G.R., Fitzharris, B.B, Chinn, T.J.H., Salinger, M.J., 2002. Interannual variations in end-of-summer snowlines of the Southern Alps of New Zealand, and relationships with Southern Hemisphere atmospheric circulation and sea surface temperature patterns. *International Journal of Climatology* 22: 107-120.
- Cockburn, J.M.H., Lamoureux, S.F., 2007. Century-scale variability in late-summer rainfall events recorded over seven centuries in sub-annually laminated lacustrine sediments, White Pass, British Columbia. *Quaternary Research* 67: 193-203.
- Cockburn, J.M.H., Lamoureux, S., 2008. Inflow and lake controls on short-term mass accumulation and sedimentary particle size in a High Arctic lake: implications for interpreting varved lacustrine sedimentary records. *Journal of Paleolimnology* 40: 923-942.

Cohen, A.S., 2003. Paleolimnology: The history and evolution of lake systems. *Oxford University Press* 500 pp.

Cook, E.R., Buckley, B.M., Palmer, J.G., Fenwick, P., Peterson, M.J., Boswijk, G., and Fowler, A., 2006. Millenia-long tree-ring record from Tasmania and New Zealand: a basis for modelling variability and forcing, past, present and future. *Journal of Quaternary Science* 21: 689-699.

Cook, E. R., Palmer, J. G. and D'Arrigo, R. D., 2002. Evidence for a 'Medieval Warm Period' in a 1,100 year tree-ring reconstruction of past austral summer temperatures in New Zealand. *Geophysical Research Letters* 29(14): 12-1-12-14.

Cossu, R., Forrest, A.L., Roop, H.A., Dunbar, G.B., Vandergoes, M.J., Levy, R.H., Stumpner, P., and Schladow, S.G., in review. The role of limnological processes for sedimentation in Lake Ohau, New Zealand—a conceptual process model. *Marine and Freshwater Research*.

Cowan, E.A., and Powell, R.D., 1990. Suspended sediment transport and deposition of cyclically interlaminated sediment in a temperate glacial fjord, Alaska, USA. *Geological Society, London, Special Publications* 53(1): 75-89.

de Geer, G., 1912. A geochronology of the last 12000 years. *Compte rendu du XI Congres Geologique International* (Stockholm 1910): 241-253.

de Geer, G., 1921. Correlation of late glacial annual clay-varves in North America with Swedish time scale. *Geologiska Foreningen i Stockholm Forhandlingar* 43(1-2): 70-73.

Desloges, J.R. and Gilbert, R., 1994. Sediment source and hydroclimatic inferences from glacial lake sediments: the postglacial sedimentary record of Lillooet Lake, British Columbia. *Journal of Hydrology* 159: 375-393.

Folland C.K., Renwick J.A., Salinger M.J., and Mullan A.B., 2002. Relative influences of the Interdecadal Pacific Oscillation and ENSO on the South Pacific Convergence Zone. *Geophysical Research Letters* 29: 1643-1647.

Folland, C.K., Parker D.E., Colman, A., and Washington, R., 1999. Large scale modes of ocean surface temperature since the late nineteenth century, in *Beyond El Nino: Decadal and Interdecadal Climate Variability*, edited by A. Navarra, *Springer-Verlag*, Berlin pp. 73-102.

Folland, C.K. and Salinger, M.J., 1995. Surface temperature trends and variations in New Zealand and the surrounding ocean, 1871-1993. *International Journal of Climatology* 15: 1195-1218.

Fowler A.M., Boswijk, G., Lorrey, A.M., Gergis, J., Pirie, M., McCloskey, S.P.J., Palmer, J.G., and Wunder, J., 2012. Multi-centennial tree-ring record of ENSO-related activity in New Zealand. *Nature Climate Change* 2: 172-176.

- Fyfe, J.C., 2003. Extratropical Southern Hemisphere cyclones: Harbingers of climate change? *Journal of Climate* 16: 2802-2805.
- Garr, C. E. & Fitzharris, B. B., 1991. A Climate Classification of New Zealand based on Numerical Techniques. *New Zealand Geographer* 47: 60-71.
- Garreaud, R.D., 2007. Precipitation and Circulation Co-variability in the Extratropics. *Journal of Climate* 20(18): 4789-4797.
- Hannah, D.M., Gurnell, A.M., and McGregor, G.R., 2000. Spatio-temporal variation in microclimate, the surface energy balance and ablation over a cirque glacier. *International Journal of Climatology* 20(7): 733-758.
- Hodder, K.R., Gilbert, R., and Desloges, D.R., 2007. Glaciolacustrine varves sediment as an alpine hydroclimatic proxy. *Journal of Paleolimnology* 38: 365-394.
- Kerr, T., 2013. The contribution of snowmelt to the rivers of the South Island, New Zealand. *Journal of Hydrology (NZ)* 52(2): 61-82.
- Kienel, U., Wulf Bowen, S., Byrne, R., Park, J., Böhnelt, H., Dulski, P., Luhr, J.F., Siebert, L., Haug, G.H., Negendank, J.F.W., 2009. First lacustrine varve chronologies from Mexico: impact of droughts, ENSO and human activity since AD 1840 as recorded in maar sediments from Valle de Santiago. *Journal of Paleolimnology* 42: 587-602.
- Kidston, J., Renwick, J. A. and McGregor, J. 2009. Hemispheric-Scale Seasonality of the Southern Annular Mode and Impacts on the Climate of New Zealand. *Journal of Climate* 22: 4765-4770.
- Kidson, J.W., 2000. An analysis of New Zealand synoptic types and their use in defining weather regimes. *International Journal of Climatology* 20(3): 299-316.
- Knudson, K. P., Hendy, I. L., and Neil, H. L., 2011. Re-examining Southern Hemisphere westerly wind behavior: insights from a late Holocene precipitation reconstruction using New Zealand fjord sediments. *Quaternary Science Reviews* 30: 3124-3138.
- Lamoureux, S.F., Gilbert, R., 2004. A 750-yr record of autumn snowfall and temperature variability and winter storminess recorded in the varved sediments of Bear Lake, Devon Island, Arctic Canada. *Quaternary Research* 61: 134-147.
- Leemann, A, Niessen, F, 1994. Varve formation and the climatic record in an alpine proglacial lake: Calibrating annually laminated sediments against hydrological and meteorological data. *The Holocene* 4: 1-8.
- Lewis, T., Gilbert, R., and Lamoureux, S.F., 2002. Spatial and temporal changes in sedimentary processes at proglacial Bear Lake, Devon Island, Nunavut, Canada. *Arctic, Antarctic and Alpine Research* 34: 119-129.

Lorrey, A., Fauchereau, N., Stanton, C., Chappell, P., Phipps, S., Mackintosh, A., Renwick, J., Goodwin, I., and Fowler, A., 2014. The Little Ice Age climate of New Zealand reconstructed from Southern Alps cirque glaciers: a synoptic type approach. *Climate Dynamics* 42(11-12): 3039-3060.

Lorrey, A., Williams, P., Salinger, J., 2008. Speleothem stable isotope records interpreted within a multi-proxy framework and implications for New Zealand palaeoclimate reconstruction. *Quaternary International* 187: 52-75.

Marshall, G.J., 2003. Trends in the southern annular mode from observations and reanalyses. *Journal of Climate* 16: 4134-4143.

Mann, M. E., Bradley, R. S. and Hughes, M. K., 1998. Global-scale temperature patterns and climate forcing over the past six centuries. *Nature* 392: 779-787.

Mann, M. E., Zhang, Z., Rutherford, S., Bradley, R.S., Hughes, M.K., Shindell, D., Ammann, C., Faluvegi, G., and Ni, F., 2009. Global signatures and dynamical origins of the Little Ice Age and medieval climate anomaly. *Science* 326: 1256-1260.

McKerchar, A.I., and Henderson, R.D., 2003. Shifts in flood and low-flow regimes in New Zealand due to interdecadal climate variations. *Hydrological Sciences Journal* 48(4): 637-654.

McKerchar, A.I., Pearson, C.P., Moss, M.E., 1996. Prediction of summer inflows to lakes in the Southern Alps, New Zealand, using the spring Southern Oscillation Index. *Journal of Hydrology* 184: 175-187.

Middleton, G.V., 1993. Sediment Deposition from Turbidity Currents. *Annual Review Of Earth And Planetary Science* 21: 89-114.

Mullan, A.B., 1995. On the linearity and stability of Southern Oscillation-climate relationships for New Zealand. *International Journal of Climatology* 15: 1365-1386.

NCEP/NCAR Reanalysis Plotting. NOAA/ESRL Physical Sciences Division, Boulder Colorado. <http://www.esrl.noaa.gov/psd/>

Neukom, R. and Gergis, J., 2011. Southern Hemisphere high-resolution palaeoclimate records of the past 2000 years. *The Holocene* 5: 501-524.

Ojala, A.E and Tiljander, M., 2004. Testing the fidelity of sediment chronology: comparison of varve and paleomagnetic results from Holocene lake sediments from central Finland. *Quaternary Science Reviews* 22: 1787-1803.

Ojala, A. E. K., Francus, P., Zolitschka, B., Besonen, M. and Lamoureux, S. F. 2012. Characteristics of sedimentary varve chronologies, A review. *Quaternary Science Reviews* 43: 45-60.

Orpin A.R., Carter, L., Page, M.J., Cochran, U.A., Trustman, N.A., Palmer, A.S., Mildenhall, D.C., Rogers, K.M., Brackley, H.L., and Northcote, L., 2010. Holocene sedimentary record from Lake Tutira; a template for upland watershed erosion proximal to the Waipaoa sedimentary system, northeastern New Zealand. *Marine Geology* 270: 11-29.

Østrem, G., Bridge, C.W., Rannine, W.F., 1967. Glacio-hydrology, discharge and sediment transport in the Decade Glacier area, Baffin Island, N.W.T. *Geografiska Annaler* 49: 268-282.

Page, M. J., Trustrum, N. A. and DeRose, R. C., 1994. A high-resolution record of storm induced erosion from lake sediments, New Zealand. *Journal of Paleolimnology* 11: 333-348.

Page, M.J., Trustrum N.A., Orpin, A.R., Carter, L., Gomez, B., and Cochran, U.A., 2010. Storm frequency and magnitude in response to Holocene climate variability, Lake Tutira, North-Eastern New Zealand. *Marine Geology* 270: 30-44.

Pepper, A. C., Shulmeister, J., Nobes, D. C., and Augustinus, P. A., 2004. Possible ENSO signals prior to the Last Glacial Maximum, during the last deglaciation and the early Holocene, from New Zealand. *Geophysical Research Letters*, 31(15): 1-4.

Pharo, C.H. and Carmack, E.C., 1979. Sedimentation processes in a short residence-time intermontane lake, Kamloops Lake, British Columbia. *Sedimentology* 26(4): 523-541.

Power, S., Casey, T., Folland, C., Colman, A., and Mehta, V., 1999. Inter-decadal modulation of the impact of ENSO on Australia, *Climate Dynamics* 15(5): 319-324.

Renwick, J.A., 2004. Trends in the Southern Hemisphere polar vortex in NCEP and ECMWF reanalyses. *Geophysical Research Letters* 31: L07209.

Renwick, J.A. and Thompson, D., 2006: The Southern Annular Mode and New Zealand climate. *Water Atmosphere* 14: 24-25.

Retelle, M.J., Child, J.K., 1996. Suspended sediment transport and deposition in a high arctic meromictic lake. *Journal of Paleolimnology* 16: 151-167.

Roop H.A., Dunbar, G.B., Levy, R., Vandergoes, M.J., Forrest, A.L., Walker, S.L., Upton, P. and Whinney, J., 2015. Seasonal controls on sediment transport and deposition in Lake Ohau, South Island, New Zealand: Implications for a high-resolution Holocene palaeoclimate reconstruction. *Sedimentology* 62(3): 826-844.

Roop, H.A., Levy, R., Dunbar, G.B., Vandergoes, M.J., Howarth, J., Fitzsimons, S., Soo Moon, H., Zammit, C., Ditchburn, R., Basiden, T., Yoon H.I., accepted. A hydroclimate-proxy model based on sedimentary facies in an annually laminated sequence from Lake Ohau, South Island, New Zealand. *Journal of Paleolimnology*.

Salinger, M.J., Renwick, J.A., Mullan, B., 2001. Interdecadal Pacific Oscillation and South Pacific Climate. *International Journal of Climatology* 21: 1705-1721.

Sinclair, M.R., Wratt D.S., Henderson R.D., Gray W.R, 1997. Factors affecting the distribution and spillover of precipitation in the Southern Alps of New Zealand—a case study. *Journal of Applied Meteorology* 36: 428-442.

Sturm, M. and Matter, A., 1978. Turbidites and Varves in Lake Brienz (Switzerland): Deposition of Clastic Detritus by Density Currents, in Modern and Ancient Lake Sediments (eds. A. Matter and M. E. Tucker), *Blackwell Publishing Ltd.*, Oxford, UK. doi: 10.1002/9781444303698.ch8

Thompson, D.W.J., and Solomon, S., 2002. Interpretation of recent Southern Hemisphere climate change. *Science* 296: 895-899.

Thompson, D.W.J. and Wallace, J.M., 2000. Annular modes in the extratropical circulation. Part I: month-to-month variability. *Journal of Climate* 13: 1000-1016.

Ummenhofer, C.C. and England, M.H., 2007. Interannual extremes in New Zealand precipitation linked to modes of Southern Hemisphere climate variability. *Journal of Climate* 20: 5418-5440.

Ummenhofer, C.C., Sen Gupta, A., and England, M.H., 2009. Causes of late twentieth century trends in New Zealand precipitation. *Journal of Climate* 22: 3-19.

Vandergoes, M.J., Dieffenbacher-Krall A.C., Newnham, R., Denton G.H, and Blaauw, M., 2008. Cooling and changing seasonality in the Southern Alps, New Zealand during the Antarctic Cold Reversal. *Quaternary Science Reviews* 27: 589-601.

Weirich, F.H., 1985. Sediment Budget for a High Energy Glacial Lake. *Geographiska Annaler, Series A. Physical Geography* 12: 83-99.

Zolitschka, B., 2013. Varved lake sediments. In: Elias, S (ed). *Encyclopedia of Quaternary Science* 3105-3114. Elsevier Academic Press, Amsterdam.

Zolitschka, B., and Pike, J., 2014. Maximizing the information yield from annually resolving natural archives. *Past Global Changes Magazine* 22(1): 4-5.

CHAPTER 2

Seasonal controls on sediment transport and deposition in Lake Ohau, South Island,
New Zealand: Implications for a high-resolution Holocene palaeoclimate
reconstruction

The content in Chapter 2 was published in the peer-reviewed journal *Sedimentology* in 2015.

CITATION

Roop H.A., Dunbar, G.B., Levy, R., Vandergoes, M.J., Forrest, A.L., Walker, S.L., Upton, P. and Whinney, J., 2015. Seasonal controls on sediment transport and deposition in Lake Ohau, South Island, New Zealand: Implications for a high-resolution Holocene palaeoclimate reconstruction. *Sedimentology* 62(3): 826-844.

Authorship contributions to this research article include the following:

Heidi A. Roop - Wrote manuscript and managed all co-author feedback, reviewer comments, and editing of proofs. This author compiled all data, developed initial interpretations, and produced all figures.

Gavin Dunbar - Academic Supervisor; provided feedback on drafts and aided in the interpretation of the results. Helped to outline the Discussion section of the manuscript.

Richard Levy - Academic Supervisor; provided feedback on drafts and aided in the interpretation of the results.

Marcus J. Vandergoes - Academic Supervisor; provided feedback on drafts and aided in the interpretation of the results.

Alexander Forrest - Provided comment on the lake hydrodynamics section in the Discussion portion of the manuscript. Reviewed two drafts of the manuscript.

Sharon L. Walker - Reviewed technical language in the Methods and Results sections regarding the turbidity sensors provided by NOAA. Provided helpful comments on a draft of the manuscript.

Jennifer Purdie - Reviewed language related to Meridian Energy inflow data in the Setting and Methods sections of the manuscript.

Phaedra Upton - Provided editorial comments on an early draft of the paper; Lake Ohau project collaborator.

James Whinney - Reviewed technical language in the Methods and Results sections related to the turbidity sensors provided by James Cook University.

ABSTRACT

Laminated sediments in Lake Ohau, Mackenzie Basin, New Zealand, offer a potential high-resolution climate record for the past 17 kyr. Such records are particularly important due to the relative paucity of detailed palaeoclimate data from the Southern Hemisphere mid-latitudes. This paper presents outcomes of a study of the sedimentation processes of this temperate lake setting. Hydrometeorological, limnological and sedimentological data were collected over a 14-month period between 2011 and 2013. These data indicate that seasonality in the hydrometeorological system in combination with internal lake dynamics drive a distinct seasonal pattern of sediment dispersal and deposition on a basin-wide scale. Sedimentary layers that accumulate proximal to the lake inflow at the northern end of the lake form in response to discrete inflow events throughout the year and display an event stratigraphy. In contrast, seasonal change in the lake system controls accumulation of light (winter) and dark (summer) laminations at the distal end of the lake, resulting in the preservation of varves. This study documents the key processes influencing sediment deposition throughout Lake Ohau and provides fundamental data for generating a high-resolution palaeoclimate record from this temperate lake.

Keywords: Grain size, modern process, palaeoclimate, sediment deposition, varves

2.1 INTRODUCTION

Annually laminated sediments from lakes offer high-resolution proxy climate records that often extend well beyond the relatively short modern instrumental record. These data are important because they provide a longer-term perspective on climate variability, prior to anthropogenic influence. While many varved lake records have been documented in the Northern Hemisphere, similar data from the Southern Hemisphere mid-latitudes exist (Ojala et al., 2012) but are less common. Lake systems in New Zealand can potentially reduce this Southern Hemisphere data gap. For example, previous high-resolution sediment cores recovered from lakes on the North Island (e.g. Page et al., 1994, 2010; Pepper et al., 2004; Augustinus et al., 2011) highlight the potential for terrestrial palaeoclimate archives from this key Southern Hemisphere location. Importantly, New Zealand is influenced by climatological patterns originating in both the tropics [El-Niño-Southern Oscillation (ENSO) and Interdecadal Pacific Oscillation (IPO)] and the Antarctic [Southern Annular Mode (SAM)]. In particular, the South Island of New Zealand shows decadal trends in rainfall recorded in its western regions that are highly correlated with the SAM (Ummenhofer et al., 2009). New palaeoclimate records in this region can provide insight into the variability in amplitude, timing and interdependence of these climate modes over time.

Lake Ohau is located in the Mackenzie Basin, South Island, New Zealand (44.234° S, 169.854° E; Fig. 1) and is well-situated to record the effect of climate modes, such as the SAM, on sediment transport and deposition because the riverine input to this lake is derived from precipitation sourced close to the main divide of the Southern Alps, which is driven predominantly by storms associated with westerly airflow (Chater & Sturman, 1998; Salinger & Mullan, 1999). Geophysical data (Boomer and Chirp systems) indicate that the lake basin contains up to 140 m of sediments that have accumulated following retreat of glacial ice from the basin ca 17 ka (Putnam et al., 2013). Several 5.5 m long Mackereth cores recovered from the top of this sedimentary sequence preserve millimetre-scale light and dark laminations. Similar laminated sediments have been recovered from nearby Lakes Tekapo and Pukaki (Fig. 1) and were interpreted as complex varves (Pickrill & Irwin, 1983) although the relation between seasonal climate, sedimentation processes and lake floor stratigraphy was not examined. Furthermore, problems with radiometric age

control have hindered attempts to confirm whether the observed layers represent varves (Graham et al., 2005; Mildenhall et al., 2006). A robust understanding of the processes that control sedimentation is required to determine whether the sedimentary couplets in Lake Ohau accumulate annually and represent true varves.

Transport and deposition of sediment in typical clastic varve environments is driven by pronounced seasonality in the hydrological regime (Zolitschka, 2007). Most process studies within these environments have been conducted in montane lakes in the Northern Hemisphere, where the primary drivers of seasonal sediment flux are spring snowmelt, glacier melt and summer precipitation events (e.g. Leemann & Niessen, 1994; Gilbert & Butler, 2004; Cockburn & Lamoureux, 2008a; Francus et al., 2008). In these systems, the flux of water and sediment is strongly controlled by this snowmelt and glacial-melt driven hydrology, and sediment dispersal and deposition is controlled by lake stratification (e.g. Weirich, 1986; Desloges & Gilbert, 1994; Hardy et al., 1996; Cockburn & Lamoureux, 2008b). Relatively large amounts of sediment are discharged into the lake during the spring nival pulse, throughout the summer glacier-melt season and episodically during summer and autumnal rainfall events when the lake is stratified. During winter these lakes are typically ice covered and isothermal. Discharge is also reduced and the fine silt and clay particles input during the summer months settle through gravitation settling and flocculation in quiescent flow conditions to form a dark winter layer (Bradley, 1999; Hodder & Gilbert, 2007). This pattern of accumulation results in the typical coarse/fine clastic varve stratigraphy.

In contrast to the snow- and glacial-melt driven system described above, sediment deposition within the temperate (mean winter air temperature of 6.2° C), and minimally glaciated (1.7%; Anderton, 1973) Lake Ohau watershed, is driven primarily by rainfall events that occur throughout the annual cycle. Minimal glacial meltwater and sediment flux, and year-round rainfall, suggest that the formation of the light and dark coloured couplets in Lake Ohau may be more similar to varves documented in other temperate, rainfall-dominated systems (e.g. Ross & Gilbert, 1999). This study describes the contemporary hydrometeorological and limnological processes that influence Lake Ohau and is designed to constrain the relation between environmental variables and sediment dispersal and accumulation throughout the annual cycle.

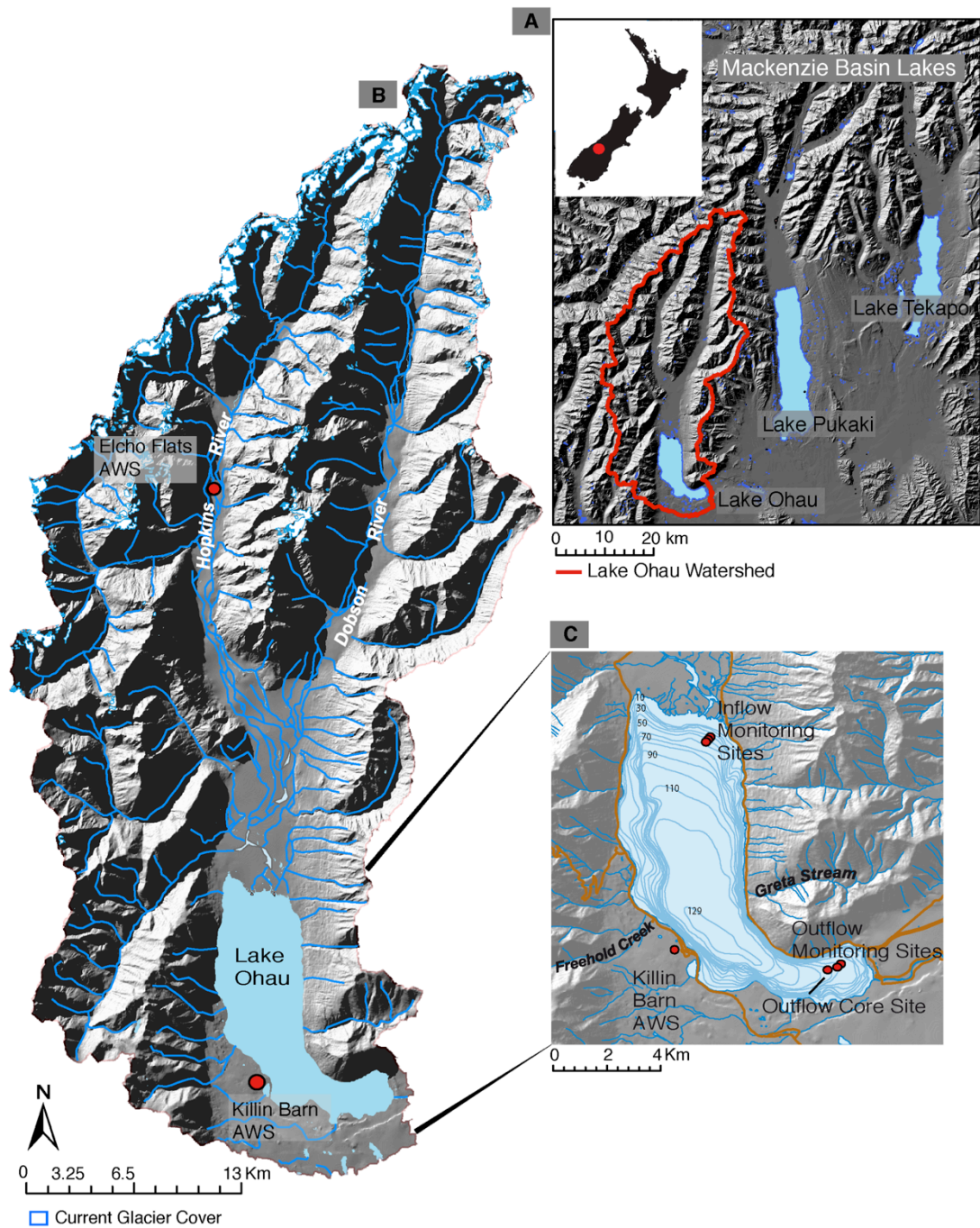


Fig. 1: Overview of the Mackenzie Basin Lakes (detail) and the Lake Ohau study area including monitoring locations, core collection sites and automatic weather stations (AWS). Isobath interval is 10 m. Bathymetric data were provided by the National Institute of Water and Atmosphere (NIWA).

2.1.1 Physical Setting

Lake Ohau is one of three north–south trending glacially-formed lakes in the intermontane Mackenzie Basin (Fig. 1A). The lake is 520 m above sea-level (asl), reaches a maximum depth of 129 m, is 18.5 km long, up to 4.9 km wide and has a surface area of 54 km² (Fig. 1B; Irwin, 1975). The lake lies immediately to the east and in the rain shadow of the south-west/north-east trending Southern Alps mountain range that reaches a maximum elevation of 3754 m asl. The Lake Ohau catchment covers 1198 km² and ranges in elevation from 520 to 2640 m asl. Catchment geology is predominately highly indurated quartzofeldspathic greywacke sandstone and argillite mudstone (Cox & Barrell, 2007).

The lake occupies a moraine-bound glacial valley with a typical glacial U-shaped cross-section. Beryllium surface-exposure ages on recessional moraines indicate that the main glacier last retreated from the Ohau Basin between 17 ka and 17.4 ka (Putnam et al., 2013). Since then, the lake basin has been partially filled with sediment derived from the Hopkins and Dobson river catchments. Today, a steep delta front occurs at the head of the lake where the bathymetry deepens to ca 100 m and eventually reaches 129 m at the depocentre between 7 km and 10 km to the south. The lake floor then gradually rises up an eastward trending slope to its natural outlet ca 18 km from the delta (Fig. 1C).

Sediment and water flux into the lake is controlled primarily by discharge from the Hopkins and Dobson rivers, which converge as they flow into the lake. Combined, these rivers contribute ca 85% of the total annual discharge (Fig. 1; Woods et al., 2006) and drain a combined area of 924 km². Small tributaries that drain directly into the lake, including Freehold Creek and Greta Stream (Fig. 1C), are additional sources of sediment and water to Lake Ohau but their catchment size and location further east of the main topographic divide makes their contribution of both sediment and water flux relatively small (< 5%; Woods et al., 2006).

Discharge into Lake Ohau is derived directly from rainfall and spring meltwater, which contributes 21% of mean annual river discharge, into Lake Ohau (Kerr, 2013). Glacier melt is a minor contributor during summer. Regionally, average rainfall in January is 58% higher than in July. The uppermost Hopkins and Dobson valleys contain small modern glaciers, which occupy ca 20.7 km² and 0.71 km², respectively, covering about 1.7% of the total catchment area (Fig. 1B; Anderton,

1973). This small volume of glacial ice is considered to have remained stable over the last several thousand years based on recent glaciological investigations in the valley (Doughty et al 2013; Putnam et al 2013) and is assumed to play a minor role in sediment generation and flux in the contemporary lacustrine environment (Roop et al 2015). Discharge into Lake Ohau shows distinct seasonality, with a marked increase in discharge during spring (October to November) and generally lower flow in winter (Fig. 2A; Table 2).

2.2 MATERIALS AND METHODS

A suite of limnological and hydrometeorological monitoring equipment was deployed from March 2012 to May 2013, with the exception of a sediment trap at the lake outflow, which was deployed over the period August 2011 to May 2013. All times and dates are reported in Greenwich Mean Time (GMT).

2.2.1 Limnological Monitoring

Lake monitoring stations were established in two areas of the lake (Fig. 1C), one proximal to the major lake inflow (44.192°S, 169.861°E; 50 m water depth), hereinafter termed ‘Inflow’ and one near the outflow (44.286°S, 169.916°E; 68 m water depth), termed ‘Outflow’. Deployment details are summarized in Table 1.

2.2.2 Water Temperature

Lake water temperature was measured using Onset HOBO Water Temperature Pro v2 dataloggers (nominal precision $\pm 0.2^{\circ}\text{C}$; Onset Computer Corporation, Bourne, MA, USA). Temperature data were collected at 5 min intervals at both the Inflow and Outflow (Table 1). Outflow bottom water temperature data were collected every 10 min using thermistors integrated into the Miniature Autonomous Plume Recorder (MAPR; resolution 0.2°C , see Turbidity section below) provided by the U.S. National Oceanic and Atmospheric Administration’s (NOAA) Pacific Marine Environmental Laboratory.

2.2.3 Turbidity

Bottom water turbidity was measured every 10 min using MAPRs (Table 1). These high-sensitivity nephelometers use optical backscatter to measure turbidity to a maximum of approximately five Nephelometer Turbidity Units (NTU). Each

instrument has a unique calibration factor resulting in values that register slightly below a maximum of 5 NTU (4.795 NTU at the Inflow and 4.775 NTU at the Outflow). Instrument saturation is reached at these values. Two optical backscatter sensors (OBS) made by James Cook University recorded surface turbidity (15 m depth) at 10 min intervals. These instruments have a horizontally aligned sensor that measures total suspended sediment concentration (Thomas & Ridd, 2004). Deployment locations and depths are listed in Table 1.

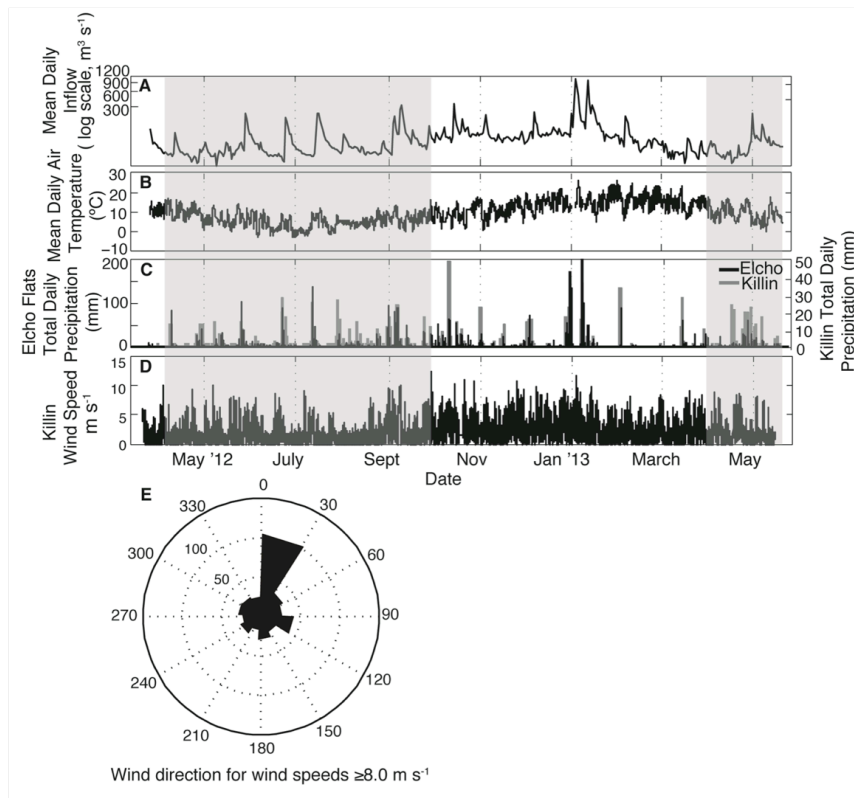


Fig. 2: Meteorological and hydrological conditions at Lake Ohau from March 2012 to May 2013: (A) Mean daily inflow into Lake Ohau; (B) Killin Barn automatic weather station (AWS) mean daily air temperature; (C) Elcho and Killin Barn AWS total daily precipitation; (D) Killin Barn AWS 10 min interval wind speed; and (E) wind direction and speed for wind speeds $\geq 8.0 \text{ m s}^{-1}$. Shading indicates period defined as winter.

2.2.4 Sediment Traps

Four 10.8 cm diameter sediment traps, based on the design of Cockburn & Lamoureux (2008b), were deployed at the Inflow and Outflow sites from June 2012 to May 2013. These traps were attached to the same mooring as the OBS sensors (Table 1). In addition, a 46 cm diameter fibreglass sediment trap mooring was deployed at the Outflow (e.g. MacPherson, 1985; Macpherson, 1986; Table 1). The

top of this trap sits ca 1 m above the lake floor. Sediment traps were recovered and exchanged every three to four months (Table 1).

Table 1 Limnological monitoring equipment deployment locations, depths, and duration.

INFLOW			
Site depth: 50 m			
Measurement (Equipment)	Location (Latitude/ Longitude)	Deployment Depth (m)	Deployment periods/Collection Date
Water Temperature	44.192°S, 169.861°E	2, 15, 30, 48	August 2011-March 2012, March-June 2012, June-October 2012, October 2012-February, 2013, February-May 2013
Turbidity (MAPR)	44.309°S, 170.053°E	47	March-June 2012, June-October 2012, October 2012-February, 2013, February-May 2013
Turbidity (JCU OBS)	44.309°S, 170.053°E	15	March-June 2012, June-October 2012, October 2012-February, 2013, February-May 2013
Sediment Traps (10.8 cm diameter)	44.309°S, 170.053°E	5, 16, 31, 47	June-October 2012, October 2012-February, 2013, February-May 2013
Core GCI_1 (0.3 m)	44.284°S, 169.913°E	50	April 2012
OUTFLOW			
Site depth: 68 m			
Water Temperature	44.517°S, 170.040°E	6, 23, 53, 67	March-June 2012, June-October 2012, October 2012-February, 2013, February-May 2013
Turbidity (MAPR)	44.517°S, 170.040°E	66	March-June 2012, June-October 2012, October 2012-February, 2013, February-May 2013
Turbidity (JCU OBS)	44.517°S, 170.040°E	15	March-June 2012, June-October 2012, October 2012-February, 2013, February-May 2013
Sediment Traps (10.8 cm diameter)	44.517°S, 170.040°E	5, 22, 52, 65	June-October 2012, October 2012-February, 2013, February-May 2013
Sediment Trap (46 cm diameter)	44.286°S, 169.916°E	67	August 2011-March 2012, March-June 2012, June-October 2012, October 2012-February, 2013, February-May 2013
Core 6m1b (5 m)	44.284°S, 169.915°E	68	October 2012
Core GCS_1 (0.3 m)	44.284°S, 169.913°E	68	May 2013

Sediment thicknesses measured in each trap were converted to a lake bottom equivalent accumulation rate (mm month^{-1}) by correcting recorded linear sedimentation for collector area using the following relation:

$$\text{Accumulation rate (mm month}^{-1}\text{)} = X = \left(\frac{S}{C}\right) / \left(\frac{A_r}{A_i}\right) \quad (1)$$

where: A_r is the cross-sectional area of the receiver (cm^2); A_i is the area of the trap mouth (cm^2); S is the thickness of accumulation in the receiver (mm); and C is the collection period (months).

This conversion enables a direct comparison between traps with different collector diameters and with accumulation measured in the sediment cores over the same period. All monthly lake floor accumulation rates were multiplied by the number of months over which the sediment trap was deployed to calculate a total accumulation rate for each deployment period. Subsamples from the sediment traps were analyzed for particle size distribution. All samples were soaked in 27% H_2O_2 for 24 hours to remove the organic component (3.2% based on Loss on Ignition (LOI); $n = 20$). Samples were rinsed with distilled water, treated with sodium hexametaphosphate (Calgon) to disperse sediment particles, sonicated for 30 min, and then continuously sonicated during analysis on a Beckman Coulter LS 13 320 laser diffraction particle size analyzer (Beckman Coulter, Inc., Brea, CA, USA). Replicates and blanks accounted for 10% of the samples run. Data were processed using Gradistat software (Blott & Pye, 2001).

2.2.5 Sediment Cores

A gravity corer was used to collect short (ca 0.3 m) sediment cores near the Inflow and Outflow sites (Table 1). Downward velocity of the corer was limited to ca 0.2 m s^{-1} using a boat-mounted winch to preserve the sediment–water interface. An Outflow core (GCS_1) was collected in May 2013. Several short (1 to 3 m) and long (5.5 m; OH6m1 and OH6m1b) sediment cores were collected near the Outflow using a Mackereth coring system in October 2012 (Fig. 1; Table 1; Mackereth, 1958). Line scan images of these cores were collected using a Geotek multi-sensor core logger (Geotek Limited, Northamptonshire, UK) at the University of Otago. Short gravity cores were split and photographed using a Lumix 10.1 Megapixel DMC LX5 camera

(Panasonic, Osaka, Japan). Thin-sections of a 5.5 m core (OH6m1) were produced following Lamoureux (1994) and scanned on a flatbed scanner at 2400 dpi.

2.3 RESULTS

2.3.1 Hydrometeorology

Limnological and meteorological data collected through the study period are summarized in Figs 2 and 3. In this paper ‘winter’ is defined as the six-month period from 1 March to 31 August and ‘summer’ is the period from 1 September to 28 February.

Average Killin Barn air temperature records show large seasonal and diurnal variability, consistent with the intermontane setting (Table 2; Fig. 2B). Highest wind speeds occur during the day in summer (Fig. 2D). Strong wind events ($> 8.0 \text{ m s}^{-1}$, the top 1% of measured wind speeds) consistently originate from the north/north-east, as down-valley ‘foehn’ winds (Fig. 2E). Based on the lake fetch and wind speeds of ca 8.0 m s^{-1} , wind-driven turbulence will only directly affect the top of the water column above the thermocline (Appendix A). As a result, wind mixing may prevent settling of sediment from the surface waters, but is predicted not to cause resuspension of bottom sediments throughout a majority of the lake.

Precipitation data from Elcho Flats and Killin Barn (Fig. 2C) show a strong correspondence in timing, but highlight a pronounced north–south gradient in precipitation, away from the headwaters of the Ohau catchment. This gradient is thought to be a result of the westerly wind flow that impinges on the Southern Alps, causing orographic precipitation to the west of the main divide. Some ‘spill over’ precipitation associated with this process falls in the Mackenzie Basin to the east (e.g. Sinclair et al., 1997; Chater & Sturman, 1998; Kerr et al., 2011). Specifically, a 76% decrease in precipitation occurs across the 37 km between the stations over the monitoring period (Table 2C). Furthermore, there is a decrease in precipitation from summer to winter at each site (46% at Elcho Flats and 29% at Killin Barn). This seasonal drop is higher than the long-term average measured at Elcho Hut (1994 to present), which indicates an average 20% seasonal decrease in precipitation from summer to winter.

Average river discharge was $61 \text{ m}^3 \text{ s}^{-1}$ (Table 2) during winter 2012 with several precipitation-driven discharge events ranging from 180 to $315 \text{ m}^3 \text{ s}^{-1}$ (Fig. 2).

Average discharge increased to $105 \text{ m}^3 \text{ s}^{-1}$ in summer with peak discharge events in January. This pattern is similar to the long-term seasonal trend in the hydrological record from 1926 to present, where annual flow peaks in December or January. However, two anomalously large discharge events, or floods, of $1005 \text{ m}^3 \text{ s}^{-1}$ and $960 \text{ m}^3 \text{ s}^{-1}$ occurred on 4 and 10 January 2013, respectively (Fig. 2A). Similar large magnitude events have only occurred eight other times in the last 87 years.

Table 2 Seasonal means of the hydrometeorological conditions measured in the Lake Ohau catchment from March 2012 to May 2013.

Variable	Winter (MAMJJA)	Summer (SONDJF)
Air Temperature	6.2°C	14.3°C
Elcho Flat Precipitation	1537.0 mm	2836.5 mm
Killin Precipitation	443.6 mm	624.4 mm
Wind Speed	1.79 m s^{-1}	3.00 m s^{-1}
Wind Direction	336°	354°
Inflow	61 $\text{m}^3 \text{ s}^{-1}$	105 $\text{m}^3 \text{ s}^{-1}$

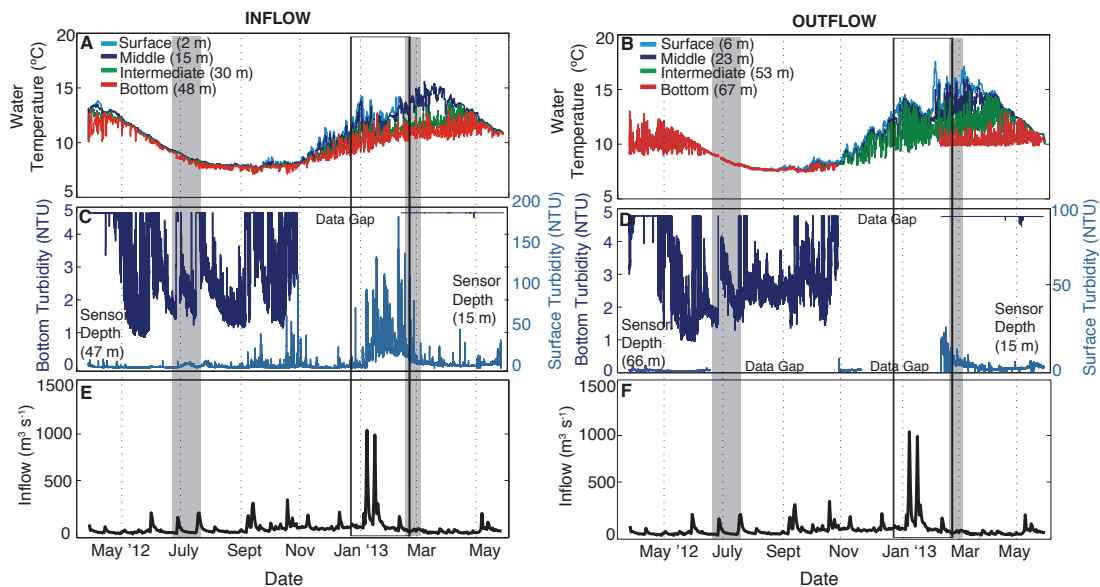


Fig. 3. Limnological conditions at the Inflow and Outflow from March 2012 to May 2013: (A) Inflow weekly mean water temperature; (B) Outflow weekly mean water temperature; (C) Inflow surface and bottom turbidity (10 min interval); (D) Outflow surface and bottom turbidity; (E) and (F) Lake Ohau mean daily inflow. Temperature data were smoothed to provide clarity. Shading indicates the period defined as winter. Black boxes indicate the periods highlighted in Figs. 4 to 6.

2.3.2 Physical Limnology

Lake Ohau is isothermal from May through to September, with a minimum water column temperature of ca 8.0°C (Fig. 3A and B). Temperature variability throughout winter is generally within the range of the sensor resolution (0.2°C) with occasional ca 0.5°C excursions evident in Inflow bottom water temperature (Fig. 4A). Intermediate and surface water temperatures at both sites remained relatively constant throughout the winter (Fig. 4A and B). Based on analysis of two of the winter events, the offset in time between the initial intrusion of cold bottom water at the Inflow and its arrival at the Outflow indicates that plumes can travel 13 km in approximately 24 hours (Fig. 4). During summer the lake is thermally stratified, with a thermocline developing around ca 20 m, although overturning occurs on several occasions (Fig. 5A and B; Table 3; Appendix A). Both sites record large fluctuations of up to 5°C throughout the water column, although the magnitude of these fluctuations is greatest at mid-depths at the Outflow (Fig. 5B).

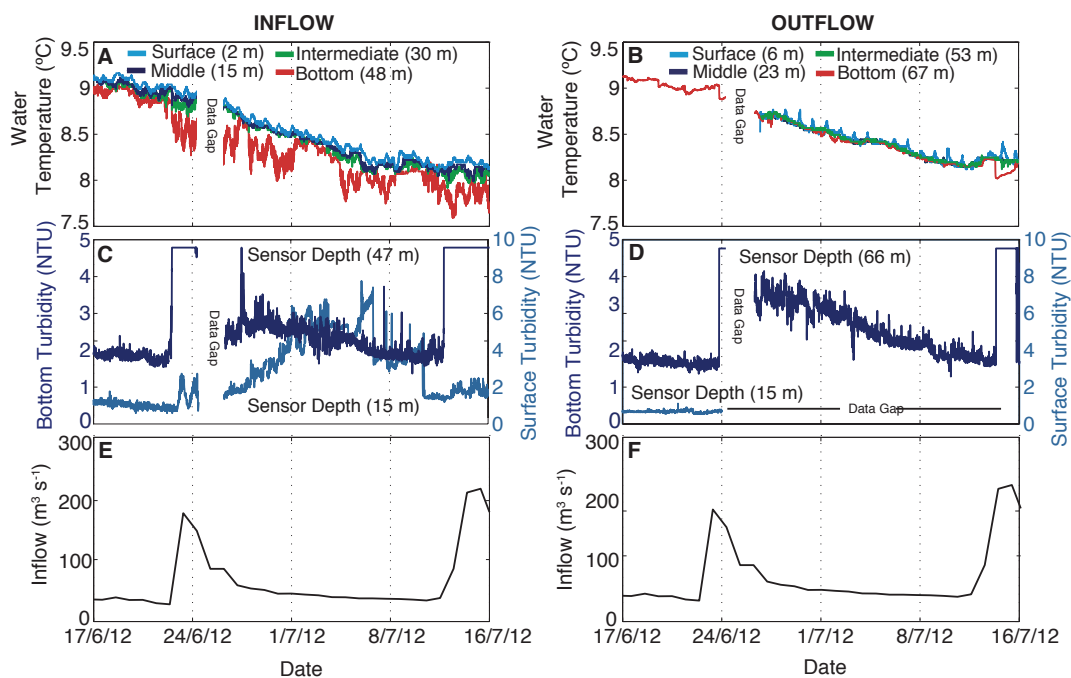


Fig. 4: Inset of background limnological and hydrological at the Inflow and Outflow during winter and winter event flow conditions throughout Lake Ohau: (A) Inflow 10 min water temperature; (B) Outflow 10 min water temperature; (C) Inflow surface and bottom turbidity; (D) Outflow surface and bottom turbidity (10 min interval); (E) and (F) Lake Ohau mean daily inflow.

The two unusually large discharge events in early January 2013 correspond with a lowering of water temperature throughout the water column (Fig. 6A and B).

The largest magnitude decrease (up to 3.5°C) occurs at middle and intermediate depths at the Outflow (Fig. 6). Water temperatures remain depressed, despite increases in air temperature, for approximately three weeks after the second event (10 January 2013) before returning to average summer values throughout the water column. During these large inflows, diurnal fluctuations in surface water temperature persist throughout the water column at both sites (Fig. 6A and B). However, immediately following each discharge event, large magnitude (ca 3.5°C) temperature variations are recorded at surface depths at the Inflow and mid-water depths at the Outflow, a feature that is not observed elsewhere in the record (Fig. 6A and B).

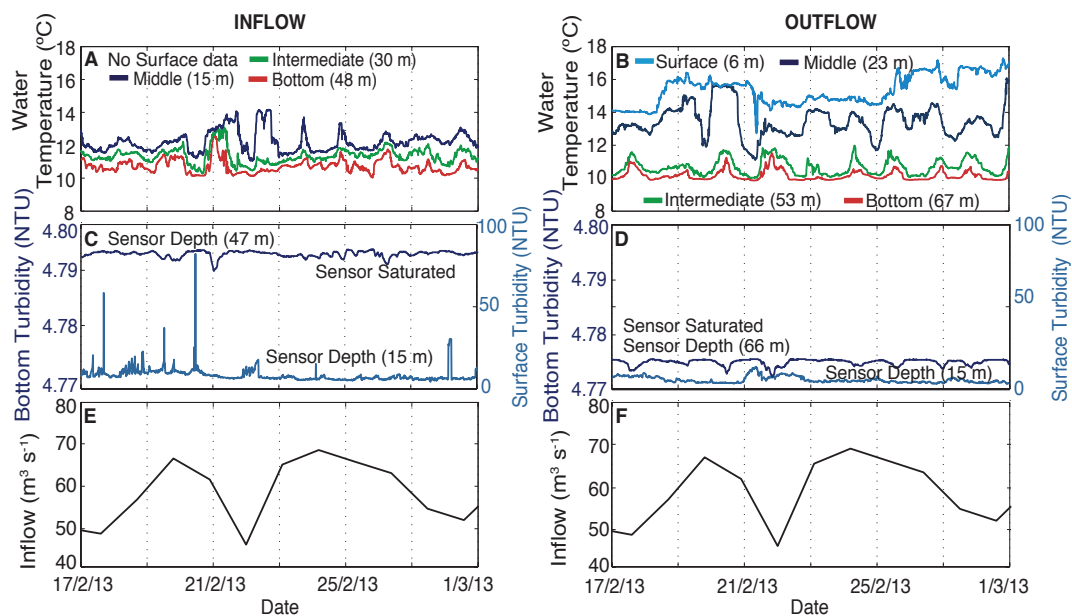


Fig. 5: Inset of background limnological and hydrological summer conditions at the Inflow and Outflow: (A) Inflow 10 min water temperature; (B) Outflow 10 min water temperature; (C) Inflow surface and bottom turbidity (10 min interval); (D) Outflow surface and bottom turbidity; (E, F) Lake Ohau mean daily inflow.

Turbidity

Measurements from optical backscatter (OBS) instruments deployed in this study indicate that both surface and bottom water turbidity is higher in the summer than in winter (Fig. 3B and C). During winter, bottom water turbidity across the depth profile is less than 4 NTU throughout the lake, with background levels around 1 NTU (Fig. 4B and C; Table 3). Following discharge events, bottom water turbidity at both sites exceeds 5 NTU (sensor maximum). These increases in turbidity are inversely correlated with bottom water temperature. Two weeks after these winter discharge

events, bottom water turbidity at the Inflow site returns to background (1-2 NTU). Inflow surface water turbidity increases to ca 6 NTU coincidental with peak discharge, followed by persistently elevated turbidity that does not return to background (ca 1 NTU) before the next increase in discharge 19 days later (Fig. 4D and F). Bottom water turbidity at the Outflow remains elevated above background during the three-week period between discharge events (Fig. 4D and F), while Outflow surface water turbidity shows no strong response to these winter flood events (Fig. 4D).

Summer is characterized by high bottom and surface turbidity (> 4 NTU, up to 90 NTU at the surface) throughout the lake (Fig. 3C and D). Bottom water turbidity consistently exceeds the maximum limit of the MAPRs (5 NTU) at both sites, with sensor saturation persisting throughout the entire summer period. Inflow surface water turbidity ranges from 5 to 90 NTU. High readings coincide with peak discharge and maximum values occur during flood events (Fig. 3C and E). Decreases in Inflow water temperature throughout the water column correspond well with increases in turbidity (Figs 5 and 6). At the Outflow, episodes of high turbidity coincide with decreases in temperature, which are limited to the intermediate and surface portions of the water column (Fig. 5A and B).

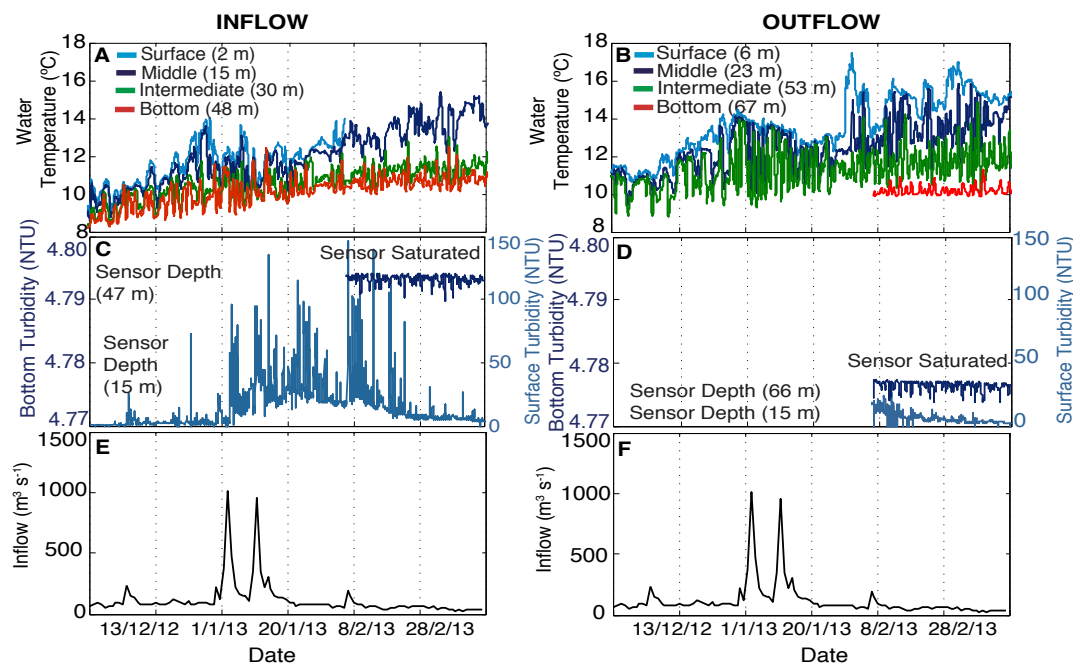


Fig. 6: Inset of background limnological and hydrological at the Inflow and Outflow during summer event flow conditions on 4 and 10 January 2013: (A) Inflow 10 min water temperature; (B) Outflow 10 min water temperature; (C) Inflow surface and bottom turbidity (10 min interval); (D) Outflow surface and bottom turbidity; (E) and (F) Lake Ohau mean daily inflow.

During summer, there is a 90% decrease in turbidity between the Inflow and Outflow (Fig. 5). Following the anomalous January increases in discharge, surface turbidity remains persistently high into mid-February, well after flows return to seasonal background (Fig. 6C and D). No Inflow bottom turbidity data are available until after the summer flood period due to equipment malfunction. The post-event data indicate bottom water saturation (> 5 NTU) at the Inflow. Similarly, Outflow turbidity data are not available until 5 February 2013, at which point turbidity is elevated in the surface and bottom waters (Fig. 6D). Observations made during a site visit on 5 February 2013 qualitatively confirmed turbid surface water conditions across the lake. Further, when the monitoring equipment was repaired in late February, turbidity was high with a slow decline to low turbidity (1 to 2 NTU) values in early March (Fig. 3D).

Table 3 Seasonal means of limnological and sedimentological data collected from March 2013 to May 2013. Accumulation and grain size data are derived from the sediment traps. Winter events are $Q = > 180 \text{ m}^3 \text{ s}^{-1}$; summer flood events are $Q = > 900 \text{ m}^3 \text{ s}^{-1}$.

INFLOW	Winter	Winter Event	Summer	Summer Event
Mean Surface Water Temp	8.3°C	8.3°C	11.6°C	12.5°C
Mean Bottom Water Temp	7.9°C	7.6°C	10.6°C	12.2°C
Mean Surface Turbidity	3 NTU	8.0 NTU	8.4 NTU	31.9 NTU
Mean Bottom Turbidity	1.2 NTU	>5 NTU	>5 NTU	n/a
Total Bottom Accumulation (l.b.e.)	74 mm	n/a	107.9 mm	102.0 mm
Primary Modal Grain Size	6.5 μm	45.8 μm	16.4 μm	41.7 μm
OUTFLOW	Winter	Winter Event	Summer	Summer Event
Surface Water Temp	8.0°C	7.8°C	11.1 °C	12.4°C
Bottom Water Temp	7.9°C	7.4°C	10.4 °C	10.5°C
Surface Turbidity	1.2 NTU	n/a	n/a	n/a
Bottom Turbidity	1.8 NTU	>5 NTU	>5 NTU	n/a
Bottom Accumulation (l.b.e)	1.57 mm	n/a	9.8 mm	4.8 mm
Primary Modal Grain Size	5.9 μm	6.5 μm	9.6 μm	10.2 μm

2.3.3 Sedimentation

Bulk sediment accumulation

Total bulk seasonal sediment accumulation, recorded at four different levels in the water column at the Inflow and Outflow sites, is summarized in Fig. 7. Accumulation at both sites is predominately allochthonous in nature, with only a small contribution of autochthonous material. Diatoms are present in the bulk sediment matrix but never in high enough proportions to form distinctive biogenic laminae. Total annual accumulation in the bottom traps is five times greater at the Inflow than at the Outflow. There is also a large seasonal difference in the accumulation pattern at the two monitoring sites: bottom trap sediment accumulation at the Inflow was 20 times greater than at the Outflow in winter and 10 times greater during summer (Fig. 7). Sediment accumulation decreases from summer to winter by 44% and 90% at the Inflow and Outflow, respectively. At both sites, sediment accumulation increases with water depth, particularly in winter. In contrast, summer Inflow accumulation is similar in the bottom two traps, representing the bottom 31 m of the water column (Fig. 7).

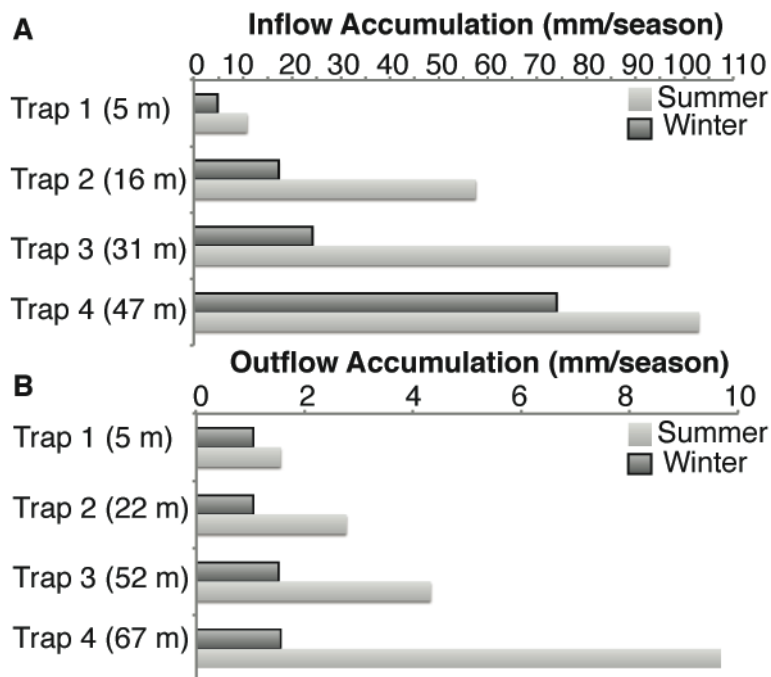


Fig. 7: Total seasonal lake bottom accumulation at the (A) Inflow and (B) Outflow. Accumulation at both sites increases in the summer. During winter, accumulation is proportional to water depth at both sites, while the summer is characterized by greater similarity in the bottom two traps at the Inflow, a result of changes in the sediment flux and dominant dispersal mechanisms.

Grain size and stratigraphy

A stratigraphic compilation of sediments captured in traps located near the lake floor at the Inflow and Outflow sites is presented in Fig. 8. Particle size is reported as the modal value, unless otherwise stated. Massive light and dark grey layers characterize winter stratigraphy at the Inflow (Fig. 8A). Dark grey winter layers are poorly sorted bimodal coarse silt (46 μm) and fine sand (86 μm), and light grey layers are fine silt (7 μm). Inflow winter surface sediment is fine silt (6 μm). Summer sedimentation at the Inflow includes two massive dark grey layers of poorly sorted medium silt (20 μm) to very fine sand (40 μm). A second coarse layer is preserved in all four traps, but is significantly coarser in the intermediate trap (169 μm) compared to 35 to 67 μm in the other traps. Subsequent particle size, representing post-event accumulation during the summer, is consistently coarse silt (16 μm) in all traps. Winter stratigraphy at the Outflow is characterized by massive grey and brown well-sorted fine silt (6 μm ; Fig. 8B). An initial 'coarse' layer (13 μm), overlain by fine silts (7 μm) defines spring/early summer accumulation. A second 'coarse' layer (10 μm) occurs in the middle of the October to February trap deployment and is overlain by more fine silt (Fig. 8B), representing the remainder of summer sediment accumulation.

2.3.4 Sediment Cores

The uppermost layers in sediment cores recovered from the Outflow site in October 2012 (OH6m1b) and May 2013 (GCS_1) directly record the progressive accumulation of sediment on the lake floor over part of the monitoring period. Correlation between the two cores indicates that 9 mm of sediment accumulated on the lake bottom between October 2012 and May 2013 (Fig. 9A). This result is consistent with 8.3 mm of lake bottom accumulation estimated from the sediment traps for the same period, indicating that the sediment traps used here have high trapping efficiency (ca 89%), and are representative of lake floor accumulation. Furthermore, down-core grain-size data show the same trends in modal size to those derived from the sediment trap analyses, providing further constraint on the timing of sediment deposition in the core (Fig. 9B). This pattern is clearly illustrated in the top 17 mm of core GCS_1, which preserves two dark coarse layers, similar to those documented in bottom sediment traps at the Outflow (Fig. 9B). We note that correlation between cores collected at the Inflow and Outflow is not straightforward

due to differences in the number of layers that accumulate at each site during corresponding time intervals, and an inherent difficulty in identifying the start and end of an annual cycle.

2.4 DISCUSSION

Seasonality in precipitation and corresponding river discharge is evident in the Lake Ohau watershed (see section 2.3.1). Although there are no data for the fluvial suspended sediment yield into Lake Ohau, the climatological setting and lithology of the Lake Ohau catchment is similar to that of other South Island river systems, which show a strong correlation between suspended sediment yield and precipitation ($r^2 = 0.71$; Hicks et al., 2011). Water column turbidity and seasonal sediment trap accumulation data indicate that suspended sediment influx to Lake Ohau is also correlated to catchment rainfall, because the greatest influx of sediment to the lake also occurs in the summer (Fig. 7). The relation between catchment precipitation and lake sedimentation is modified by lake hydrology. The relative difference in density between inflowing river water and lake water determines whether suspended sediment travels primarily as overflows, interflows or underflows and, thus, how widely it is dispersed within the lake (see also Carmack et al., 1979; Weirich, 1986; Sturm & Matter, 1978).

In winter, the relatively cold and dense inflow water is more likely to travel along the lakebed as turbid underflows. In summer, the relatively warmer inflowing water and highly thermally stratified lake means that inflows are more likely to be dispersed as interflows or overflows. This process results in seasonal variations in accumulation and particle size at the Outflow due to the change in the dominant sediment flow pathways. Furthermore, these differing processes allow for a demarcation between winter and summer layers at the Outflow, and an interpretation of the distinct light/dark laminations preserved at the Outflow as varves. The anomalous January 2013 floods provided an opportunity to observe the deposition mechanisms in the lake during flood conditions.

2.4.1 Winter 'Inflow' and 'Outflow' Conditions

Cumulative accumulation in the sediment traps at the Inflow during winter includes dark layers of relatively thick, coarse (46 μm) sediment that probably formed by rapid

deposition from turbidity currents during winter flow events and fine-grained (7 μm) light grey layers forming by slow suspension settling during lower/background flow conditions. Relatively low wind speeds through winter enhance settling from suspension, because turbulent mixing through the water column is limited during this period. Lake temperature profiles at the Inflow show that most variability in the winter occurs near the bed.

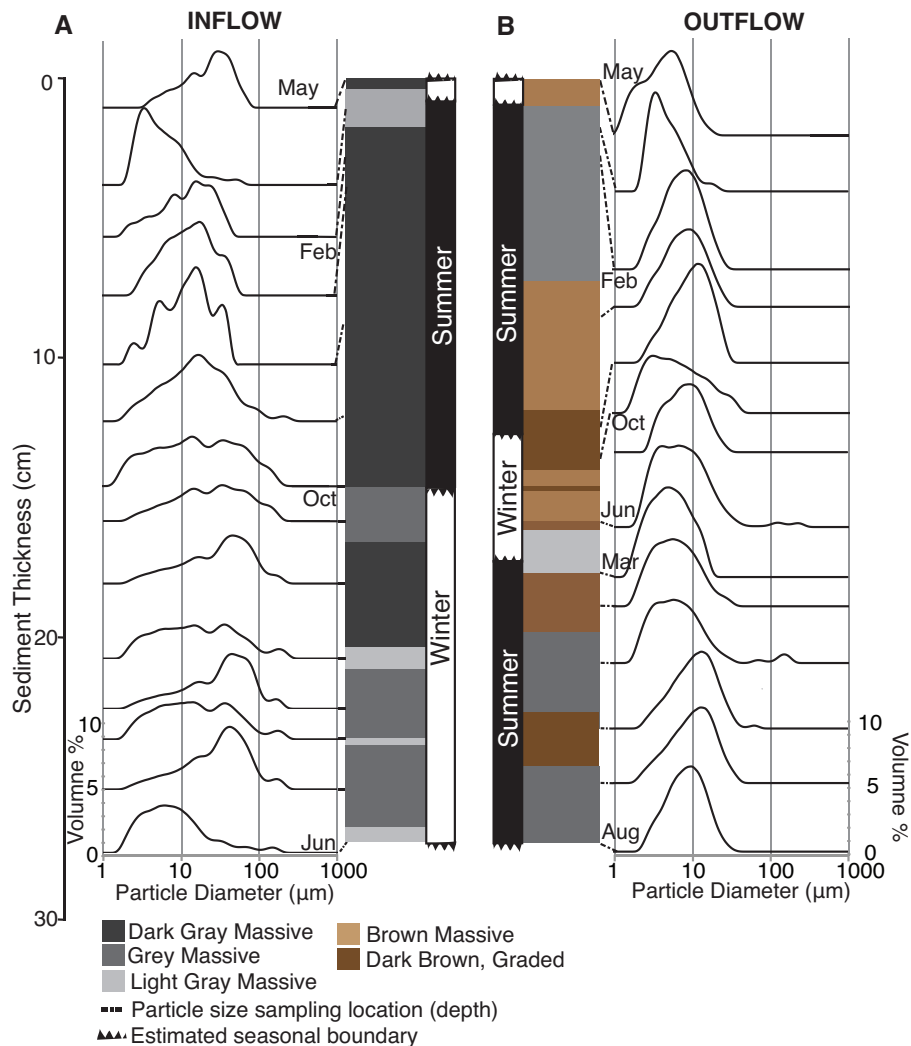


Fig. 8: Composite stratigraphic diagram and particle size measured in the lake bottom sediment traps at the (A) Inflow and (B) Outflow show that, in general, the light and dark layering are associated with fine and coarse accumulation, respectively. The Inflow preserves an event-based stratigraphy with coarse/fine accumulation occurring throughout the annual cycle. At the Outflow, coarse grain sizes correspond with initial deposition in the summer with fine accumulation isolated to the late summer and winter periods. Accumulation is based on the total measured thickness (cm) of bottom trap sediment at each site. Grain size curves are tied to relevant depths and are plotted as volume percent (same scale throughout). Months are listed where the top and bottom accumulation was constrained by sample collection and redeployment. Note that accumulation was measured from June 2012 to May 2013 at the Inflow and from August 2011 to May 2013 at the Outflow.

Cold winter night air temperatures cause incoming water temperatures to be colder, and therefore denser, than the lake water. These cold inflows probably account for a majority of the quasi-diurnal temperature fluctuations measured at the deepest sensors.

The authors therefore interpret these repeating temperature departures at the bed as caused by underflows. Furthermore, enhanced accumulation in the bottom sediment traps at both sites points to the predominance of sediment-laden underflows during winter. It is important to note that trap accumulation probably represents a minimum when underflows dominate, because the traps are designed for vertical deposition and are likely to under-trap during strong underflows when the sediment plumes have a significant lateral component (Cockburn & Lamoureux, 2008b). The absence of coarse silt and sand accumulation at the Outflow during winter indicates that only fine silt is transported to the distal basin during winter events. Sandy material deposited in bottom traps at the Inflow during these events accumulates on the delta front and along the downslope axis of the lake, but does not travel into the shallower eastern arm of the basin. This suggests that only the fine fraction of the sediment load carried by the cold turbid underflows originating at the delta propagates upslope to the Outflow in winter (e.g. Chikita et al., 1996; Gilbert et al., 2006). Indeed, evidence for this process is seen in changes in river inflow temperature that begin predominantly as interflows and overflows at the Inflow but are detected by subtle changes in bottom water turbidity about 24 hours later at the Outflow (Fig. 4). Slight variations in surface water turbidity coincident with the arrival of these turbid underflows may be the result of some of the suspension plume penetrating to the surface waters, a situation similar to that documented by Fischer & Smith (1983).

The presence of very fine silt ($6\ \mu\text{m}$), with a settling velocity of $0.025\ \text{mm s}^{-1}$ (Gibbs et al., 1971), helps to explain the persistence of turbid bottom water at the Outflow following event flow and supports the interpretation of slow suspension settling as the driver of deposition during the winter. The lack of variability in the temperature with depth at the Outflow, combined with low sediment accumulation, implies a strong horizontal gradient in winter deposition in Lake Ohau.

2.4.2 Summer ‘Inflow’ and ‘Outflow’ Conditions

Inflow accumulation during summer in the sediment traps shows thicker, coarser (42

μm) dark layers which probably form by rapid deposition of coarse particles during episodic event flows, while finer ($16 \mu\text{m}$) lighter layers form by suspension settling during lower flow conditions (Fig. 8A). While the fine fraction is coarser during the summer, the coarse fraction remains similar to that of winter (Fig. 8A). The Inflow site continues to preserve a complex coarse/fine stratigraphy similar to that of the winter period, while a more pronounced seasonal shift in grain size and accumulation occurs at the Outflow (Fig. 8).

The summer temperature profile at the Inflow shows significant diurnal temperature variability throughout the water column, with the lowest amplitude changes near the bed and the greatest at mid to upper water depths. This suggests that inflowing river water is propagating through the lake primarily in the surface waters (top ca 20 m) as overflows, with internal waves and wind stress likely helping to keep the top waters mixed and sediment in suspension. Elevated surface turbidity data support this interpretation, while high bottom water turbidity shows that the bottom waters remain turbid during the whole summer period (Fig. 3C). Turbid bottom waters probably occur in response to both settling of particles from the upper portions of the water column and occasional turbidity currents that enter the lake as underflows, when the incoming river water temperature is lower, and has a corresponding higher density, than that of the bottom waters.

In contrast to the winter months, transport of sediment-laden water to the Outflow is primarily by interflows and overflows during the summer months due to the relatively lower density of inflowing river water and the well developed thermocline (e.g. Bloesch & Uehlinger, 1986). The predominance of interflows and overflows in Lake Ohau is evident in the greatly enhanced accumulation of sediment in the traps at the Outflow during summer relative to winter. At the Outflow there are rapid changes in temperature throughout the water column, most pronounced in the mid and upper levels, which also implies the passage of sediment-laden water by internal waves (Mortimer, 1953). The sediment trap stratigraphy shows an initial change in particle size from 6 to $10 \mu\text{m}$ occurring around early October, probably coincident with increased discharge and lake stratification associated with the onset of the summer period. This initial deposit of dark coloured coarse material is interpreted as the nival pulse signature. The first pulse of coarse sediment following fine deposition is often associated with this seasonal increase in discharge from snowmelt, and hence suspended sediment, carrying coarser material throughout the lake system

due to its higher energy and the developing lake stratification (Desloges & Gilbert, 1994; Lewis et al., 2002). Particle sizes fine slightly (to ca 7 μm) following this initial pulse, but coarsen again in response to an abrupt, massive influx of turbid water during the large January flood events. These events created the second dark coarse layer, and contributed a large portion of the light coloured, fine material that accumulated during the remainder of the summer. These layers are clearly preserved in the sediment cores (Fig. 9B).

Most sediment, therefore, enters the lake in the summer due to enhanced summer rainfall and discharge. Suspended sediment is also more widely dispersed, leading to a nearly three-fold increase in accumulation at the Outflow compared to the winter period (Fig. 7B). Following large summer discharge events, the finer particles transported during these events progressively settle during reduced flow periods, resulting in a depositional pattern similar to those documented at other montane sites (Gilbert, 1975; Desloges & Gilbert, 1994).

2.4.3 Flood Conditions

Two large floods events in excess of $950 \text{ m}^3 \text{ s}^{-1}$ occurred in January 2013. This large input of sediment-laden water perturbed the lake system in a manner not observed during lower summer flow conditions. At the Inflow, immediately following the first event, the water column became destratified in temperature and displayed a rapid increase in surface and bottom water turbidity (Figs 3A and 6A). This pattern was repeated during the second event, after which the turbidity throughout the water column remained elevated above pre-flood levels into March 2013.

At the Outflow, flood events appeared as a marked decreases in surface water temperature (Figs 3B and 6B), related to large overflow transport of cooler inflowing water that persisted until 28 January. However, the limited turbidity data (which begin on 5 February) suggest that consistently high turbidity also persisted throughout the water column until March 2013. These floods deposited a second coarse layer (10 μm) at the Outflow. The deposition of multiple coarse dark layers within a single varve indicates the potential for the generation of complex stratigraphy during the summer months. These floods also input anomalously large amounts of material into the system, similar to lacustrine deposition documented during large flood events in other montane settings (Gilbert et al., 2006). For example, the two January events

contributed approximately 95% of the summer sediment deposition at the Inflow and 51% of total summer accumulation at the Outflow. Post-event deposition preserved in the gravity core at the Outflow is marked by a thick, 7 mm light layer with a mean grain size of 6 μm .

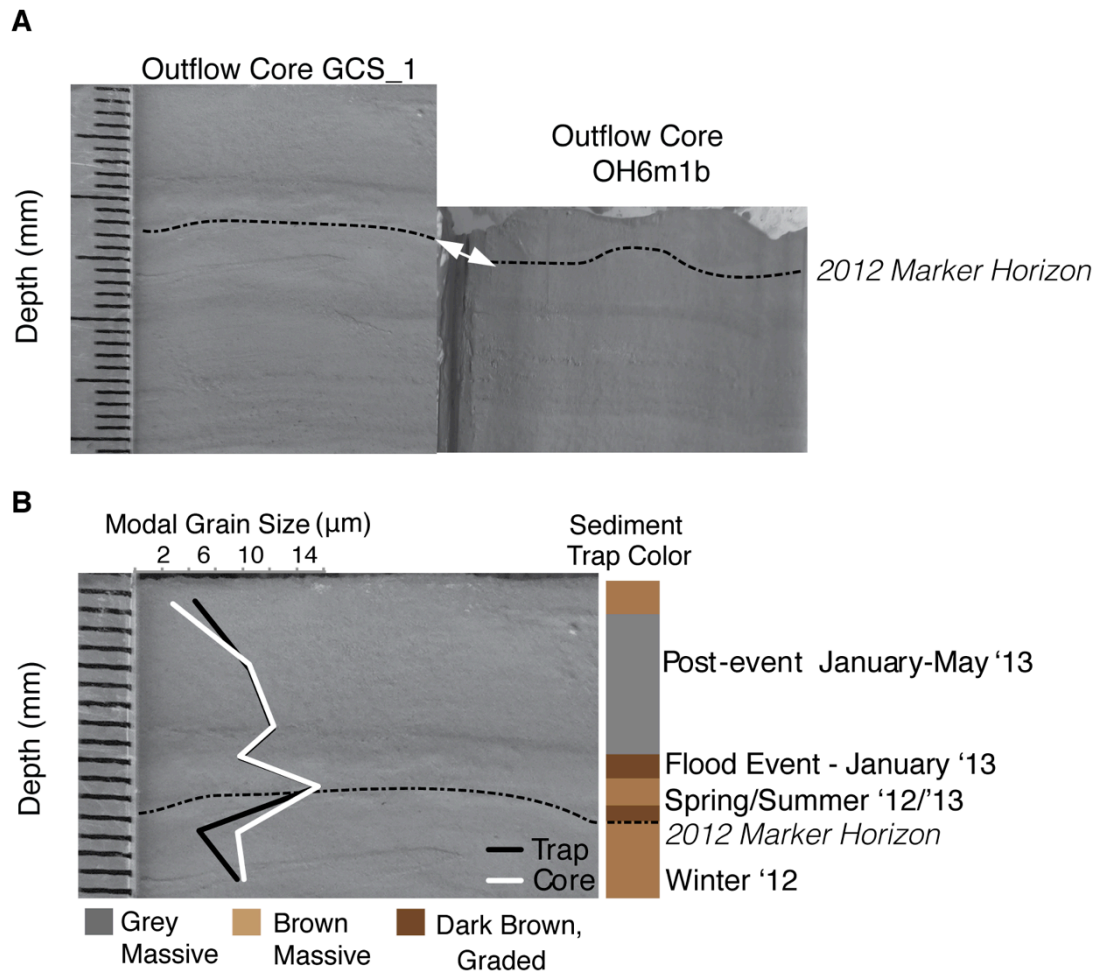


Fig. 9: (A) Comparison between surface sediments in cores GCS_1 (collected May 2013) and OH6m1b (collected October 2012). A light band near the top of OH6m1b is interpreted as the end of winter layer and is referred to here as the 2012 marker horizon, as can be seen clearly in GCS_1. (B) A comparison of colour and grain sizes measured in the May 2013 gravity core and the Outflow bottom sediment trap. Sediment trap grain sizes are the modal grain size measured in the same stratigraphic layers and then plotted on the same depth scale as the samples measured in the core. Sediment trap stratigraphy is based on visual colour for layers greater than 1.5 mm. There is close correlation of both grain size and colour between the sediment cores and sediment traps.

2.4.4 Characteristics of the Longer Sediment Sequence

To place these observations in context with the longer record and to see if there is a recognizable seasonal stratigraphy preserved in lake bottom sediments, a thin-section

scan from core OH6m1 was examined. The summer (coarse) and winter (fine) layers were identified visually using grain size or light/dark colouration (Fig. 10). This image preserves approximately nine couplets and contains both complex and simple varves (Fig. 10). At the 17.5 cm core depth, a coarse (14 lm) layer may be a similar flood event to that monitored in 2013, given the grain-size fraction and relative thickness of the couplet (7.0 mm). Micro-laminations or complex stratigraphy are widely documented in varved sediments (Desloges & Gilbert, 1994; Hambley & Lamoureux, 2006; Chutko & Lamoureux, 2008), and have been used to develop robust palaeoclimate reconstructions. These complexities in Lake Ohau may be derived from unseasonal high-magnitude flow events, similar to those observed in the present study, or other disturbances in the catchment and lake system (e.g. earthquakes). Ongoing work with radiometric isotopes (^{210}Pb , ^{137}Cs and ^{14}C) and layer counting will help to place these observations in context with the past, to determine whether these modern-day mechanisms can be attributed to accumulation patterns further down-core. Furthermore, the complexities in this system highlight a key need for ongoing monitoring in order to better constrain the causes of the complex stratigraphy.

2.4.5 Primary Mechanisms of Varve Formation

In Lake Ohau the relatively lower precipitation in winter, paired with the inability for the coarse fraction of winter turbidity currents to travel to the distal Outflow result in the deposition of only fine-grained sediments, similar to that observed in lakes characterized by winter ice cover where deposition is limited to fine particles. In summer, increased discharge resulting from both snowmelt and increased precipitation generate a coarse layer, with deposition at the outflow aided by lake density stratification, which enables the propagation of warmer sediment laden water to penetrate the length of the lake as interflows and overflows. Simply, the coarsening of sediment in the summer produces dark layers, while the fine winter accumulation creates a light layer. Therefore, despite the differences between this temperate mid-latitude location and higher-latitude polar locations, the data herein show that the intrinsic processes remain the same as those more typical clastic varve depositional environments, where distinct seasonal changes in lake dynamics and hydrometeorology result in the formation of clastic varves.

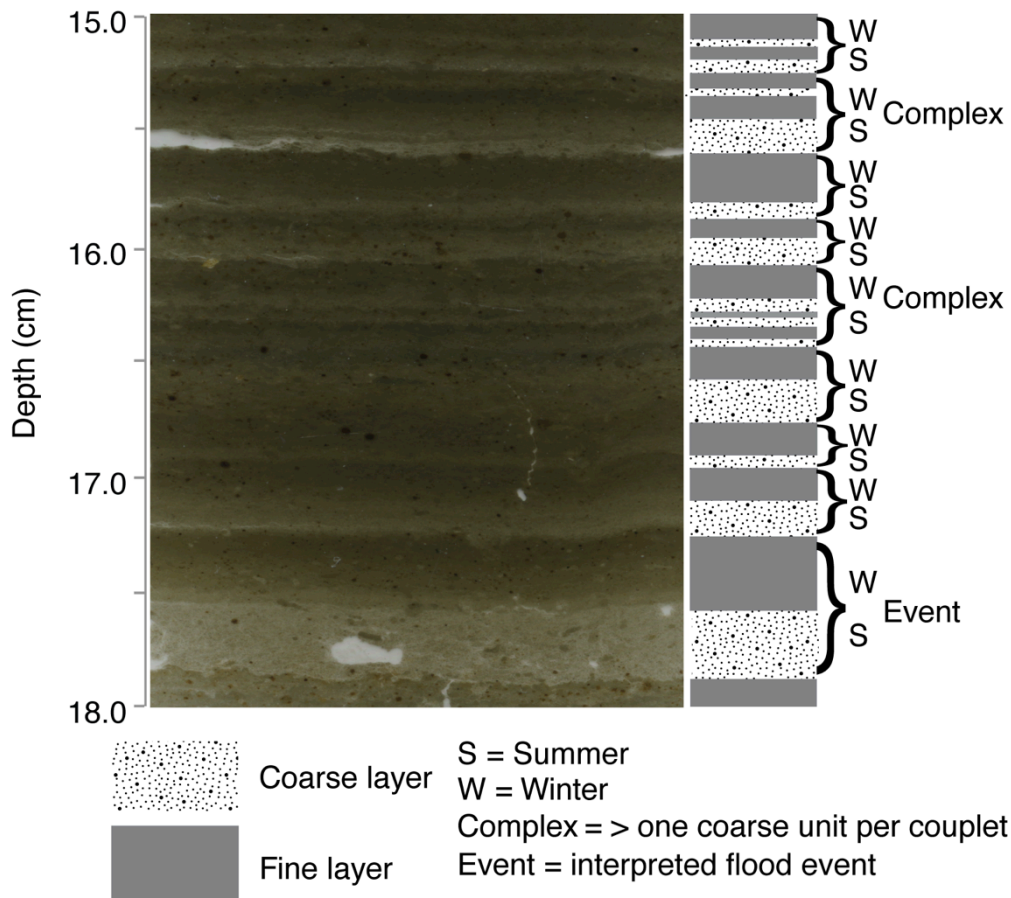


Fig. 10: Thin-section scan and corresponding stratigraphic column from a representative section of core OH6m1. Light layers in the thin section correspond to coarse layers, as more light penetrates through more porous layers during scanning. Summer and winter layers were defined based on visual estimation of the particle size in the thin section. Complex stratigraphy was similarly ascribed based on grain size and relative thickness of interbedded coarse laminae, yielding 9 years of accumulation between 15.0 and 18.0 cm.

2.5 CONCLUSIONS

Through detailed lake monitoring, this study demonstrates that the character and amount of sediment deposition in Lake Ohau is controlled by strong basin-wide seasonality in precipitation, river discharge and internal lake dynamics. This provides a mechanism for explaining the formation of the light and dark layers observed at the Outflow and further points to the Outflow as an ideal target site for the development of a high-resolution palaeoclimate record.

Large flood events observed in January 2013 caused a multi-week perturbation in temperature and turbidity throughout the lake environment, and significantly increased deposition throughout the lake. Future work will place these

events in context with the past and help to constrain and understand flood characteristics and frequency through comparison with other similar layers preserved at depth in the sediment cores. Ongoing lake monitoring will help to further develop current understanding of the complex processes occurring throughout Lake Ohau, particularly with the addition of instrument strings in the lake depocentre.

Ultimately, this study contributes a detailed framework for understanding seasonal sedimentation processes in Lake Ohau and provides important context for interpreting the longer Outflow sediment sequence. The temperate environment of southern New Zealand and the Lake Ohau catchment is suitable for preserving varves, thus providing the opportunity to develop a robust, high-resolution lacustrine palaeoclimate record from the Southern Hemisphere mid-latitudes.

2.6 ACKNOWLEDGEMENTS

The GNS Science Global Change through Time program, the Sarah Beanland Memorial Scholarship, and the ANZICE program (VICX0704), PMEL Contribution Number 4122, and the Eggers fund supported this work financially. We would like to thank Gary Wilson and the Marine Sciences Department, University of Otago for logistical support. Thank you to Sean Fitzsimons at the University of Otago and Jamie Howarth at GNS Science for their help with core collection and initial core characterization. Thank you to Geoff Schladow and Paul Stumpner at the University of California Davis and the United States Geological Survey and Remo Cossu at the University of Tasmania for their contribution to this work. The National Science Foundation East Asia and Pacific Summer Institute supported Paul Stumpner. We would also like to thank Peter Ridd at James Cook University for providing nephelometers and plentiful advice, the staff at Meridian Energy Ltd. For logistical support, Chris and Rae Spiers for their hospitality and large workspace at the Killin Barn, and the Inkersell family at Lake Ohau Station for land access and ongoing support. Thoughtful reviews by R. Gilbert and M. De Batist significantly improved this paper.

2.7 REFERENCES

- Anderton, P. (1973) The significance of perennial snow and ice to the water resources of the South Island, New Zealand. *Journal of Hydrology New Zealand*, 12, 6-18.
- Augustinus, P., D'costa, D., Deng, Y., Hagg, J. and Shane, P. (2011) A multi-proxy record of changing environments from ca. 30 000 to 9000 cal. a BP: Onepoto maar palaeolake, Auckland, New Zealand. *Journal of Quaternary Science*, 26, 389-401.
- Bloesch, J. and Uehlinger, U. (1986) Horizontal sedimentation differences in a eutrophic Swiss lake. *Limnology and Oceanography*, 31, 1094-1109.
- Blott, S.J. and Pye, K. (2001) GRADISTAT: a grain size distribution and statistics package for the analysis of unconsolidated sediments. *Earth Surface Processes and Landforms*, 26, 1237-1248.
- Bradley, R.S. (1999) Paleoclimatology: reconstructing climates of the Quaternary, Access Online via *Elsevier* 68, 1-613.
- CACR Wave Calculator (2014) University of Delaware. <http://www.coastal.udel.edu/faculty/rad/wavetheory.html>. Accessed 1st January 2014.
- Carmack, E.C., Gray, C.B., Pharo, C.H. and Daley, R.J. (1979) Importance of lake-river interaction on seasonal patterns in the general circulation of Kamloops Lake, British Columbia. *Limnology and Oceanography*, 634-644.
- Chater, A.M. and Sturman, A.P. (1998) Atmospheric conditions influencing the spillover of rainfall to lee of the Southern Alps, New Zealand. *International Journal of Climatology*, 18, 77-92.
- Chikita, K. A., Smith, N. D., Yonemitsu, N., & Perez-Arlucea, M. (1996) Dynamics of sediment-laden underflows passing over a subaqueous sill: glacier-fed Peyto Lake, Alberta, Canada. *Sedimentology*, 43(5), 865-875.
- Chutko, K.J. and Lamoureux, S.F. (2008) Identification of coherent links between interannual sedimentary structures and daily meteorological observations in Arctic proglacial lacustrine varves: potentials and limitations. *Canadian Journal of Earth Sciences*, 45, 1-13.
- Cockburn, J.M. and Lamoureux, S.F. (2008a) Hydroclimate controls over seasonal sediment yield in two adjacent High Arctic watersheds. *Hydrological Processes*, 22, 2013-2027.
- Cockburn, J.M. and Lamoureux, S.F. (2008b) Inflow and lake controls on short-term mass accumulation and sedimentary particle size in a High Arctic lake: implications for interpreting varved lacustrine sedimentary records. *Journal of Paleolimnology*, 40, 923-942.

Cox, S. and Barrel, D. (2007) Geology of the Aoraki area, Institute of Geological and Nuclear Sciences 1: 250000 Geological Map. *Lower Hutt, New Zealand (GNS Science)*, 71.

Desloges, J.R. and Gilbert, R. (1994) Sediment source and hydroclimatic inferences from glacial lake sediments: the postglacial sedimentary record of Lillooet Lake, British Columbia. *Journal of Hydrology*, 159, 375-393.

Fischer, H. B., & Smith, R. D. (1983). Observations of transport to surface waters from a plunging inflow to Lake Mead [Nevada]. *Limnology and Oceanography*, 28.

Francus, P., Bradley, R., Lewis, T., Abbott, M., Retelle, M. and Stoner, J. (2008) Limnological and sedimentary processes at Sawtooth Lake, Canadian High Arctic, and their influence on varve formation. *Journal of Paleolimnology*, 40, 963-985.

Gibbs, R.J., Matthews, M.D. and Link, D.A. (1971) The relationship between sphere size and settling velocity. *Journal of Sedimentary Research*, 41, 7-18.

Gilbert, R. (1975) Sedimentation in Lillooet Lake, British Columbia. *Canadian Journal of Earth Sciences*, 12, 1697-1711.

Gilbert, R. and Butler, R.D. (2004) The physical limnology and sedimentology of Meziadin Lake, northern British Columbia, Canada. *Arctic, Antarctic, and Alpine Research*, 36, 33-41.

Gilbert, R., Crookshanks, S., Hodder, K. R., Spagnol, J., & Stull, R. B. (2006). The record of an extreme flood in the sediments of montane Lillooet Lake, British Columbia: implications for paleoenvironmental assessment. *Journal of Paleolimnology*, 35(4), 737-745.

Graham, I. (2005) Sedimentology, Geochronology and Micropaleontology of Post- and Immediately Pre-European Lake Tekapo Sediment (Based on Analysis of Core L1395). *Institute of Geological & Nuclear Sciences*.

Hambley, G.W. and Lamoureux, S.F. (2006) Recent summer climate recorded in complex varved sediments, Nicolay Lake, Cornwall Island, Nunavut, Canada. *Journal of Paleolimnology*, 35, 629-640.

Hardy, D.R., Bradley, R.S. and Zolitschka, B. (1996) The climatic signal in varved sediments from Lake C2, northern Ellesmere Island, Canada. *Journal of Paleolimnology*, 16, 227-238.

Hicks, D.M., Shankar, U., McKerchar, A.I., Basher, L., Lynn, I., Page, M. and Jessen, M. (2011) Suspended sediment yields from New Zealand rivers. *Journal of Hydrology (New Zealand)*, 50, 81-142.

Hodder, K. R., & Gilbert, R. (2007). Evidence for flocculation in glacier-fed Lillooet Lake, British Columbia. *Water Research*, 41(12), 2748-2762.

Irwin, J. (1975) *Checklist of New Zealand lakes*. Department of Scientific and Industrial Research.

Kerr, T. (2013). The contribution of snowmelt to the rivers of the South Island, New Zealand. *Journal of Hydrology (New Zealand)*, 52(2), 61.

Kerr, T., Owens, I., and Henderson, R. (2011). The precipitation distribution in the Lake Pukaki catchment. *Journal of Hydrology (New Zealand)*, 50, 361-382.

Lamoureux, S.F. (1994) Embedding unfrozen lake sediments for thin section preparation. *Journal of Paleolimnology*, 10, 141-146.

Leemann, A. and Niessen, F. (1994) Varve formation and the climatic record in an Alpine proglacial lake: calibrating annually-laminated sediments against hydrological and meteorological data. *The Holocene*, 4, 1-8.

Lewis, T., Gilbert, R. and Lamoureux, S.F. (2002) Spatial and Temporal Changes in Sedimentary Processes at Proglacial Bear Lake, Devon Island, Nunavut, Canada. *Arctic, Antarctic, and Alpine Research*, 34, 119-129.

Mackereth, F.J.H. (1958). A portable core sampler for lake deposits. *Limnology and Oceanography*, 3(2), 181-191.

MacPherson, A. (1985) Mactrap 85. *Antarctic field report*. Victoria University of Wellington.

Macpherson, A.J. (1986) *Glaciological Oceanographic and Sedimentological Data from Mackay Glacier and Granite Harbour Antarctica*. Victoria University of Wellington.

Mildenhall, D., Cochran, U. and Cook, R. (2006) Reconnaissance sediment and microfossil analyses of a laminated short piston core from Lake Tekapo, South Island, New Zealand. *New Zealand Journal of Geology and Geophysics*, 49, 463-476.

Mortimer, C. H. (1953). The resonant response of stratified lakes to wind. *Aquatic Sciences-Research Across Boundaries*, 15(1), 94-151.

Ojala, A.E.K., Francus, P., Zolitschka, B., Besonen, M. and Lamoureux, S.F. (2012) Characteristics of sedimentary varve chronologies: A review. *Quaternary Science Reviews*, 43, 45-60.

Page, M., Trustrum, N., Orpin, A., Carter, L., Gomez, B., Cochran, U., Mildenhall, D., Rogers, K., Brackley, H. and Palmer, A. (2010) Storm frequency and magnitude in response to Holocene climate variability, Lake Tutira, North-Eastern New Zealand. *Marine Geology*, 270, 30-44.

Page, M.J., Trustrum, N.A. and DeRose, R.C. (1994) A high resolution record of storm-induced erosion from lake sediments, New Zealand. *Journal of Paleolimnology*, 11, 333-348.

- Pepper, A., Shulmeister, J., Nobes, D. and Augustinus, P. (2004) Possible ENSO signals prior to the Last Glacial Maximum, during the last deglaciation and the early Holocene, from New Zealand. *Geophysical Research Letters*, 31, L15206.
- Pickrill, R. and Irwin, J. (1983) Sedimentation in a deep glacie-fed lake, Lake Tekapo, New Zealand. *Sedimentology*, 30, 63-75.
- Putnam, A.E., Schaefer, J.M., Denton, G.H., Barrell, D.J., Birkel, S.D., Andersen, B.r.G., Kaplan, M.R., Finkel, R.C., Schwartz, R. and Doughty, A.M. (2013) The Last Glacial Maximum at 44°S documented by a ¹⁰Be moraine chronology at Lake Ohau, Southern Alps of New Zealand. *Quaternary Science Reviews*, 62, 114-141.
- Salinger, M. and Mullan, A. (1999) New Zealand climate: temperature and precipitation variations and their links with atmospheric circulation 1930-1994. *International Journal of Climatology*, 19, 1049-1071.
- Sinclair, M. R., Wratt, D. S., Henderson, R. D., and Gray, W. R. (1997) Factors affecting the distribution and spillover of precipitation in the Southern Alps of New Zealand-A case study, *Journal of Applied Meteorology*, 36, 428-442.
- Sturm, M. and Matter, A. (1978) Turbidites and Varves in Lake Brienz (Switzerland): Deposition of Clastic Detritus by Density Currents. In: *Modern and Ancient Lake Sediments*, pp. 147-168. Blackwell Publishing Ltd.
- Thomas, S.V. and Ridd, P.V. (2004) Review of methods to measure short time scale sediment accumulation. *Marine Geology*, 207, 95-114.
- Ummenhofer, C.C., Sen Gupta, A. and England, M.H. (2009) Causes of late twentieth-century trends in New Zealand precipitation. *Journal of Climate*, 22, 3-19.
- Weirich, F. (1986) The record of density-induced underflows in a glacial lake. *Sedimentology*, 33, 261-277.
- Woods, R., Hendricks, J., Henderson, R. and Tait, A. (2006) Estimating mean flow of New Zealand rivers. *Journal of Hydrology New Zealand*, 45, 95.
- Zolitschka, B. (2007) Varved lake sediments. *Encyclopedia of Quaternary Science*. Elsevier, Amsterdam, 3105-31.

CHAPTER 3

A hydroclimate-proxy model based on sedimentary facies in an annually laminated sequence from Lake Ohau, South Island, New Zealand

The content in Chapter 3 is published in the *Journal of Paleolimnology*.

CITATION

Roop, H.A., Levy, R., Dunbar, G.B., Vandergoes, M.J., Howarth, J., Fitzsimons, S., Moon, H.S., Zammit, C., Ditchburn, R., Baisden, T., Yoon, H.I, in review. A hydroclimate-proxy model based on sedimentary facies in an annually laminated sequence from Lake Ohau, South Island, New Zealand. *Journal of Paleolimnology*. DOI :10.1007/s10933-015-9853-3.

Authorship contributions to this research article include the following:

Heidi A. Roop - Wrote manuscript and managed all co-author feedback, conducted all data compilation, developed initial interpretations and outline of statistical tests, and developed all figures.

Richard Levy - Academic Supervisor; provided feedback on manuscript drafts and aided in the interpretation of the results.

Gavin Dunbar - Academic Supervisor; provided feedback on draft manuscript.

Marcus J. Vandergoes - Academic Supervisor; provided feedback on drafts and helped with radiometric dating.

Jamie Howarth - Provided comment on draft version of manuscript, helped with age-modeling, core collection and scanning; ongoing Lake Ohau project collaborator.

Sean Fitzsimons - Ongoing Lake Ohau project collaborator who helped to guide initial discussions about geomorphology and catchment controls on sedimentation and provided core material.

Heung Soo Moon - Sampled core and ran ITRAX scanner on core slabs to generate X-rays and the greyscale curve used for layer counting.

Christian Zammit - Provided editorial comments on a draft of the paper related to hydrologic interpretations and provided Topnet model data; ongoing Lake Ohau project collaborator.

Robert Ditchburn - Conducted all lab analyses for ^{210}Pb and ^{137}Cs radiometric dating.

Troy Baisden - Helped with ^{210}Pb age model development and provided comment related to the age model on a draft of this manuscript; ongoing Lake Ohau project collaborator.

Ho Il Yoon - Reviewed draft of manuscript and provided access to ITRAX scanner and equipment at the Korean Polar Research Institute; ongoing Lake Ohau project collaborator.

ABSTRACT

Annually laminated sediments collected from Lake Ohau, New Zealand offers a opportunity to generate a high-resolution paleoclimate record for the Southern Hemisphere mid-latitudes. Correlation between regional precipitation and synoptic climate indices like the Southern Annular Mode, paired with a correlation between Ohau catchment precipitation, lake inflow and suspended sediment yield suggest that the Lake Ohau varves are a potentially powerful tool for interrogating the amplitude, timing and interdependence of different climate modes operating in the Southern Hemisphere mid-latitudes over time. A robust chronology and sound climate-proxy model are fundamental requirements for all high-resolution proxy environmental records. Here we present a chronology derived from layer counts, and ^{137}Cs and ^{210}Pb ages for the top 60 cm of sediments from the distal basin of Lake Ohau that confirm the varved nature of the sedimentary sequence. Sedimentary facies of different varve motifs are used to develop a hydroclimate-proxy model which links stratigraphy to seasonal hydrology. To establish this relationship we use a model accuracy statistic, which shows a quantitative difference between the annual hydrographs associated with each of three primary varve motifs. Distribution of above average inflow events points to summer and autumn hydrologic regimes as the primary control on the deposition of different motifs. This hydroclimate-proxy model will serve as a tool to reconstruct lake inflow, and by extension precipitation, on an annual basis, potentially throughout the late Holocene, for the South Island of New Zealand.

Key Words: Varves; Proxy; Hydroclimate; Stratigraphy; Complexity

3.1 INTRODUCTION

High-resolution paleoclimate records that capture environmental change on sub-decadal timescales play an important role in bridging the gap between short instrumental records and longer, lower resolution paleoclimate sequences (Zolitschka and Pike 2014). Only a few types of records capture environmental change at such high resolution—these include tree rings, ice cores, varved sediments, corals and speleothems (Bradley 1999; Zolitschka and Pike 2014). A number of these records are documented across the Northern Hemisphere (Mann et al. 1998; Ojala et al. 2012), but there remains a need to develop high-resolution paleoclimate reconstructions from the Southern Hemisphere (Neukom and Gergis 2012). New Zealand is one of only few landmasses that lie in the core of the climatically important Southern Hemisphere westerly wind belt but very few high-resolution terrestrial paleoclimate records have been recovered from the North and South Islands (Cook et al. 2006, 2002; Lorrey et al. 2008; Page et al., 2010, 1994; Orpin et al. 2010; Augustinus et al. 2011; Fowler et al. 2012; Striewski et al. 2013). Sediment cores collected from the distal end of Lake Ohau, South Island, New Zealand (Fig. 1) contain clastic varves, providing an opportunity to produce a high-resolution proxy climate record from this important mid-latitude region (Roop et al. 2015).

Process-network studies of the climatic, physical and biological processes in contemporary lacustrine systems that are targeted for paleoclimate record development provide an important means by which the relationship between climate and core stratigraphy can be examined in detail and aid in the interpretation and calibration of varved sediment sequences (Hodder et al. 2007; Ojala et al. 2012; Stockhecke et al. 2012; Lamoureux and Francus 2014; Zolitschka and Pike 2014). The Lake Ohau process-network study demonstrates that seasonal thermal stratification of the water column plays an important role in regulating the transfer of relatively coarser or finer grains from the river mouth to the distal (Outflow) end of the lake (Fig. 1; Roop et al. 2015). Sediment accumulation in winter at the Outflow is limited to very fine silt particles (3 - 5 μm) as cold, turbid underflows originating at the delta do not transport coarser silts and sands upslope beyond the depocentre. Increased discharge and sediment flux, paired with pronounced thermal stratification in summer, enables transport of fine silt particles (8 - 13 μm) to the core site along pycnoclines in the upper portions of the water column (Roop et al. 2015). These

observations provide a clear mechanism for the deposition of annual laminations, or varves, in the contemporary system (Roop et al. 2015).

This study builds on this physical process model to describe and explain seasonal controls on sedimentation in Lake Ohau beyond the process-network monitoring period (2011-2013) discussed in Roop et al. (2015) and aims to: a) confirm that sediment laminations preserve a seasonal signal over the instrumental record (1900-2011), and; b) investigate the hydroclimatic and sedimentological variability over the instrumental record in order to establish a sound climate-proxy model. This model will serve as the primary tool for interpreting paleoclimate variability in a ~17,000 year record (~80 m) expected to be collected from Lake Ohau in mid-2016.

3.1.1 Study Site

Lake Ohau (44.234°S, 169.854°E; 520 m asl) is a temperate lake (mean winter air temperature 6.2 °C) located in the intermontane Mackenzie Basin, South Island, New Zealand (Fig. 1). This glacially formed lake is 54 km² and reaches a maximum depth of 129 m. The 924-km² Ohau catchment ranges from 520 m to 2640 m asl and is drained primarily by the Hopkins and Dobson Rivers (Fig. 1). The catchment geology is characterized by highly indurated quartzofeldspathic greywacke sandstone and argillite mudstone (Cox and Barrell 2007). The Hopkins and Dobson valleys have relatively small modern glaciers at their head, which occupy 1.7% of the total catchment area (Fig. 1; Anderton 1973). This small volume of glacial ice is considered to have remained stable over the last several thousand years based on recent glaciological investigations in the valley (Doughty et al 2013; Putnam et al 2013) and is assumed to play a minor role in sediment generation and flux in the contemporary lacustrine environment (Roop et al 2015).

The Hopkins and Dobson Rivers account for 85% of the total fluvial input into Lake Ohau, with smaller tributaries contributing the remaining 15% (Fig. 1; Woods et al. 2006). River inflow is highest during austral summer (average inflow 105 m³ s⁻¹) and lowest in winter (61 m³ s⁻¹). Spring and early summer snowmelt contribute approximately 21% of mean annual inflow (Kerr 2013). Monthly headwater precipitation and lake inflow are correlated over the instrumental record (1926-2014; $r = 0.74$, $p = <0.0001$). There is a strong precipitation gradient over the 37 km long catchment, with headwaters receiving 76% more precipitation than at the lake (Roop

et al. 2015). This gradient is the result of westerly wind driven orographic precipitation on the western side of the Southern Alps ‘spilling over’ the main divide into the upper part of the Ohau catchment (Chater and Sturman 1998; Salinger and Mullan 1999). Lake Ohau is seasonally stratified and experiences frequent overturning during the austral summer (October - March; Roop et al 2015).

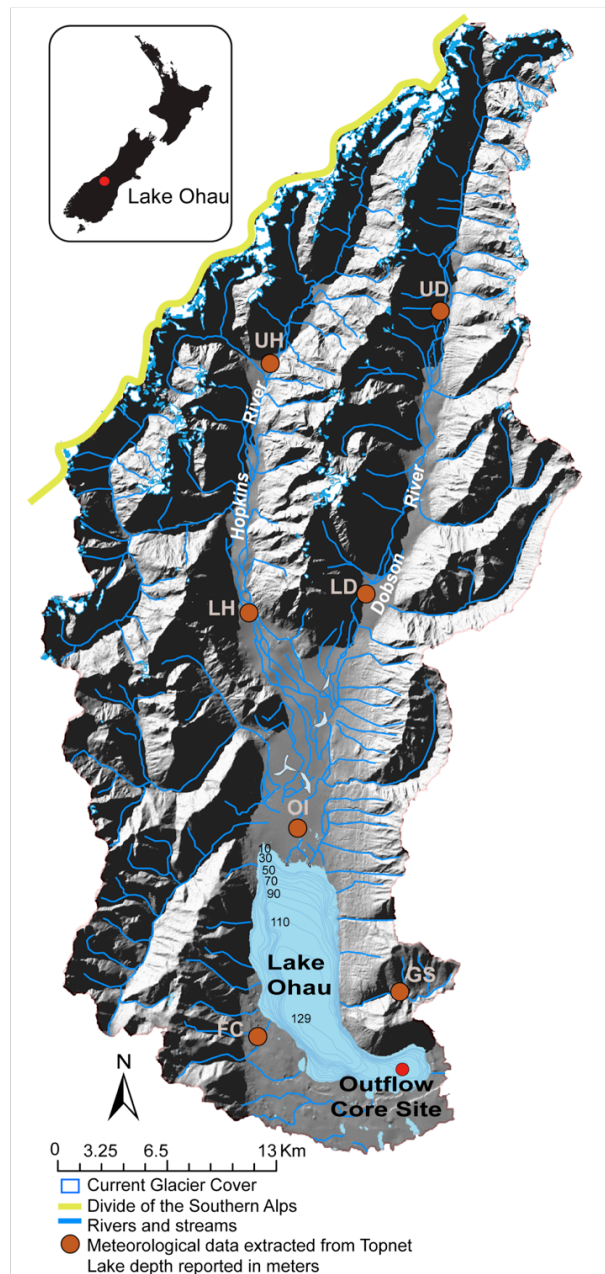


Fig. 1: The Lake Ohau catchment located on the eastern slope of the Southern Alps on the South Island, New Zealand. Sediment cores were collected near the lake outflow. Isobath interval is 10 m. Topnet derived precipitation time-series were generated for seven points in the Ohau catchment including: Upper Hopkins (UH), Upper Dobson (UD), Lower Hopkins (LH), Lower Dobson (LD), near the Ohau inflow (OI), at the based of Freehold Creek (FC) and in the Greta Stream catchment (GS).

3.2 MATERIALS AND METHODS

Three short gravity cores (0.3 m) and three longer Mackereth cores (5.5 m; Mackereth, 1958) were recovered near the outflow of Lake Ohau at ~68 m water depth between July 2009 and May 2013 (Fig. 1). Gravity cores were used to recover the sediment-water interface. The cores discussed in this paper include Mackereth cores OH1m1 (1m; collected July 2009), OH6m1c (5.5 m; collected October 2012), OH6m1 (5.5 m; collected July 2009), and gravity core GCS_1 (0.23 m; collected May 2013).

3.2.1 Physical Properties

Density, compressional (p)-wave velocity, magnetic susceptibility (whole core), and line scan RGB data (split core) were collected from cores OH6m1c, OH1m1, and OH6m1 using a Geotek multi-sensor core logger at the University of Otago. GCS_1 was split and photographed using a Lumix 10.1 Megapixel DMC LX5 camera. Thin-sections from core OH6m1 were made following Lamoureux (1994) and scanned at 2400 dpi on a flatbed scanner. X-radiographs (X-rays) were acquired from 30 cm x 0.5 cm x 0.5 cm u-channel samples taken from OH6m1c (Fig. 2A). Each u-channel sub-sample was offset with an overlap of 1.5 cm. X-ray data were collected at twenty-micron resolution using an ITRAX™ core scanner housed at the Korea Polar Research Institute (KOPRI). X-rays were generated using a 3 kw Mo tube running at 40 Kv and 35 mA with scanning time of 500 ms. Greyscale data were extracted from 16-bit X-ray positive (where lower density is represented by a lighter tone) TIFF images generated by the ITRAX™ using ImageJ (Schneider et al. 2012). Images were adjusted for brightness and contrast to fit within a range of intensity between 33,000-36,500.

Particle size was measured on selected high and low-density laminae from GSC_1 to verify that density variation is primarily due to changes in particle-size-influenced porosity (Supplementary Fig. 1). Discrete samples were dispersed with sodium hexametaphosphate (Calgon), continuously stirred and sonicated for 30 minutes, and passed through a Beckman Coulter LS 13 320 laser diffraction particle size analyzer equipped with a Micro Liquid Module (MLM). The MLM is capable of measuring small (~0.03 g) samples, ensuring material from lamina < 2 mm thick

could be obtained. Particle size data statistics were generated using Gradistat software (Blott and Pye 2001).

3.2.2 Chronology

One-centimeter sections extracted at various depths from core OH1m1 were analyzed for both ^{137}Cs and ^{210}Pb activity (Supplementary Table 1). ^{137}Cs was measured directly by gamma spectrometry using a high-resolution low background germanium (well-crystal) detector and total ^{210}Pb was determined from its granddaughter ^{210}Po measured by alpha spectrometry. Unsupported ^{210}Pb was calculated from the total by subtracting supported ^{210}Pb , which was estimated by measuring ^{226}Ra using gamma spectrometry. All analyses were conducted at GNS Science, New Zealand. The CRSmodel program, which assumes a Constant Rate of Supply (CRS), was used to determine the ^{210}Pb age-depth relationship (<https://code.google.com/p/crsmodel/>, accessed Nov 19, 2014; Fig. 2). Correlation between OH1m1 and OH6m1c was conducted visually in Corelyzer (<http://andrill.org/~jareed/corewall.org/www/>) and indicated an average ~1 cm offset between the cores for the top 60 cm (Supplementary Table 1). The offset is a result of the difference in the year of core collection and disturbance of the surface from coring. For example, gravity core GCS_1 and OH6m1c (recovered with a Mackereth system) were both collected in 2012. Correlation between these two cores shows that two full laminations were lost in the Mackereth core, which means that the surface of OH6m1c represents varve year 2010.

Layer Counting

Sedimentation patterns in Lake Ohau are dominated by a signal comprised of a coarse and fine couplet, represented in greyscale by high (~35,000-36,500) and low intensity values (~33,000-35,000), respectively (Fig. 3). This dominant pattern is often overprinted by the occurrence of additional coarse sublaminae (greyscale intensities of ~34,000-36,000), as observed by Roop et al. (2015). Based on our studies of modern sedimentation processes, the coarse-fine couplets are interpreted as annual layers and were counted accordingly.

Three layer counts were generated by two independent operators (Roop and Levy) from a combination of X-ray images, line-scan images, and thin sections for the top 60 cm of OH6m1c and OH6m1 (Fig. 2A). Each operator assigned a ‘varve year’

(VY) to each couplet based the occurrence of a sharp density change and a visual change in particle size in thin-section. HR conducted two separate counts. A more objective method was used to generate a layer count by recording all points in the X-rays greyscale curve where a positive gradient equivalent to ~20% of the total amplitude occurred ≤ 0.5 mm (after Wheatley et al. 2012). We also assumed that annual sediment accumulation must be > 2 mm based on prior monitoring (Roop et al. 2015), so concurrent greyscale peaks that were < 2 mm apart were not counted as separate years but classified as sublaminae. The resulting layer counts are shown in Figure 2. Sedimentation rate and layer thickness vs. year are derived from these age-depth relationships. Because the major coarse layer in the sedimentary couplet is the easiest feature to identify in the greyscale record and is caused by an influx of sediment in spring, a varve year is defined as September 1st - August 31st (which differs slightly from Roop et al. 2015 who defined a VY as October 1st - September 31st). This modification enables an investigation of variability in spring inflow conditions.

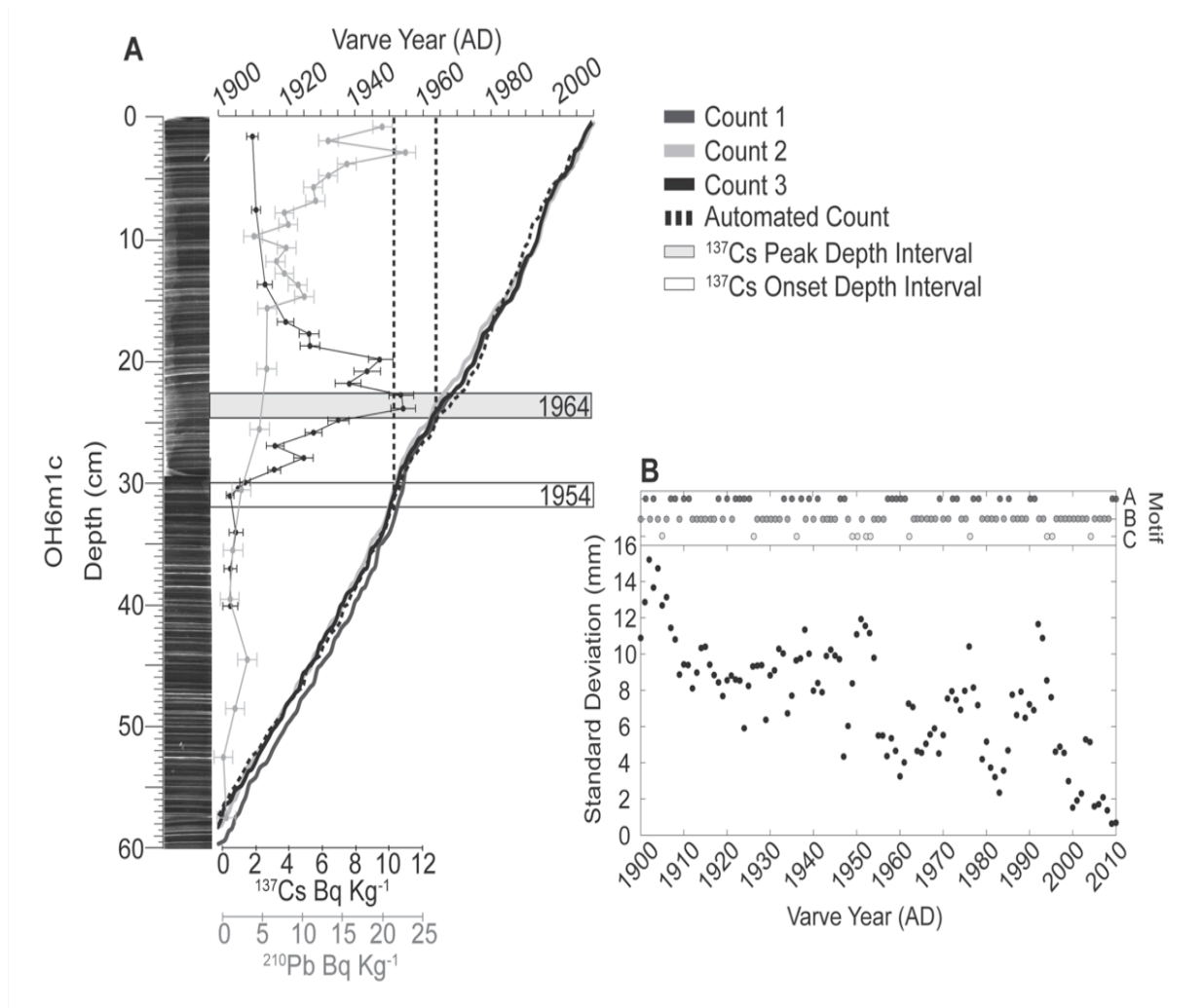


Fig. 2: A) ^{137}Cs and ^{210}Pb activity profiles compared to manual operator and automated counts for the top 60 cm of core OH6m1c. All counts are consistent with the depth intervals associated with the 1964 peak in ^{137}Cs and onset of ^{137}Cs in the early 1950's. B) 1σ standard deviation for all manual and automated counts compared to the three described motifs. The maximum deviation is 15.2 mm or ± 5.8 years (2σ) based on the ^{137}Cs -derived sedimentation rate. The greatest deviation between counts is associated with motif C, or event stratigraphy.

3.2.3 Hydrometeorological data

Three hydrometeorological datasets were used in this study including: (1) a record of daily mean inflow calculated from lake level and measured outflow that extends from 1926 to present (Meridian Energy Ltd., unpublished data); (2) a continuous time-series of precipitation and temperature (1926-present) measured at Lake Tekapo Air Safaris, 40 km north of Lake Ohau and outside of the Ohau surface water catchment (44.00°S, 170.43° E; Station ID 4970); and (3) modeled precipitation, air temperature and inflow data extracted for seven different locations in the Lake Ohau catchment from the National Institute of Water and Atmosphere (NIWA) Topnet model (Clark et al. 2009; Fig. 1). Topnet is based on a 30 m Digital Elevation Model (DEM) and simulates hydrological processes based on total precipitation and temperature provided as a 0.05° latitudinal/longitudinal grid based on an interpolation of data from a national network of automated weather stations (Tait et al. 2006). The hydrological model was calibrated against hourly total lake inflows over the period 1980-1990 and validated over the period 1980-2008. Seven samples sites were selected to provide upstream catchment average precipitation and temperature and total inflow, including: Upper Hopkins (UH), Upper Dobson (UD), Lower Hopkins (LH), Lower Dobson (LD), near the Ohau inflow (OI), at the base of Freehold Creek (FC) and in the Greta Stream catchment (GS; Fig. 1).

Comparisons between varve thickness (VT) and hydrometeorological data were run for seven different temporal increments including: full twelve months, spring (September, October, November, referred to as SON), summer (December, January, February, referred to as DJF), autumn (March, April, May, referred to as MAM), winter (June, July, August, referred to as JJA), spring and summer (SONDJF), and autumn and winter (MAMJJA). Averages and totals of the three hydrometeorological datasets over these temporal increments were tested against the full VT time-series and all varve motifs and sub-types for five different varve features including: 1) total thickness; 2) coarse unit thickness; 3) fine unit thickness; 4) fine unit thickness minus sublaminae; 5) sublaminae thickness. Lag correlations between VT characteristics and hydrometeorological parameters were also tested for the preceding one and two years. All statistical relationships between each measured varve feature and hydrometeorological variables were tested using Spearman's rank

correlation (non-parametric) as all datasets were non-normally distributed. Relationships where $p \leq 0.05$ are considered significant.

Varve year hydrographs were compared using the Nash-Sutcliffe model accuracy statistic (Nash and Sutcliffe 1970). The Nash-Sutcliffe coefficient tests values for goodness of fit between measured and modeled hydrographs. The goodness of fit, represented here as r , is analogous to the sum of squares, where 1 is a perfect fit and values ≤ 0 indicate that the model hydrograph is a poor predictor of the measured discharge values compared to the average discharge over the period considered. In this study, the Nash-Sutcliffe coefficient was used to compare the mean of measured hydrographs for differing varve motifs and types. Annual and seasonal (as above) hydrographs for each primary sedimentary motif were also compared using the Spearman's rank correlation.

3.3 RESULTS

3.3.1 X-ray density and particle size

Less dense layers (light grey and white tones in X-rays) are consistently associated with coarser particles (modal size $> 8.0 \mu\text{m}$), while the densest layers (dark tones in X-rays) are associated with finer particles (modal size $3.7 \mu\text{m}$; Supplementary Fig. 1). Particle size variability between the light and dark layers in X-ray is similar to the annual range measured in surface cores and sediment traps by Roop et al. (2015).

3.3.2 Varve classification

Three primary varve motifs (labeled A, B and C) were identified based on variations in complexity (e.g. presence/absence and number/position of sub-laminae) and total thickness (Table 1; Fig. 3). Motif A consists of a fine silt basal layer that grades into a very fine silt layer. These 'simple' varves are divided into sub-types A1 and A2, which are separated based on the relative thickness of the coarse and fine units (Table 1; Fig. 3). Motif A accounts for 34% of the total lamination stratigraphy in the top 60 cm of OH6m1c. Motif B is characterized by the presence of one or more grain-supported 0.5 - 1.5 mm-thick sublaminiae within the primary coarse/fine stratigraphy. These 'complex' varves account for 56% of the total lamination stratigraphy in the top 60 cm of OH6m1c. Motif B is sub-divided into four types (B1, B2, B3, B4) to account for the variations in the number and position of sublaminiae within the annual

couplet (Table 1; Fig. 3). Motif C includes layers that are ≥ 9.0 mm thick and comprise a basal fine silt layer that grades into a relatively thick (~ 3.5 mm) homogeneous very fine silt layer (Table 1; Fig. 3). Thin sub-laminae (≤ 1.0 mm) commonly occur immediately above the basal unit. Motif C accounts for 10% of the varve stratigraphy in the top 60 cm of OH6m1c. Total VT ranges from 3.4 - 3.5 mm in motif A, 4.5 - 7.1 mm in motif B, and 9.0 - 12.9 mm motif C (Table 1; Fig. 3).

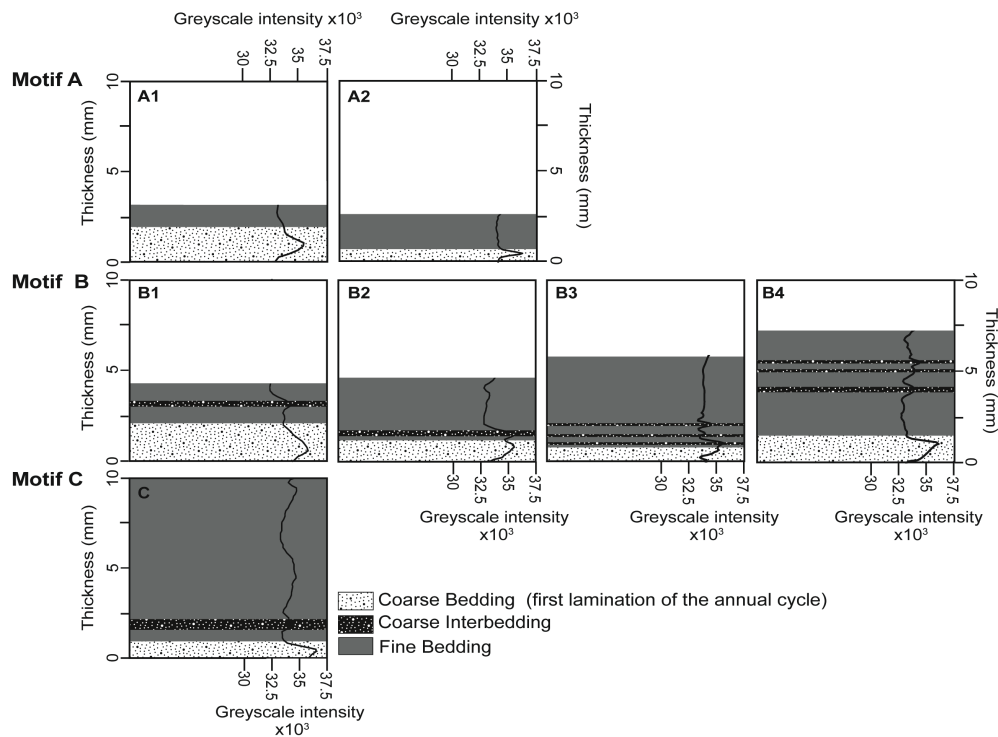


Fig. 3: An example of the differing stratigraphic patterns and greyscale curve for each of the seven different varve types characterized by motifs A, B, C. Each example shows the relative thickness of each unit and the presence and stratigraphic position of sublaminae in motifs B and C. Unit thickness is based on the mean of each varve type.

Table 1 Varve classification for the different varve motifs and sub-types

	Description	Mean Thickness (mm)	Mean Coarse Unit Thickness (mm)	Mean Fine Unit Thickness (mm)	Mean Number of Sublaminae	Occurrence *	Interpretation (Note: Spring (SON); Summer (DJF); Autumn (MAM); Winter (JJA))
<i>Motif A- defined by a coarse/fine couplet lacking sublaminae.</i>							
A 1	Composed of fine silt basal layer grading into a very fine silt layer. Silt layer is thicker than very fine silt layer. Contains no sublaminae.	3.5	2.0	1.5	0	7	Simple varve dominated by spring discharge.
A 2	Composed of silt basal layer grading into a very fine silt layer. Fine silt layer is thicker than the silt layer. Contains no sublaminae.	3.4	1.1	2.3	0	27	Simple varve dominated by late spring discharge.
<i>Motif B- defined by coarse/fine couplet with one or more coarse sublaminae.</i>							
B1	Composed of fine silt basal layer grading into a very fine silt layer. Very fine silt layer contains one coarse-grained ≤ 1.5 mm thick sublaminae.	4.7	1.2	1.6	1	19	Complex annual hydrograph; spring-dominated signal with late season inflow event.
B2	A fine silt basal layer grades into the very fine silt layer. ≤ 1.0 mm fine silt sublaminae are present proximal (≤ 0.8 mm) to the fine silt basal layer. Sublaminae are not present near the top of the very fine silt unit.	4.8	1.1	2.2	1	12	Complex annual hydrograph; dynamic spring hydrograph with late spring/early summer peak inflow event.
B3	A fine silt basal layer grades into the very fine silt layer. One or more ≤ 1.0 mm fine silt sublaminae are present proximal to the fine silt basal layer. Sublaminae are not present near the top of the very fine silt unit.	5.6	0.9	1.7	2	9	Complex annual hydrograph; numerous peaks in summer discharge.
B4	Composed of fine silt basal layer grading into a very fine silt layer. Very fine silt layer contains several fine silt ≤ 1.0 mm thick sublaminae.	7.1	1.1	2.1	3	16	Complex annual hydrograph; numerous peaks in summer and autumn discharge.
<i>Motif C- defined by graded coarse deposits overlain by a (≥ 3.5 mm) fine unit. Total unit thicknesses $> 9mm$</i>							
C 1	Composed of a basal silt layer which grades into a thick (≥ 3.5 mm) non-graded fine silt layer. Sublaminae are common in basal layer.	10.0	1.5	3.4	2	10	Event layer; large summer discharge exceeding $\sim 880 \text{ m}^3 \text{ s}^{-1}$

*Percent occurrence since 1900 AD based on varve counts.

3.3.3 Core chronology

Cesium-137 and lead-210 radiometric dating techniques and layer counts provide both a robust age-depth model for the instrumental record and a method to test whether the lamination stratigraphy preserves an annual signal. Southern Hemisphere onset and maximum ^{137}Cs fallout, a by-product of nuclear weapons testing, occurs in 1954 and 1964, respectively (UNSCEAR 2000). These tie-points offer important age-control for the top portion of the sediment record. Peak ^{137}Cs (1964) occurs between 24.0 - 25.0 cm and onset (1954) occurs between 31.0 - 32.0 cm in OH6m1c (Supplementary Table 1).

Chronology determined by layer counts (manual and automatic) is consistent with the depth intervals associated with the ^{137}Cs profile (Fig. 2A). Specifically, layer counts place varve year (VY) 1964 between 23.7 - 24.8 cm and VY 1954 between 28.8 - 30.5 cm. Similar sediment accumulation rates (SAR) are calculated using ^{137}Cs and ^{210}Pb activity profiles and layer counts (Fig. 2A). The ^{137}Cs derived SAR is $5.1 \pm 0.3 \text{ mm yr}^{-1}$, the ^{210}Pb SAR is $6.0 \pm 1.1 \text{ mm yr}^{-1}$ and the layer count derived SAR is $5.2 \pm 0.5 \text{ mm yr}^{-1}$. The instrumental record commenced in 1926 and the ^{210}Pb -derived and layer counts age-depth relationships are in close agreement; ^{210}Pb places 1926 (± 6.1 years) at 44.0 - 45.0 cm while an average layer count places 1926 (± 2 years) at 44.5- 45.0 cm.

A 2σ standard deviation of the ages assigned to a given depth is used as a means to quantify offset between the four different layer counts (three manual and one automated; Fig. 2B). A maximum deviation of 15.2 mm or ± 5.8 years occurs at VY 1900. The largest deviation between counts generally occurs in sections of the core that are characterized by motif C and the total error then propagates with depth (Fig. 2B). Maximum agreement and consistency between layer counts occurs in sections that are characterized by motif A. Given the similarity and small error between the layer count- and radiometric-derived age-depth relationships, hydroclimatic relationships over the instrumental record were tested against an average of the manual and automated layer counts.

3.3.4 Hydroclimate-varve relationships

Regression statistics were calculated to compare all five 'iterations' of VT with average modeled air temperature, aeral total and average modeled and measured

precipitation, and total and average inflow for the seven different temporal/monthly breakdowns of the annual cycle. These tests yield few statistically significant results (Supplementary Table 2). One of the strongest correlations is a basin-wide negative correlation between total SON precipitation and coarse unit thickness. This correlation is weakly significant for six of the seven sites for which modeled precipitation was extracted; the strength of the correlation only ranges from $r = -0.29$, $p = 0.08$ at Freehold Creek (FC) to the strongest correlation of $r = -0.36$, $p = 0.03$ at Greta Stream (GS). The correlation is not significant for the Upper Hopkins site. The same regression statistics were tested on the three major varve motifs and seven types, which yielded similar non-robust and weakly statistically significant results (Supplementary Table 2).

In order to explore the relationship between varve motif/type and hydroclimate, the hydrographs for each annual layer during the correlation period of 1926-2010 were compared using the Nash-Sutcliffe model accuracy statistic (inflow derived from the Lake Ohau inflow time-series provided by Meridian Energy Ltd.) To mitigate the impact of potential mismatches between varve type and hydrology arising from errors in our annual layer chronology, we compared hydrographs for a subset of years of close chronologic sequence (1-5 sequential years) defined by each motif and varve type (Table 2). The annual inflow time-series for the subsets of years corresponding to motifs A, B, C and varve types A1, A2, B1, B2, B3, B4, C respectively, were grouped and averaged to produce a characteristic hydrograph for each motif and type (Fig. 4). These characteristic hydrographs were compared to each other using the Nash-Sutcliffe model accuracy statistic and Spearman's rank correlation (Tables 2 and 3; Nash and Sutcliffe 1970).

Comparisons between each characteristic (mean) hydrograph for the subsets of years were made using a complete data series and both a 30- and 15-point running mean (Fig. 4). Results from analysis of the 15-pt smoothed data series for the subset of chronologically sequential varves ($n = 5$ or 6) show poor fit between the hydrographs that characterize motif A and C and close agreement between those that characterize motifs B and C (Table 2). Hydrographs for subtypes A1 and A2 are in close agreement with B1 and B2 (Table 2). To increase the statistical power of the correlations, hydrographs for the sum of all of the years represented by each of the three major motifs were also compared (minimum $n = 11$ for motif C). The strong

positive correlation between the subset of annual hydrographs (15-pt smooth) for all motifs weakens significantly when weekly data are considered (Table 3).

Table 2 Nash-Sutcliffe coefficients (r) for 15-point smooth hydrographs. Mean hydrographs are derived from the listed subset of years. Sequential years were selected, where possible, in order to minimize potential error associated with the varve chronology. For type A1, no chronologic sequence of years was available for testing. Hydrographs are derived from the Lake Ohau inflow time-series.

Varve type	A1	A2	B1	B2	B3	B4	C1
A1	1	0.54	0.70	0.56	0.40	0.40	0.45
A2	0.54	1	0.50	0.72	0.50	0.50	0.47
B1	0.70	0.5	1	0.69	0.45	0.68	0.62
B2	0.56	0.72	0.69	1	0.50	0.37	0.61
B3	0.40	0.50	0.45	0.50	1	0.30	0.61
B4	0.40	0.50	0.68	0.37	0.30	1	0.26
C1	0.45	0.47	0.62	0.61	0.61	0.26	1
Years Compared	2009	1973	1968	2008	1980	1999	1995
	1991	1972	1966	2005	1979	1996	1994
	1977	1961	1965	2001	1975	1993	1953
	1958	1960	1964	1948	1956	1932	1952
	1947	1959	1963	1945	1954	1930	1950
	1939			1943		1929	1949

Table 3 Nash-Sutcliffe coefficients (r) for the weekly smoothed annual hydrograph for each of the three major sedimentary motifs. The hydrograph for each motif is derived from a mean of all of the years characterized by each sub-type (e.g. A1, A2 = A). Each motif is characterized by a unique hydrologic regime.

Motif	A	B	C
A	1	-0.27	-0.46
B	-0.27	1	0.32
C	-0.46	0.32	1
n	22	52	11

To explore seasonal biases in inflow, characteristic hydrographs for the major motifs and types were divided into four temporal increments including: spring (SON), summer (DJF), autumn (MAM), and winter (JJA) and compared using a Spearman's rank correlation and outlier plots (Table 4; Fig. 5). The hydrographs for each motif during SON show close correlation while the relationship between the seasonal hydrologic regimes and varve motifs weakens for the rest of the annual cycle (Table 4). Outlier plots show similar patterns for all of the varve types, with the range of

hydrologic variability the lowest during SON. The number of hydrologic outliers increases most notably in summer and autumn (Fig. 5). Outliers in seasonal discharge are mostly associated with motif B varve types, while type A varves show the smallest range of variability across the annual cycle, and the fewest number of anomalous peaks in inflow (Fig. 5).

Table 4 Regression statistics (r) for the seasonal mean hydrology of each of the three major motifs (for all years, as in Table 3). Correlation between the three motifs is greatest in the spring (SON).

Motifs Compared	Season			
	SON (Spring)	DJF (Summer)	MAM (Fall)	JJA (Winter)
A – B				
r	0.53	0.18	0.15	0.26
p -value	<0.0001	<0.0001	<0.0001	<0.0001
A – C				
r	0.35	0.23	0.02	0.02
p -value	<0.0001	<0.0001	0.21	0.30
B – C				
r	0.62	0.17	0.02	0.17
p -value	<0.0001	<0.0001	0.17	<0.0001

3.4 DISCUSSION

Meaningful paleoclimate reconstructions from annually laminated sediments require a detailed understanding of the relationship between sedimentation and climate (Hodder et al. 2007). In the Lake Ohau region, there is significant correlation between headwater precipitation and lake inflow ($r = 0.74$ $p = <0.0001$), as well as spatially-averaged precipitation and suspended sediment yield for South Island greywacke catchments ($r = 0.71$; reported here as r ; Hicks et al. 2011). This regional relationship suggests there should be a link between rainfall and sediment accumulation in Lake Ohau. The original hypothesis was that this link would be reflected in VT based on previous paleoclimatic reconstructions in many clastic varve settings (e.g. Desloges and Gilbert 1994; Tomkins and Lamoureux 2008; Kaufman et al. 2011). However, results indicate that such a relationship does not exist. This is not entirely surprising as direct relationships between VT and hydroclimatic variables can be difficult to establish (Hodder et al. 2007). Geologic processes such as earthquakes and slope failure can, in geologic time, instantly alter the availability of sediment to a basin (Dadson et al. 2004; Howarth et al. 2012). The climate system itself operates on various temporal and spatial scales and can be complicated in mountainous terrain by

microclimates, which are poorly resolved in modeled data and generally underrepresented in meteorological time-series (Hannah et al. 2000). In addition to the aforementioned complexities, internal lake dynamics can further attenuate dispersal and accumulation patterns of sediments (Pharo and Carmack 1979; Desloges and Gilbert 1994; Hodder et al. 2007). Regardless of these complexities, our results suggest that varve stratigraphy, instead of varve thickness, is a good indicator of hydroclimatic variability in Lake Ohau. In the following discussion we explore the probable causes of stratigraphic variability and show that varve stratigraphy can be used to establish a hydroclimate-proxy model.

3.4.1 Varve thickness and hydroclimatic variability

A strong correlation between riverine suspended sediment yield and precipitation and inflow has been shown for nearby catchments (Hicks et al. 2011) and a similar relationship is assumed to be true for Lake Ohau. However, the predominance of negative correlations between total precipitation, inflow and varve thickness at the distal core site (Supplementary Table 2) suggests that sediment accumulation and inflow are decoupled due to seasonal lake hydrodynamics. Specifically, inflow events in spring occur when the lake is isothermal, which influences sediment transport pathways and affects the relationship between inflow (discharge) and suspended sediment flux (Roop et al. 2015). However, errors in sediment flux derived from SSC rating curves can be in excess of 50% and tend to produce low estimates during high SSC conditions and vice versa (Walling and Webb 1988; Horowitz 2003). This demonstrates that relationships between inflow and SSC, and subsequent sediment transport and deposition, are complicated and cannot be assumed to be linear or constant through time.

Eight large magnitude ($\geq 880 \text{ m}^3 \text{ s}^{-1}$) inflow events were measured between 1926 and 2011 and eleven $\geq 9.0 \text{ mm}$ laminations (motif C layers) were identified in the cores during the same period. Further, only fifty percent of layers characterized as motif C coincide temporally (± 2 years) with measured large magnitude inflow events. This mismatch suggests that some large sedimentation events are potentially related to non-climatic events including subaqueous mass wasting. These observations are not surprising, as other studies have shown that peaks in SSC do not always correlate with peak inflow (Sawada and Johnson 2000; Orwin and Smart 2004). In addition, unusually dry conditions and associated high soil infiltration capacity can attenuate

the sediment transport response following extreme precipitation events and affect expected SSC (Favaro and Lamoureux 2014). One or more of the processes outlined above could explain the observed mismatch between thick event layers and precipitation-driven extreme event inflow and the anti-correlation between precipitation, inflow and varve thickness.

3.4.2 Lamination stratigraphy

Sedimentary couplets without sublaminae (motif A) represent varves that form in years with limited high magnitude summer/autumn inflow events (Figs. 4 and 5). A1 varves form during years that are characterized by an annual hydrograph with a late-spring onset of high inflow that peaks in December/January and exhibits limited spring freshet input (Figs. 4 and 5). This late season flux may account for the proportionally thicker coarse unit in A1 as peak flow occurs when the lake is fully stratified, which may provide a more direct conduit for coarser sediment delivery to the distal basin. A2 varves form during years characterized by a hydrograph exhibiting higher peak inflow in spring when lake stratification is developing, which may cause flow separation that delivers less sediment to the distal basin and produces the proportionally thinner basal coarse unit (Fig. 4). This interpretation may also explain the basin-wide negative correlation between coarse unit thickness and total SON precipitation. High spring rain may prolong isothermal conditions in the lake through the continued input of relatively colder precipitation and snowmelt. More persistent isothermal conditions would likely limit the transport of coarse particles to the core site and produce thinner coarse basal units. Overall, the lack of complexity in motif A is likely associated with fewer peak inflow events in summer and autumn (Fig. 5).

Sedimentary couplets that contain sublaminae characterize motif B. Sediment grain size in the basal layer of each sublamination is similar to the primary spring/summer coarse unit, which suggests that these units are deposited during inflow events of similar magnitude that occur between October and May when the lake is fully stratified (Roop et al. 2015; Fig. 4). However, we suggest that the thinner units reflect lower total suspended sediment flux due to lower total inflow volume, duration, or sediment availability. Sublaminae in motif B are similar to those documented in other records with complex lamination stratigraphy (Desloges and Gilbert 1994; Chutko and Lamoureux 2008; Cockburn and Lamoureux 2008) and

reflect short-lived summer and autumn rain events. This interpretation is consistent with Roop et al. (2015), who observed discrete sublaminae deposited during summer inflow events and captured in sediment traps at the Outflow site. Further, each sub-type of motif B includes several outliers in discharge during the stratified period in the summer and autumn (Fig. 5), which are likely responsible for producing the sublaminae characterizing motifs B and C. Type A2 is an exception, as it lacks sublaminae but has a summer hydrologic regime that includes numerous outliers in summer discharge; these peaks in inflow may be responsible for the proportionally thicker fine unit in A2 (compared to A1) and the lack of sublaminae potentially associated with internal lake dynamics.

Motif B is subdivided into four sub-types based on the position and thickness of sublaminae. The stratigraphic position of the sublaminae may, in general, reflect the position of summer and autumn inflow events within the annual hydrograph (Fig. 4). For example, sub-type B2 includes sublaminae that occur within the lower portion of the primary fine unit and has a characteristic hydrograph that is dominated by high magnitude spring and summer peaks in inflow (Figs. 4 and 5). In contrast, sub-type B1 includes sublaminae that occur within the upper portion of the primary fine unit and is characterized by a hydrograph with a greater concentration of peak inflow events in the autumn (Figs. 4 and 5).

Motif C is comprised of a thick fine (dense) unit that includes sublaminae thicker than those observed in motifs B. This stratigraphy suggests that these varves form in years that include extreme inflow events. These extreme event flows generally range between 880-1300 m³ s⁻¹ and can deposit sediment at nearly double the average annual sedimentation rate (Roop et al. 2015).

One annual hydrograph with a large (1,200 m³ s⁻¹) peak inflow event correlates with motif sub-type B4 (Fig. 4) and highlights that misclassification can occur. However, general agreement between the Nash-Sutcliffe correlation and regression statistics show that all three major motifs, and sub-types, are characterized by unique annual hydrologic regimes (Fig. 4; Table 3). High correlation between spring discharge and varve motif (and sub-types) suggests that the primary hydrologic causes for the different varve types occurs in summer and autumn. During summer and autumn, characteristic hydrographs for motifs B and C contain significant outliers in discharge (Fig. 5), which likely produce complex laminae.

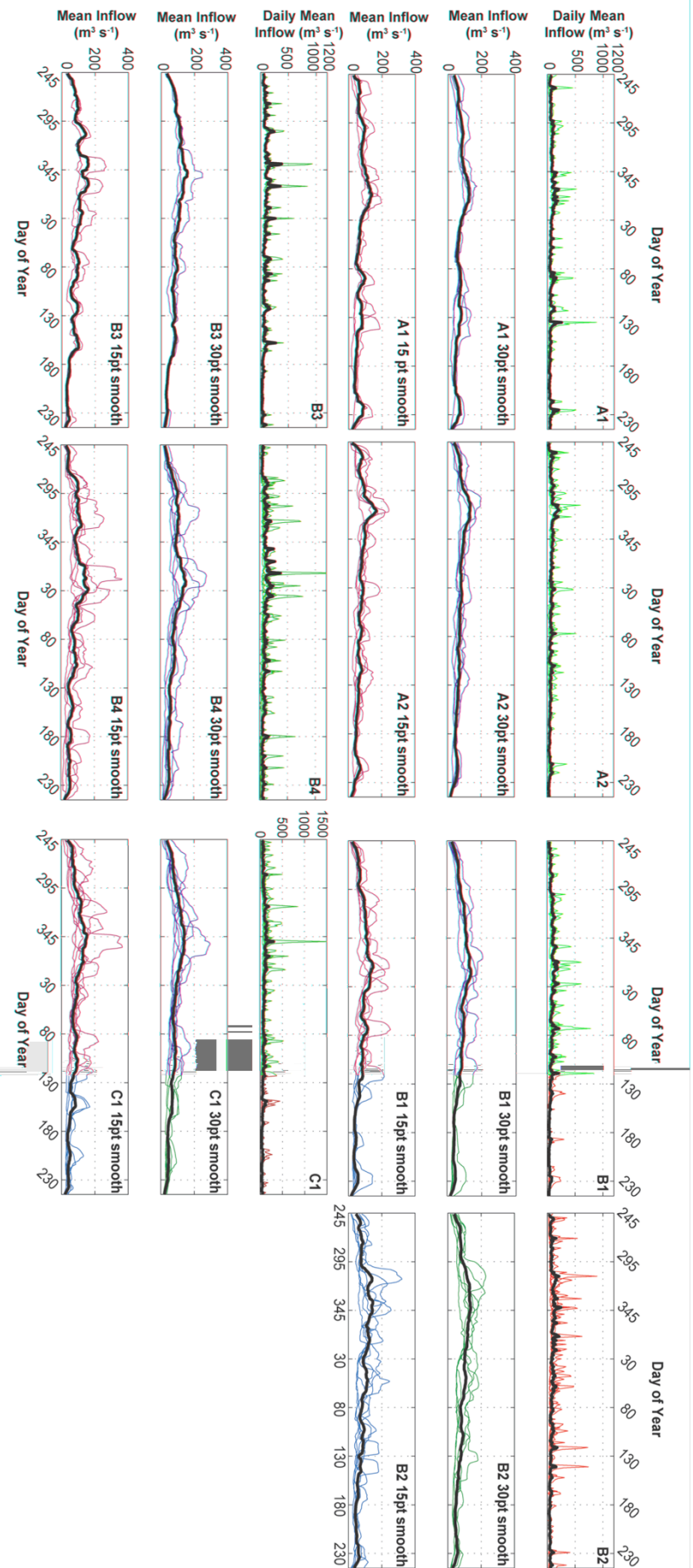


Fig. 4: Plots showing the full, 15-point and 30-point smoothed hydrographs for each motif sub-type. Dark bold lines are the mean of all years in each comparison (Table 2). Motif A varves are characterized by a spring season dominated hydrograph, motif B varves are characterized by a more complex hydrograph displaying a high degree of variability throughout the annual cycle. Motif C is similar to B, but is characterized by extreme summer event flows. Each of the three motifs is significantly different based on the Nash-Sutcliffe model accuracy statistic (Table 3).

Furthermore, general agreement between the stratigraphic position of sublaminae and the number and timing of anomalous summer-autumn inflow events (outliers) suggests that stratigraphic pattern and hydrodynamics are closely related.

Monitoring data through winter (JJA) showed that isothermal conditions prohibit the transport and deposition of coarse material to the Outflow (Roop et al. 2015). Therefore, changes in varve stratigraphy are interpreted as variations in the number and intensity of peak inflow events during the summer and autumn seasons. Specifically, the three primary motifs are interpreted to represent the following: (1) limited summer and autumn precipitation-driven inflow events (motif A; inferred drier summer catchment conditions); (2) frequent summer inflow events (motif B; inferred wetter summer catchment conditions); and (3) large magnitude summer inflow (flood) events ($> 880 \text{ m}^3 \text{ s}^{-1}$; motif C).

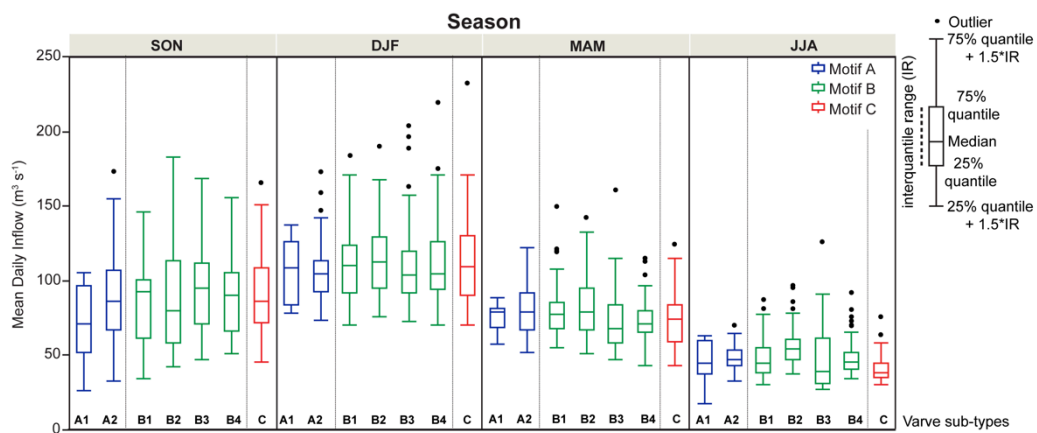


Fig. 5: Outlier box plots organized by season for each of the varve types. The hydrographs used for this comparison are derived from a mean of all of the years characterized by each varve type. Outliers represent anomalous flow, or event flow. A higher density of inflow events, particularly in summer and autumn, characterizes motif B.

3.4.3 Towards a hydroclimate-proxy model for the pre-instrumental era

A link between varve stratigraphy and hydrology provides a foundation for developing a hydroclimate-proxy model for the Lake Ohau outflow site. This model, however, is complicated by a lack of pronounced statistical relationship between varve thickness and hydrology, indicating that important mediating variables are at play in the system which accentuate and/or decouple sediment deposition from

sediment flux and transport—and hydroclimatic variables such as precipitation and inflow.

The ability to characterize the hydrologic signal by the general accumulation pattern of the different motifs provides a potentially powerful tool for interpreting a longer sediment sequence. Recognizing a range of processes influences sedimentation in Lake Ohau, the demonstrated link between annual hydrology and sedimentary motif can be used to reconstruct pre-historic hydrology. Specifically, sedimentation patterns preserved in cores from the Outflow can be used to reconstruct the general shape of the annual hydrograph, with different sedimentological packages changing in response changes in summer and autumn hydrologic regimes. Given that each of the three major motifs are demonstrably different from one another, observed changes in sedimentary motif can be used to infer changes in seasonal event flow, and by extension storm events, experienced at Lake Ohau. Initial examination of the 5.5 m OH6m1c indicates that the range of facies described herein characterizes the majority of down-core sediment stratigraphy. Similar methods to those described here, including motif descriptions and layer-counting methods, will be employed to ensure we capture any pre-historic variations in the system that were not observed in this study of the instrumental era. Future work will also utilize reanalysis data and synoptic typing specific to New Zealand (Kidson 2000) to establish links to the climate system. The potential correlation between synoptic types and hydrology will allow for a more comprehensive interpretation of the hydroclimatic signal preserved in the Lake Ohau sedimentary sequence.

3.5 CONCLUSIONS

We have assessed the utility of sedimentary facies of different varve motifs from Lake Ohau to develop a hydroclimate-proxy model which links stratigraphy to the shape of the annual hydrograph. Few robust correlations result from our comprehensive statistical tests of the relationship between varve thicknesses and measured and modeled hydroclimatic variables such as precipitation and inflow at Lake Ohau. Varve thickness is a poor climate proxy at this site, due to the complex interplay between sediment flux and internal lake sediment transport processes. Seasonal thermal stratification, as documented by Roop et al. (2015), has a major influence on sediment accumulation throughout Lake Ohau.

Despite the lack of a clear relationship between varve thickness and hydroclimate, there is a quantitative relationship between sediment stratigraphy and summer and autumn inflow patterns. Three primary lamination types presented here represent years with: (1) limited summer and autumn precipitation-driven inflow events (motif A); (2) frequent summer inflow events (B); and (3) large magnitude summer inflow (flood) events ($> 880 \text{ m}^3 \text{ s}^{-1}$; C). These relationships provide a tool for characterizing hydrology and storm event frequency for the longer pre-instrumental period. The method used here to compare hydrology and sedimentary facies may be of use for investigating and developing climate-proxy models from other sites where it is difficult to quantitatively link varve thickness and hydroclimatic variability. Overall, this work provides a solid foundation for the development of the Lake Ohau paleoclimate record and is a step towards addressing the current paucity of high-resolution terrestrial paleoclimate reconstructions from the Southern Hemisphere mid-latitudes.

3.6 ACKNOWLEDGEMENTS

Financial support was provided through the GNS Science Global Change through Time Program, Sarah Beanland Memorial Scholarship, ANZICE Program (VICX0704), Royal Society of New Zealand Marsden Fund (GNS1302), and KOPRI Project #PP15010. Thanks to Brian Anderson, Lionel Carter, Andrew Lorrey, Christian Ohlendorf and Peter Neff for numerous scientific discussions and ongoing interest in the Lake Ohau Project. We would like the staff at Meridian Energy Ltd. and the University of Otago Marine Sciences Department for logistical support. Sincere thanks to Chris and Rae Spiers for their hospitality and large workspace at the Killin Barn, and the Inkersell family at Lake Ohau Station for land access and continuing project support.

3.7 REFERENCES

Anderton P (1973) The significance of perennial snow and ice to the water resources of the South Island, New Zealand. *J Hydrol (NZ)* 2: 6-18.

Augustinus P, D'costa D, Deng Y, Hagg J, and Shane P (2011) A multi-proxy record of changing environments from ca. 30 000 to 9000 cal. a BP: Onepoto maar palaeolake, Auckland, New Zealand. *J Quat Sci* 26: 389-401.

Blott SJ and Pye K (2001) GRADISTAT: a grain size distribution and statistics package for the analysis of unconsolidated sediments. *Earth Surf Process Landf* 26: 1237-1248.

Bradley RS (1999) Paleoclimatology: reconstructing climates of the Quaternary. Accessed Online via *Elsevier* 68: 1-613.

Chater AM and Sturman AP (1998) Atmospheric conditions influencing the spillover of rainfall to lee of the Southern Alps, New Zealand. *Int J Climatol* 18: 77-92.

Chutko KJ and Lamoureux SF (2008) Identification of coherent links between interannual sedimentary structures and daily meteorological observations in Arctic proglacial lacustrine varves: potentials and limitations. *Can J Earth Sci*, 45: 1-13.

Clark MP, Rupp DE, Woods RA, Zheng X, Ibbitt RP, Slater AG, Schmidt J, and Uddstrom MJ (2008) Hydrological data assimilation with the ensemble Kalman filter: Use of streamflow observations to update states in a distributed hydrological model. *Adv. Water Resour* 31: 1309–1324.

Cockburn JM and Lamoureux SF (2008) Inflow and lake controls on short-term mass accumulation and sedimentary particle size in a High Arctic lake: implications for interpreting varved lacustrine sedimentary records. *J Paleolimnol* 40: 923-942

Cook, ER, Buckley, BM, Palmer, JG Fenwick P, Peterson MJ, Boswijk G, and Fowler, A (2006). Millennia-long tree-ring records from Tasmania and New Zealand: A basis for modelling climate variability and forcing, past, present and future. *J Quat Sci* 21(7): 689-699.

Cook, ER, Palmer JG, and D'Arrigo, RD (2002). Evidence for a 'Medieval Warm Period' in a 1,100 year tree-ring reconstruction of past austral summer temperatures in New Zealand. *Geophys Res Lett* 29(14): 12-1.

Cox S and Barrel D (2007) Geology of the Aoraki area, Institute of Geological and Nuclear Sciences 1: 250000 Geological Map. *Lower Hutt, New Zealand (GNS Science)* 71:1.

Dadson SJ, Hovius N, Chen H, Dade WB, Lin JC, Hsu ML, Lin CW, Horng MJ, Chen TC, Milliman J, and Stark CP (2004) Earthquake-triggered increase in sediment delivery from an active mountain belt. *Geology* 32(8): 733-736.

- Desloges JR and Gilbert R. (1994) Sediment source and hydroclimatic inferences from glacial lake sediments: the postglacial sedimentary record of Lillooet Lake, British Columbia. *J Hydrol* 159: 375-393.
- Favaro EA and Lamoureux, SF (2014) Antecedent Controls on Rainfall Runoff Response and Sediment Transport in a High Arctic Catchment. *Geografiska Annaler: Series A, Phys Geo* 96: 433-446.
- Fowler AM, Boswijk G, Lorrey AM, Gergis J, Pirie M, McCloskey S, Palmer JG, and Wunder J (2012) Multi-centennial tree-ring record of ENSO-related activity in New Zealand. *Nat Clim Chang* 2(3): 172-176.
- Hannah DM, Gurnell AM, and McGregor GR (2000) Spatio-temporal variation in microclimate, the surface energy balance and ablation over a cirque glacier. *International J Climatol* 20(7): 733-758.
- Hicks DM, Shankar U, McKerchar AI, Basher L, Lynn I, Page M and Jessen M (2011) Suspended sediment yields from New Zealand rivers. *J Hydrol (NZ)* 50: 81-142.
- Hodder KR, Gilbert R and Desloges JR (2007) Glaciolacustrine varved sediment as an alpine hydroclimatic proxy. *J Paleolimnol* 38(3): 365-394.
- Horowitz AJ (2003) An evaluation of sediment rating curves for estimating suspended sediment concentrations for subsequent flux calculations. *Hydrol Process*, 17: 3387-3409.
- Howarth JD, Fitzsimons SJ, Norris RJ, and Jacobsen GE (2012) Lake sediments record cycles of sediment driven by large earthquakes on the Alpine Fault, New Zealand. *Geology* 40: 1091-1094.
- Kaufman CA, Lamoureux SF, and Kaufman DS (2011) Long-term river discharge and multidecadal climate variability inferred from varved sediments, southwest Alaska. *Quat Res* 76(1): 1-9.
- Kerr T (2013) The contribution of snowmelt to the rivers of the South Island, New Zealand. *J Hydrol (NZ)* 52(2): 61-82.
- Kidson JW (2000) An analysis of New Zealand synoptic types and their use in defining weather regimes. *Int J Climatol* 20(3): 299-316.
- Lamoureux, SF (1994) Embedding unfrozen lake sediments for thin section preparation. *J Paleolimnol* 10: 141-146.
- Lamoureux SF and Francus P (2014) Layers within layers: quantifying seasonal versus event processes in Arctic clastic varved sediments. *Past Global Changes Magazine* 22(1): 6-7.

- Lorrey AM, Williams P, Salinger J, Martin T, Palmer J, Fowler, A, Zhao J, Neil H (2008) Speleothem stable isotope records interpreted within a multi-proxy framework and implications for New Zealand palaeoclimate reconstruction. *Quat Int* 187(1): 52-75.
- Mackereth FJH (1958) A portable core sampler for lake deposits. *Limnol Oceanogr* 3: 181-191.
- Mann ME, Zhang Z, Hughes MK, Bradley RS, Miller SK, Rutherford S, and Ni F (2008) Proxy-based reconstructions of hemispheric and global surface temperature variations over the past two millennia. *Proc Natl Acad Sci USA* 105(36): 13252-13257.
- Nash J and Sutcliffe JV (1970) River flow forecasting through conceptual models part I—A discussion of principles *J Hydrol* 10(3): 282-290.
- Neukom R and Gergis J (2012) Southern Hemisphere high-resolution palaeoclimate records of the last 2000 years. *Holocene* 22(5): 501-524.
- Ojala AEK, Francus P, Zolitschka B, Besonen M and Lamoureux SF (2012) Characteristics of sedimentary varve chronologies: A review. *Quat Sci Rev* 43: 45-60.
- Orpin AR, Carter L, Page MJ, Cochran UA, Trustrum NA, Gomez B, Midenhall DC, Rogers KM, Brackely HL and Northcote, L (2010) Holocene sedimentary record from Lake Tutira: A template for upland watershed erosion proximal to the Waipaoa Sedimentary System, northeastern New Zealand. *Mar Geol* 270(1): 11-29.
- Orwin JF and Smart CC (2004) Short-term spatial and temporal patterns of suspended sediment transfer in proglacial channels, Small River Glacier, Canada. *Hydrol Process* 18(9): 1521-1542.
- Page M, Trustrum N, Orpin A, Carter L, Gomez B, Cochran U, Mildenhall D, Rogers K, Brackley H and Palmer A (2010) Storm frequency and magnitude in response to Holocene climate variability, Lake Tutira, North-Eastern New Zealand. *Mar Geol* 270: 30-44.
- Page MJ, Trustrum NA and DeRose RC (1994) A high resolution record of storm-induced erosion from lake sediments, New Zealand. *J Paleolimnol* 11: 333-348.
- Pharo CH and Carmack EC (1979) Sedimentation processes in a short residence-time intermontane lake, Kamloops Lake, British Columbia. *Sedimentology* 26(4): 523-541.
- Roop HA, Dunbar GB, Levy R, Vandergoes MJ, Forrest AL, Walker SL, Upton P, and Whinney J (2015) Seasonal controls on sediment transport and deposition in Lake Ohau, South Island, New Zealand: Implications for a high-resolution Holocene palaeoclimate reconstruction. *Sedimentology* 62(3): 826-844.

Schneider CA, Rasband WS, Eliceiri KW (2012) NIH Image to ImageJ: 25 years of image analysis. *Nat Methods* 9(7): 671-675.

Stockhecke M, Anselmetti FS, Meydan AF, Odermatt D and Sturm M (2012) The annual particle cycle in Lake Van (Turkey). *Palaeogeogr Palaeoclimatol Palaeoecol* 333: 148-159.

Striewski B, Shulmeister J, Augustinus PC, and Soderholm J (2013) Late Holocene climate variability from Lake Pupuke maar, Auckland, New Zealand. *Quat Sci Rev* 77: 46-54.

Tait A, Henderson R, Turner R and Zheng X (2006) Thin plate smoothing spline interpolation of daily rainfall for New Zealand using a climatological rainfall surface. *Int J Climatol* 26(14): 2097-2115.

Tomkins JD and Lamoureux SF (2005) Multiple hydroclimatic controls over recent sedimentation in proglacial Mirror Lake, southern Selwyn Mountains, Northwest Territories. *Can J Earth Sci* 42(9):1589-1599.

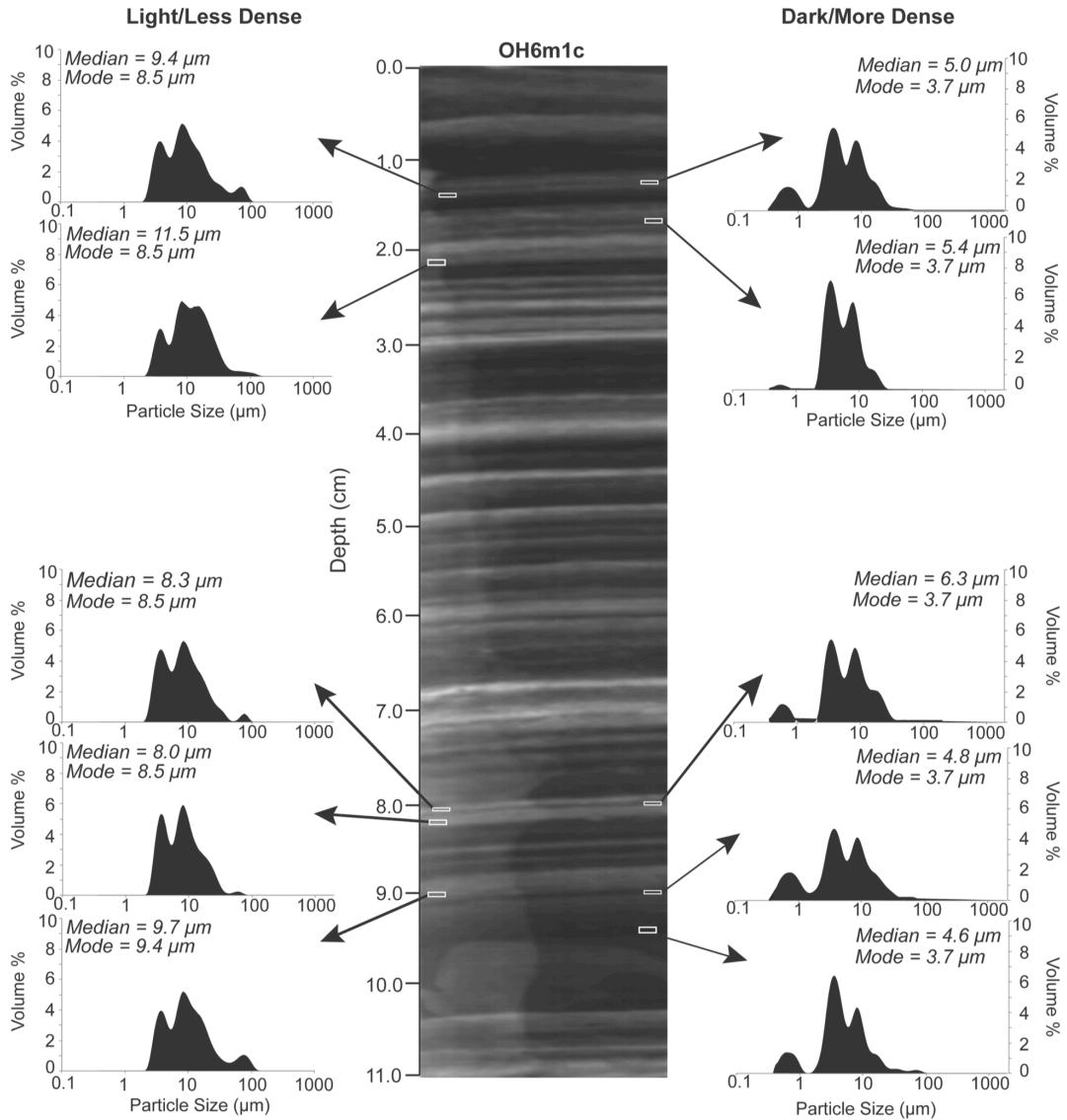
UNSCEAR Annex C (2000) Exposures to the public from man-made sources of radiation. *Sources and Effects of Ionizing Radiation: Sources UNSCEAR 1*:158-287.

Walling DE and Webb BW (1988) The reliability of rating curve estimates of suspended sediment yield: some further comments. *Sediment Budgets, IAHS Publ* 174.

Wheatley JJ, Blackwell, PG, Abram NJ, McConnell JR, Thomas ER, and Wolff EW (2012) Automated ice-core layer-counting with strong univariate signals. *Clim Past* 8:1869-1879.

Woods R, Hendricks J, Henderson R and Tait A (2006) Estimating mean flow of New Zealand rivers. *J Hydrol (NZ)* 45(2): 95-109.

Zolitschka B and Pike J (2014) Maximizing the information yield from annually resolving natural archives. *Past Global Changes Magazine* 22(1): 4-5.



Supplementary Fig. 1: Example of the relationship between particle size and the less dense (light) and more dense (dark) portions of the X-ray positives. The light layers are consistently associated with coarser particles (modal size $> 8 \mu\text{m}$), while the darker layers are associated with finer particles (modal size $3.7 \mu\text{m}$). The range of particle size fractions is similar to those measured in cores and sediment traps by Roop et al. (2015).

Supplementary Table 1 ¹³⁷Cs and ²¹⁰Pb sampling depths, depth correction for OH6m1c, concentrations, and modeled age-depth for the ²¹⁰Pb CRS model

OH1m1 ¹³⁷ Cs Mid-point Sample Depth (cm)	OH6m1c ¹³⁷ Cs Equivalent Mid- point Sample Depth (cm)	¹³⁷ Cs Concentration (Bq Kg ⁻¹)	OH1m1 ²¹⁰ Pb Mid- point Sample Depth (cm)	OH6m1c ²¹⁰ Pb Equivalent Mid-point Sample Depth (cm)	²¹⁰ Pb Excess Concentration (Bq Kg ⁻¹)	CRS Modeled Years	Age Uncertainty (± years)
1.5	2.5	1.33	0	0.5	19.99	2009	0.5
7.5	8.5	1.55	0.5	1.5	13.24	2009	0.5
13.5	14.5	2.10	1.5	2.5	22.91	2007	1.5
16.5	17.5	3.36	2.5	3.5	15.58	2004	1.5
17.5	18.5	4.79	3.5	4.5	13.21	2002	1.6
18.5	19.5	4.84	4.5	5.5	11.33	2000	1.6
19.5	20.5	9.13	5.5	6.5	11.61	1998	1.7
20.5	21.5	8.31	6.5	7.5	7.66	1996	1.7
21.5	22.5	7.15	7.5	8.5	8.23	1995	1.8
22.5	23.5	10.39	8.5	9.5	3.82	1993	1.8
23.5	24.5	10.50	9.5	10.5	8.20	1993	1.8
24.5	25.5	6.57	10.5	11.5	6.64	1991	1.9
25.5	26.5	5.05	11.5	12.5	7.75	1989	1.9
26.5	27.5	2.72	12.5	13.5	9.39	1988	2.0
27.5	28.5	4.44	13.5	14.5	10.22	1985	2.1
28.5	29.5	2.67	14.5	15.5	5.58	1983	2.1
29.5	30.5	0.89	19.5	20.5	5.53	1974	2.6
30.5	31	0.49	24.5	25.5	4.56	1963	3.3
31.5	31.5	0.00	29.5	30.5	2.38	1953	4.2
34.5	34.5	0.34	34.5	35.5	1.33	1945	4.9
37.5	37.5	0.00	39.5	39.5	0.93	1940	5.2
40.5	40.5	0.00	44.5	44.5	3.11	1930	6.1
			49.5	48.5	1.59	1906	10.7
			54.5	52.5	0.15	1891	12.6
			59.5	57.5	0.51	1884	6.7

Supplementary Table 2 Example of Spearman's rank correlations between hydrometeorological variables, varve thickness and varve motif. Correlations include here include only those with $r \geq 0.20$. There are no robust and significant correlations between varve thickness or type and hydrometeorology over the instrumental record. See Methods for a list of all correlations tested in this study and a description of temporal increments.

Site (listed from south to north up the catchment)	Temporal Increment	Varve Type (All refers to full time- series)	Meteorological Variable	Total Varve Thickness		Coarse Unit Thickness		Fine Unit Thickness		Fine Unit without Interbeds Thickness		Interbed Thickness	
				<i>r</i>	<i>p</i>	<i>r</i>	<i>p</i>	<i>r</i>	<i>p</i>	<i>r</i>	<i>p</i>	<i>r</i>	<i>p</i>
Freehold Creek	Total SON	All	Inflow			-0.29	0.08						
Freehold Creek	Total SONDJF	All	Precipitation	0.20	0.07								
Freehold Creek	Total MAMJJA	All	Precipitation					-0.30	0.06				
Freehold Creek	Avg MAMJJA	All	Precipitation	-0.30	0.07								
Freehold Creek	Total JJA	All	Precipitation					-0.38	0.02				
Freehold Creek	Total JJA	All	Precipitation	-0.36	0.03								
Greta Stream	Total Annual	All	Precipitation			-0.28	0.09						
Greta Stream	Total SON	All	Inflow			-0.36	0.03						
Greta Stream	Total MAMJJA	All	Precipitation					-0.28	0.09				
Greta Stream	Total JJA	All	Precipitation					-0.32	0.05				
Greta Stream	Total JJA	All	Precipitation	-0.28	0.09								
Lower Dobson	Total SON	All	Inflow			-0.32	0.05						
Lower Dobson	Total MAMJJA	All	Precipitation					-0.27	0.10				
Lower Dobson	Total JJA	All	Precipitation					-0.35	0.03				
Lower Dobson	Total JJA	All	Precipitation	-0.34	0.04								
Lower Hopkins	Total SON	All	Inflow			-0.31	0.06						
Lower Hopkins	Total SONDJF	All	Precipitation	0.30	0.11								
Lower Hopkins	Total MAMJJA	All	Precipitation					-0.29	0.08				
Lower Hopkins	Total MAMJJA	All	Precipitation	-0.29	0.08								
Lower Hopkins	Total JJA	All	Precipitation	-0.34	0.04								
Ohau Inflow	Total SON	Type A	Inflow			-0.41	0.05						
Ohau Inflow	Total SON	All	Inflow			-0.29	0.08						
Ohau Inflow	Total SON	All	Precipitation			-0.26	0.11						
Ohau Inflow	Total DJF	Type C	Inflow					0.55	0.08				
Ohau Inflow	Average DJF	Type C	Inflow					0.55	0.09				
Ohau Inflow	Total SONDJF	All	Inflow			-0.23	0.04						
Ohau Inflow	Average SONDJF	All	Inflow			-0.23	0.04						
Ohau Inflow	Total MAMJJA	All	Precipitation					-0.32	0.05				
Ohau Inflow	Total MAMJJA	All	Precipitation	-0.33	0.04								
Ohau Inflow	Total JJA	Type A	Inflow					-0.37	0.08				
Ohau Inflow	Total JJA	All	Inflow					-0.20	0.08				
Ohau Inflow	Total JJA	All	Inflow							-0.20	0.08		
Ohau Inflow	Total JJA	All	Precipitation	-0.41	0.09								
Ohau Inflow	Average JJA	All	Inflow					-0.20	0.08				
Ohau Inflow	Average JJA	Type A	Inflow					-0.37	0.08				
Upper Dobson	Total SON	All	Inflow			-0.32	0.05						
Upper Dobson	Total MAMJJA	All	Precipitation	0.28	0.10								
Upper Dobson	Total JJA	All	Precipitation					-0.29	0.08				
Upper Dobson	Total JJA	All	Precipitation	-0.32	0.05								
Upper Hopkins	Total SON	All	Precipitation					-0.29	0.08				
Upper Hopkins	Total JJA	All	Precipitation					-0.35	0.03				
Upper Hopkins	Total JJA	All	Precipitation	-0.26	0.11								

CHAPTER 4

Hydroclimate variability and regional atmospheric circulation over the past 1,350 years reconstructed from Lake Ohau, New Zealand

This chapter is in preparation for submission to the peer-reviewed journal *Quaternary Science Reviews*.

Anticipated Authorship List:

Heidi A. Roop

Gavin B. Dunbar

Marcus J. Vandergoes

Richard Levy

Andrew M. Lorrey

Jamie Howarth

ABSTRACT

The current lack of high-resolution paleoclimatic records from the Southern Hemisphere mid-latitudes limits our ability to place observed climate over instrumental record in context with the preindustrial period. Continuous, high-resolution terrestrial records of climate offer a means with which to fill this gap. Here we present a 1,350-year record of hydroclimatic variability and regional circulation derived from an annually laminated sediment record from Lake Ohau, South Island, New Zealand. The clastic laminae in Lake Ohau can be subdivided into three major motifs, each of which is associated with changes in the frequency of summer and autumn precipitation-induced inflow events, or relative wet/dry conditions. Inflow and precipitation in New Zealand's western South Island climate district are well correlated with a regional synoptic climate regime classification scheme that associates 1,000-hPa geopotential height synoptic patterns with temperature and precipitation anomalies across New Zealand. Utilizing this classification scheme to assign synoptic regimes to 25-year time slices from Lake Ohau and a nearby tree-ring temperature reconstruction from Oroko Swamp provides a means to generate a paleo-atmospheric circulation index for the western South Island of New Zealand. This circulation index shows significant periods of change, most notably 835 – 985 AD when northerly airflow dominated and from 1385 – 1710 when strong southerly airflow persisted. Comparison with regional reconstructions of SAM and ENSO show both in-phase and anti-phase relationships, which point to the oscillating role of the high-latitudes and tropics as drivers of New Zealand's climate over the last ~1,350 years. A notable shift in circulation occurs during the 'Little Ice Age' (1385-1710 AD) and coincides with a negative phase SAM and weak tropical teleconnection, which highlights the role that these phenomena can play in driving climate across the South Pacific.

Keywords: Southern Hemisphere; varves; paleocirculation; SAM; ENSO

4.1 INTRODUCTION

Detailed understanding of past and projected variability in climate systems operating in the Southern Hemisphere (SH) is, in part, limited by the paucity of high-resolution paleoclimate reconstructions from this region (Mann and Jones, 2003; Mann et al., 2008; Neukom and Gergis, 2012). In the SH mid- to high-latitudes, instrumental measurements show that on inter-annual timescales the distribution of precipitation and temperature is strongly controlled by synoptic climate drivers originating in both the tropics and Antarctica (Ummenhofer et al., 2009; Renwick, 2011; Ding et al., 2012; Abram et al., 2014). Two primary SH climate drivers are the Southern Annular Mode (SAM) and the El-Niño-Southern Oscillation (ENSO), which influence both the strength and position of the SH westerly winds and consequently regional temperature and rainfall patterns (e.g. Ummenhofer and England, 2007; Fogt et al., 2011; Abram et al., 2014).

However, trends over the instrumental period point to significant anthropogenic influences including the recent persistence of the positive phase SAM, which is attributed mainly to stratospheric ozone depletion and greenhouse gases (Thompson et al., 2011). Existing instrumental records are too short to confidently attribute anthropogenically-driven climate impacts to the observed inter-decadal and multi-decadal variability in ENSO (Stevenson et al., 2012; Li et al., 2013). Thus, the amplitude, timing and interdependence of SAM and ENSO remain poorly constrained beyond the instrumental record, limiting understanding of the range of natural variability in these systems (Neukom and Gergis, 2012; Li et al., 2013; Abram, et al., 2014).

Because these drivers can vary on daily to annual (SAM) and decadal (ENSO) timescales (Fogt and Bromwich, 2006; Yeo and Kim, 2015), highly resolved proxies (annual to decadal) are required to reconstruct variability in these features. Improving the spatial and temporal coverage of such reconstructions is challenging because the core of the SH westerlies is only intersected by a few landmasses, limiting the regions from which high-resolution terrestrial climate records can be generated (Fig. 1; Neukom and Gergis, 2012). New Zealand's South Island intersects the SH westerly winds in the SW Pacific basin. Thus, temperature and precipitation fields over the western South Island (WSI) are accordingly well correlated with both ENSO and SAM (Renwick, 2011; Jiang et al., 2013; Lorrey et al., 2014). This

suggests that the WSI is particularly well situated for examining variability in, and interactions between, these synoptic climate features affecting the entire SH.

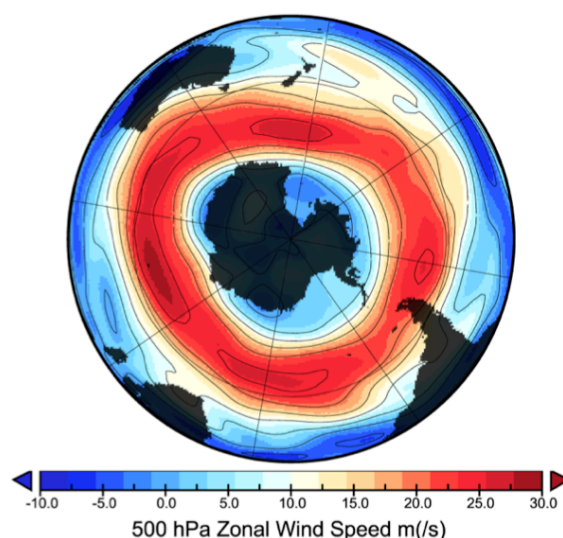


Fig. 1: The circumpolar westerly winds are a key feature of Southern Hemisphere atmospheric circulation, and are only intercepted by a few landmasses. Long-term (1948-2014) mean zonal wind speeds from reanalysis data provided by NOAA/OAR/ESRL PSD (www.esrl.noaa.gov/psd/).

One of the first clastic varve sequences identified in New Zealand was recently recovered from Lake Ohau in the WSI (Fig. 2; 44.234°S, 169.854°E), and may be a powerful tool for investigating the interplay between the southern high latitude and equatorial circulation patterns beyond the instrumental period. In particular, the stratigraphy of this lacustrine record records changes in austral warm period (December-May) inflow (Roop et al., accepted (Chapter 3)). Constraints on timing and amount of lake inflow can help to determine variability in hydrologic resources including the length and duration of drought or flood conditions. Furthermore, regional precipitation and inflow are sensitive to subtle changes in the strength and direction of westerly airflow (Salinger et al., 2004; Lorrey et al., 2007; Ummenhofer and England, 2007). Therefore, precipitation- and inflow-sensitive proxies from New Zealand can provide an important perspective on paleo-atmospheric circulation.

Specifically, we construct a WSI paleo-atmospheric circulation index derived from the reoccurrence of inflow-sensitive varve facies from Lake Ohau over the last 1.3 ka in combination with a regional tree-ring-derived summer temperature

reconstruction (Cook et al., 2002). This index is based on the regional climate regime classification scheme and associated temperature and precipitation anomalies defined by Kidson (2000). While the climate regimes and types characterize local circulation patterns, they also show annual and seasonal sensitivity to tropical and SH high-latitude synoptic circulation patterns including SAM and ENSO (Table 2; Kidston et al., 2009; Jiang et al., 2011; Renwick, 2011; Jiang et al., 2013). Therefore, reconstructed changes in Kidson regimes are interpreted as the result of specific combinations in the strength and phase of these synoptic climate drivers back in time. Comparisons of this southern New Zealand circulation index to recently published SAM (Abram et al., 2014) and ENSO (Li et al., 2013) reconstructions help to elucidate the varying influence of tropical and austral high latitude climate drivers on late Holocene climate in southern New Zealand, and the broader South Pacific region.

4.1.1 Geographic and Climatic Setting

Lake Ohau is situated in the WSI climate district as defined by Kidson (2000; Fig. 2A). The headwaters of the lake lie in the Southern Alps and experience ~76% higher precipitation than the lake itself (Roop et al., 2015 (Chapter 2); Fig 2B). This gradient is the result of overspill of orographic precipitation along the axial Southern Alps, which intersect westerly airflow (Fig. 2B, Sinclair et al., 1997).

In the Pacific sector of the SH, westerly wind circulation is influenced by a combination of high-latitude and tropically induced variability associated with SAM and ENSO, respectively (Ummenhofer and England, 2007; Renwick, 2011; Ding et al., 2012; Jiang et al., 2013). The SAM, also known as the Antarctic Oscillation, is described by the zonally symmetric dipole in sea level pressure between 60°S and 40°S, and serves as a measure of westerly airflow (Marshall, 2003). The SAM is associated with up to 64% of year-to-year variability in WSI precipitation during austral summer (December to February (DJF); Ummenhofer et al., 2009). It is therefore expected to have a strong influence on Lake Ohau climate and the climate-proxy record preserved in the sediments, as lake inflow and sediment accumulation are greatest during the austral warm period (Roop et al., 2015).

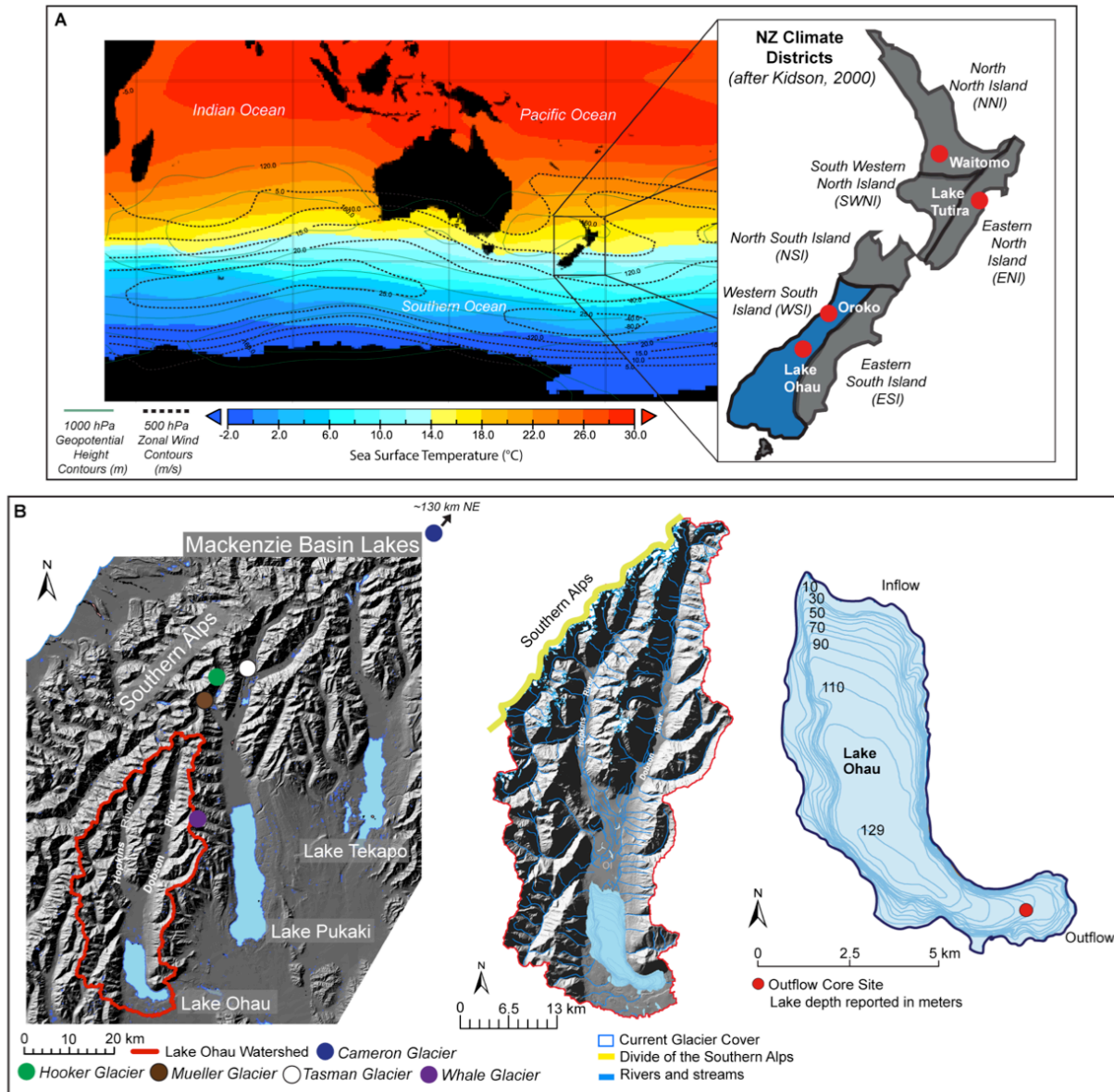


Fig. 2: A) Long-term mean sea surface temperature (SST) from HadISST (Hadley Centre Sea Ice and Sea Surface Temperature dataset), geopotential height (m) at 1000-hPa and zonal wind contours at 500 hPa from NCEP reanalysis (NOAA/OAR/ESRL PSD; www.esrl.noaa.gov/psd/) showing the regional oceanic and atmospheric setting of the New Zealand region. Inset map of New Zealand's six climate districts as defined by Kidson (2000) and regional paleoclimate studies referred to in this study. B) Hydrologic setting of Lake Ohau, including location of local glaciers (see Section 4.3.2).

While SAM primarily results from high-latitude atmospheric dynamics, the intensity, latitudinal position and variability of the SAM are also influenced by meridional circulation initiated in the central tropical Pacific (Ding et al., 2012; Kidson, 1998). In particular, ENSO and SAM show significant correlation that is strongest during austral summer and winter (Fogt and Bromwich, 2006; L'Heureux and Thompson, 2006; Fogt et al., 2011; Ding et al., 2012). ENSO is a coupled oceanic-atmospheric climate mode whose intensity is frequently described by sea

surface temperature (SST) anomalies in regions of the central tropical Pacific Ocean (e.g. in the Niño 3.4 region, positive anomaly = El Niño, negative anomaly = La Niña; See Chapter 1). These SST fluctuations are linked to variations in the SAM through the origin, position and propagation of planetary atmospheric (Rossby) waves, which in turn influence the position of the mid-latitude jet (Grassi et al., 2005; Ding et al., 2012). Approximately 25% of the variance in SAM has been attributed to ENSO through similar mechanisms (L'Heureux and Thompson, 2006).

However, understanding of the relationship between high-latitude and equatorial Pacific zonal circulation is complicated by short instrumental records (~100 years), which reflect both natural variability and that forced by anthropogenic influences including stratospheric ozone depletion and greenhouse gas-induced warming (Thompson and Solomon, 2002; Thompson et al., 2011). The Lake Ohau varved record, enhanced by comparison with similarly-resolved records of SAM (Abram et al., 2014) and ENSO (Li et al., 2013) from other regions, aims to explore circulation patterns and the relative role of the tropics and SH high-latitudes as drivers of regional and South Pacific climate over the last 1,350 years.

4.2 ANALYTICAL APPROACH AND RESULTS

A 5.5 m-long Mackereth core (OH6m1c) was collected from the Lake Ohau Outflow site in October 2012 and is the focus of this research. Correlation between gravity core GCS_1 (collected May 2013 from the same location as OH6m1c, and includes the sediment water interface) indicates that the core top of OH6m1c represents varve year 2010. A varve year is defined as September 1st - August 31st (Roop et al., accepted (Chapter 3)).

4.2.1 Age Model Development

Age model development for the 5.5-m Lake Ohau sedimentary sequence is on its own a dedicated research investigation as part of the broader Lake Ohau climate history project. The full details of the dating and age model development are being prepared for subsequent publication (Vandergoes et al., in prep.) but are summarized here and in the supplementary information.

The age model for core OH6m1c is constructed from a combination of methods. First, manual layer counts were conducted using thin-sections and X-radiographs (following Roop et al., accepted (Chapter 3)). Each laminae was counted,

measured and described according to the facies model outlined in Chapter 3 (Supplementary Fig. 2). A ‘varve year’ is assigned to each couplet based the occurrence of a sharp density change in the X-radiographs and a visual change in particle size observed in thin-section. Multiple operators were used for manual layer counting to 60 cm. A single operator applied the established criteria to count to the base of OH6m1c. Manual layer counts yielded a total of 1379 years, equivalent to 632 AD. Secondly, direct and independent ages from ^{137}Cs analysis, pollen marker horizons (Supplementary Methods Fig. 1), radiocarbon dating of terrestrial plant macrofossils and *Cladocera* spp. (water flea) concentrates were used to provide independent age control for the Lake Ohau age model (see Supplementary Methods).

Both the layer counts and independent chronologies were integrated using the P_Sequence prior model in OxCal 4.2.4 to produce an age model for the Ohau6m1c core (Bronk Ramsey and Lee, 2013). The P_Sequence prior model can incorporate information about random variability in sedimentation processes as opposed to other models such as the U_Sequence model where sedimentation processes are held constant (Bronk Ramsey, 2008). The specific design of the P_Sequence prior model makes it particularly suitable for capturing uncertainty associated with layer count chronologies, such as complex annual or missing layers, while at the same time integrating independent chronological data (Bronk Ramsey 2008). The ability to capture uncertainty associated with anomalous layers is important for accurate age modeling of the Ohau6m1c core because the layer counts for the full 6m sequence were derived from a single operator and lack estimates of error. The set up of the P_Sequence model for Ohau6m1c is outlined in the Supplementary Methods and follows published methodologies (e.g. Blockley et al., 2007; 2008; Bronk Ramsey, 2008). The chronology produced by the model provides an average precision of ± 25 years (2σ) and a basal age of 646 ± 86 AD (2σ).

Lake Ohau Age Model

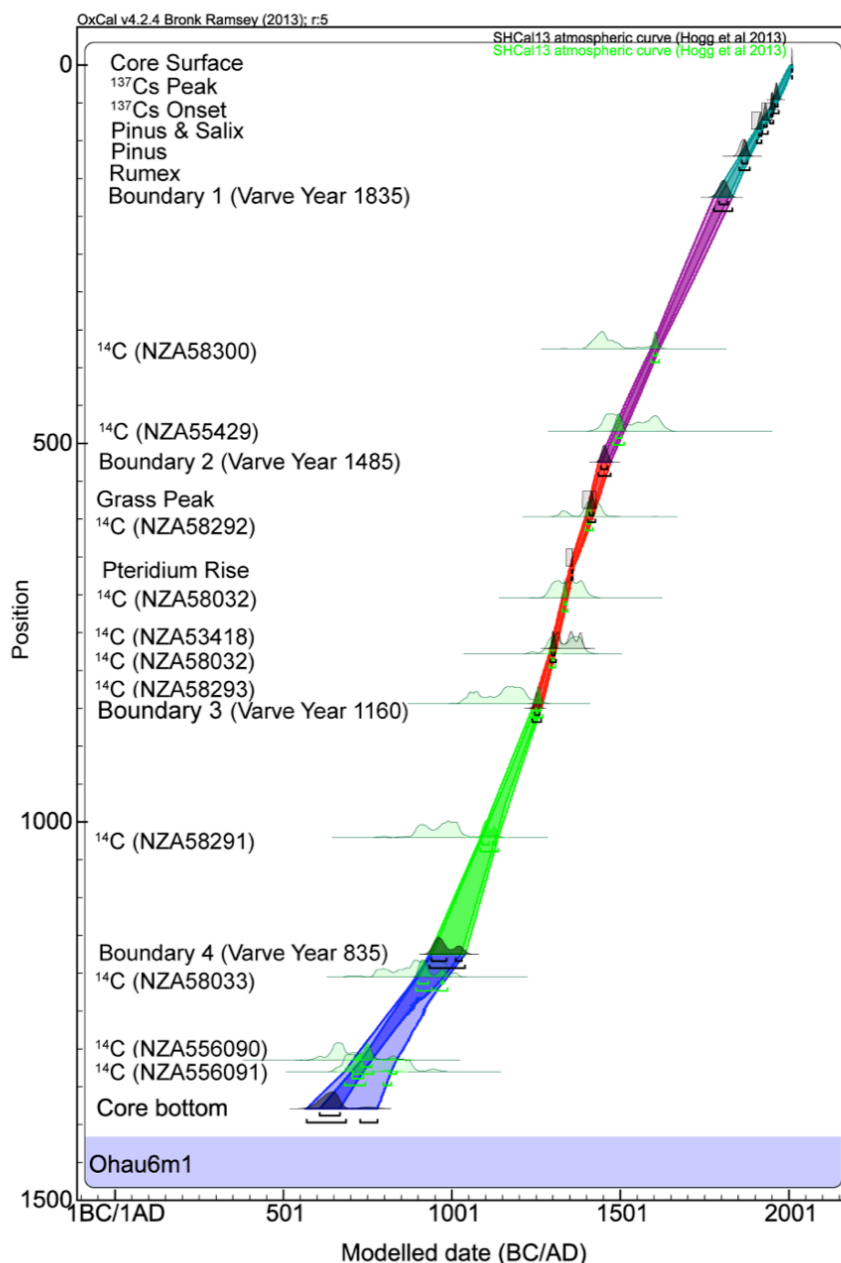


Fig. 3: A) Calendar year age model for the Lake Ohau record based on ^{137}Cs , ^{14}C dating, and age marker horizons including pollen and layer counting. The chronological model was produced in OxCal v4.2.4 (Bronk Ramsey, 2013) using the SHCal 13 calibration curve (Hogg et al. 2013). The model uses the P_sequence algorithm applied against layer counts. The figure includes the calendar age likelihood (light grey and light green) and posterior probability density functions (dark grey and dark green), as well as the age models at the 95% level of confidence. Colored sections (teal, purple, red, green, and blue) reflect four noted changes, or boundaries, in sedimentation rate as determined by varve motif (e.g. Change 1; see text). The y-axis refers to layer count position.

4.2.2 Varve Classification and Distribution

The lamination stratigraphy in OH6m1c is characterized by three primary motifs (labeled A, B and C) (Table 1; Supplementary Fig. 1; Roop et al., accepted (Chapter 3)). Each motif results from different hydrologic conditions during the austral warm period (December - May (DJFMAM)) when rainfall and associated sedimentation are highest (Roop et al., accepted (Chapter 3)). Motif A is produced under inferred average-to-below (dry) lake inflow conditions. Motif B is characterized by thin silt layers, which form as a result of frequent precipitation-induced inflow events throughout the austral warm period. Motif B is the most frequently occurring type during the instrumental record and is interpreted to represent average-to-above (wet) inflow conditions. Over the instrumental record, total seasonal inflow between December and May is on average 14% greater during years characterized by motif B than years defined by motif A.

Motifs A and B therefore represent an aggregate of the seasonal conditions prevailing during their deposition (e.g. summers with multiple inflow events). In contrast, Motif C laminae form in response to extreme inflows, or floods, which our observations suggest may be the result of individual short-duration (hours) but intense, and often single meteorological events. The significant change in sediment and water flux into the lacustrine system during these events subsequently masks the annual sediment cycle (Roop et al., 2015). By linking sedimentation patterns to inflow we are further able to associate sediment deposition directly with rainfall, as headwater precipitation in the Ohau catchment and inflow are correlated at $r = 0.74$, $p = 0.0001$ (Roop et al., accepted (Chapter 3)). These relationships form the basis of the methodological approach and interpretations.

Each varve is characterized as one of these three motifs (Table 1). To examine the frequency distribution of each motif over time, the number of occurrences of motifs A, B and C were counted in 25-year increments (Fig. 4A). A 25-year bin was used as it approximates the 2σ uncertainty associated with the age model (± 25 years) and is of sufficient length to associate variability with potential shifts in the base climate state (Lorrey et al., 2014). As the focus for this chapter is on seasonal average, rather than event-dominated conditions, we omit motif C from further analysis for this study.

Table 1 Characteristics of the three primary varve motif preserved in OH6m1c. Descriptions and interpretations adapted from Roop et al. (accepted (Chapter 3)).

Varve Motif	A	B	C
Basic Description*	Fine silt unit grading into a very fine silt unit, lacks sublaminae.	Fine silt unit grading to a very fine silt unit containing one or more matrix supported fine silt sublaminae	Fine silt basal unit grading into a thick (~3.5 mm) ungraded fine silt layer; one or two silt laminae commonly occur immediately above the basal unit.
Median Thickness^	2.50 mm	4.26 mm	8.54 mm
Percent of Record	40.0 %	56.3 %	3.7 %
Climate Interpretation	Average-to-below inflow/precipitation	Average-to-above inflow/precipitation	Flood Event-dominated

*After Roop et al. (accepted (Chapter 3)); ^See *Supplementary Fig. 2 for distributions*

To examine seasonal conditions over the last 1,350 years, the counts of motifs A and B in each 25-year bin were treated in three steps. First, the frequency of occurrence of motifs A and B were converted to an anomaly relative to the 20th century by subtracting the mean of the 25-year bin occurrences between 1900-1999 (motif A = 7.5; motif B = 14.75) of each motif. Second, these anomalies were converted to a ratio of B/A (Fig. 4B). This ratio is used as a relative index of ‘wet’ to ‘dry’ austral warm period conditions based on the relationship between varve motif, inflow and precipitation with positive values indicting an increase in motif B, or wet conditions. Finally, this wet/dry index was linearly detrended to remove insolation and CO₂ forcing effects (Fig. 4B). This helps to isolate changes resulting specifically from variability in atmospheric circulation (Lorrey et al., 2008).

4.2.3 Regional Climate Regime Classification

A Regional Climate Regime Classification (RCRC) for New Zealand (Kidson, 2000) provides a basis for interpreting paleoclimate proxy data in the context of paleo-atmospheric circulation patterns (Lorrey et al., 2007; 2008; 2014). The RCRC is based on twelve different synoptic weather types (Fig. 5; Kidson, 2000), determined using a k-means clustering of twice-daily fields of 1,000-hPa height from the National Centers for Environmental Prediction/National Center for Atmospheric Research (NCEP/NCAR; Kidson, 2000; Lorrey et al., 2014). These synoptic types are then grouped into three regimes: Trough, Zonal and Blocking, which represent similar synoptic situations (Fig. 5; Kidson, 2000).

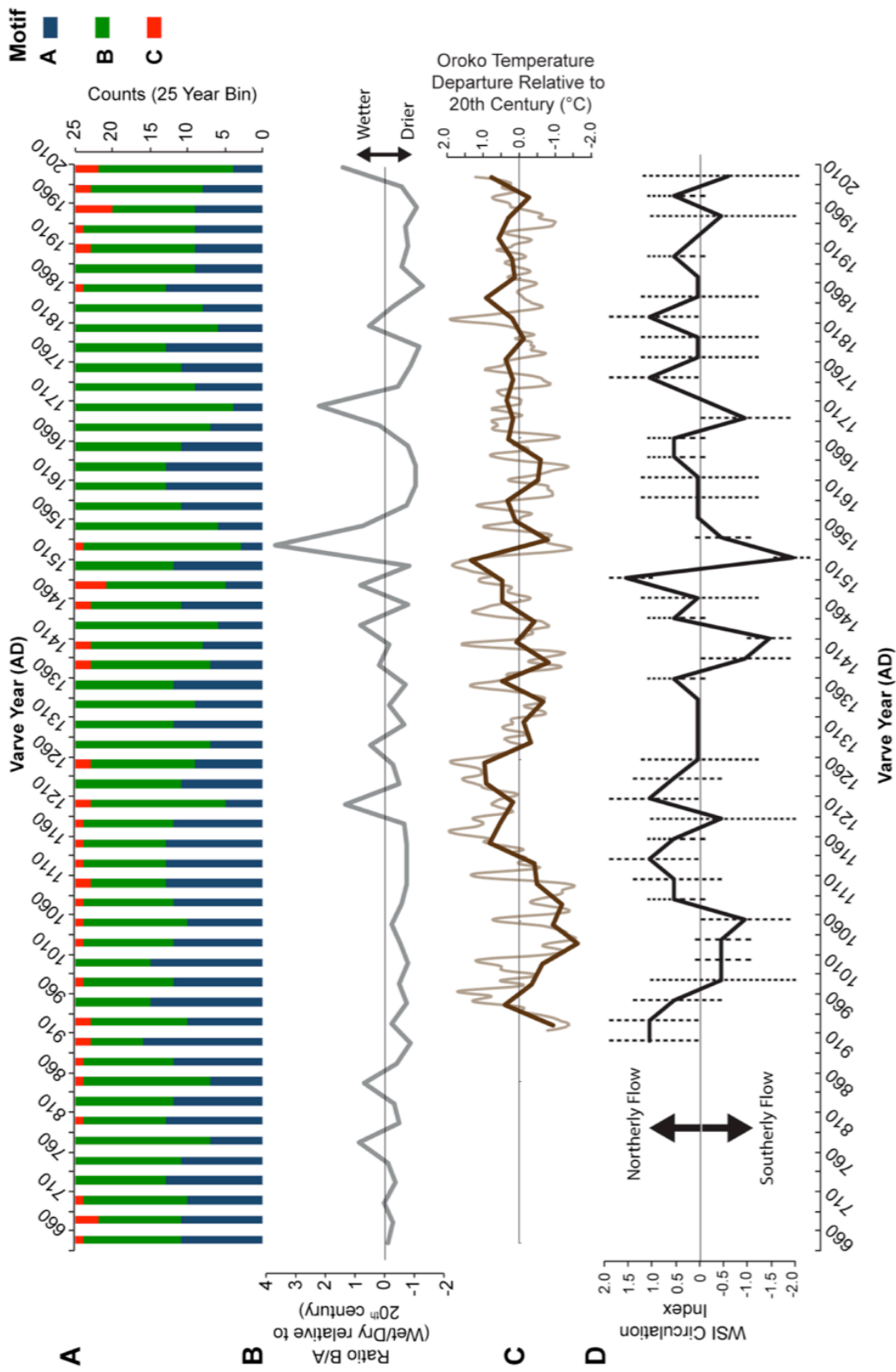


Fig. 4: A) Ohau motif counts in 25-year bins from 2010-635 AD; B) Ratio of motifs B/A as a semi-quantitative index of wetter/drier summer conditions; C) Oroko Swamp temperature reconstruction binned in 25-year intervals and smoothed with a 25-point LOESS filter (Section 4.2.4; Cook et al., 2002); and D) western South Island circulation index constructed from synoptic conditions the inferred from the Lake Ohau precipitation and Oroko Swamp temperature indices (Section 4.2.4).

The Trough regime primarily results in unsettled conditions over New Zealand, with the Zonal regime characterized by strong westerly airflow, while the Blocking regime is associated with settled, anti-cyclonic conditions (Kidson, 2000; Renwick, 2011).

To categorize and calculate the temperature and precipitation anomalies that result from these different synoptic regimes, Kidson (2000) utilized the six climate districts determined by Mullan (1998; Fig 2A; Fig. 6). These districts were designated based on mean monthly precipitation and temperature departures measured across New Zealand (Fig. 6; Mullan, 1998; Kidson, 2000). This regional classification and the associated anomalies are also linked to extreme rainfall events and river inflows in New Zealand, with Trough conditions being predominately associated with the unsettled conditions that lead to these events on the South Island (McKerchar et al, 2010; Griffiths, 2011).

To determine whether a particular regime type influences Lake Ohau inflow, and by extension sediment accumulation patterns, an analysis the prevailing synoptic conditions immediately prior to peak inflow was conducted for all 159 inflow events exceeding $400 \text{ m}^3 \text{ s}^{-1}$ between 1948 and 2011 (after McKerchar et al., 2010). Synoptic conditions were considered preceding the inflow event by 12-hours, as there is a lag between rainfall and the resultant hydrologic response (after McKerchar et al., 2010).

4.2.4 Assigning Paleo-regimes

For each 25-year bin of the B/A wet/dry index (Fig. 4B), a scale was used to assess the extent to which calculated inflow within each bin of the B/A index was above, below or near normal. For this scale, shifts to values above (below) one were assigned as wetter (drier) conditions at Lake Ohau. Values between 0 and 0.5 (-0.5) were assigned normal-to-above (-below) conditions, while zero indicated 'normal' conditions. The cut-offs on this scale were assigned arbitrarily, but serve as a means for categorizing and classifying these data. The results of this scaling for each 25-year time slice are summarized in the second column of Table 3. The scale is the first step in categorizing the Ohau proxy data in order to determine the dominant weather regime (i.e. Zonal, Blocking or Trough; see below).

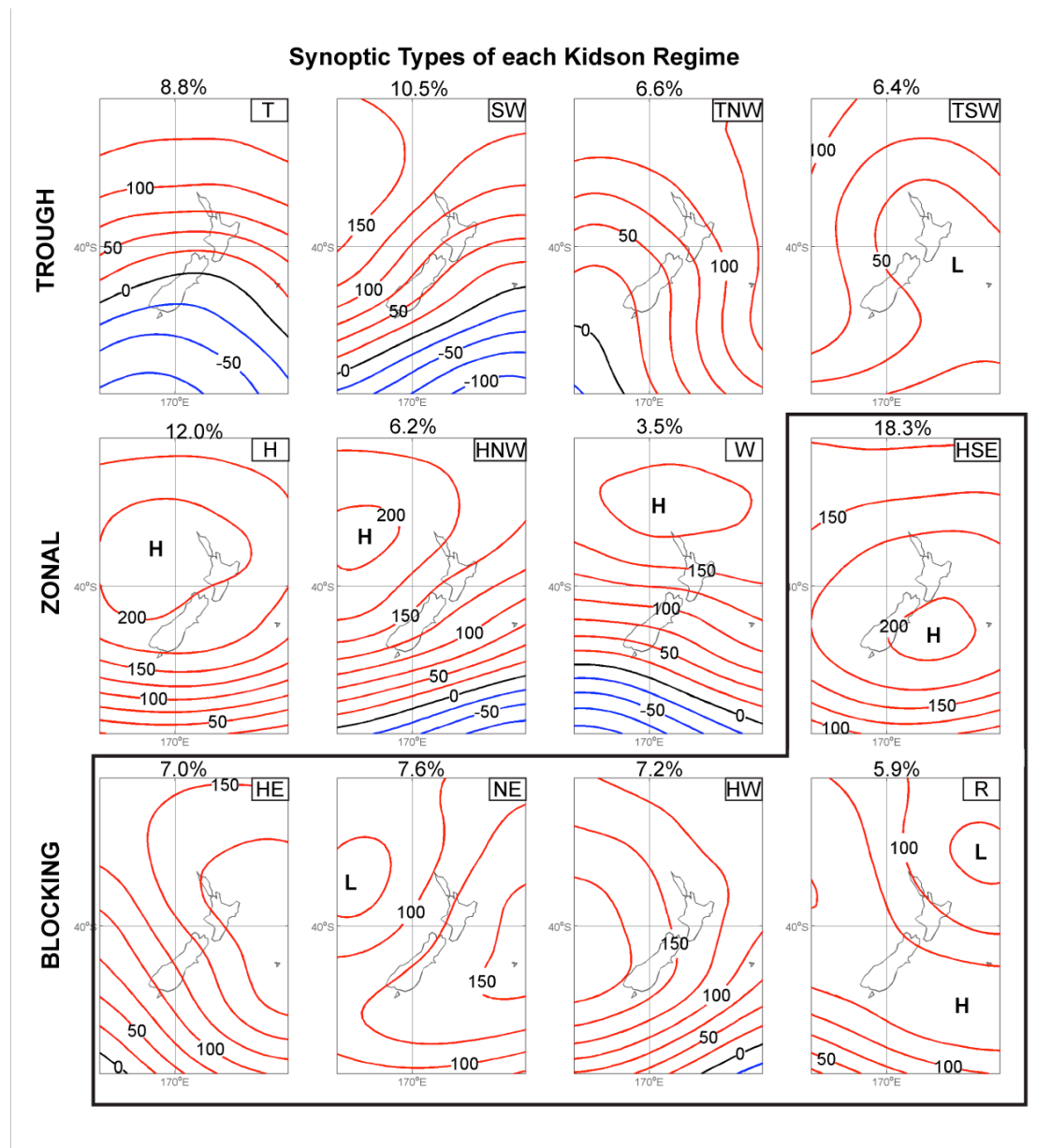


Fig. 5: Twelve different synoptic types grouped into three Kidson regimes (after Renwick, 2011). The percent occurrence from 1948 to 2013 is shown at the top of each box. Contours are 1,000-hPa geopotential height (m). Where: T= westerly flow, low near South Island (SI); TNW= Trough to west of New Zealand (NZ); SW= south-west flow, high to north-east; H= high over NZ; HNW= High west of North Island (NI); W= westerly flow, high over NI; HSE= high to south east of NZ; HE= High to east of NI; NE = north-east flow; HW= high to west of SI; and R= high over SI (after Kidson (1994)).

Regional New Zealand Climate Districts and Regimes

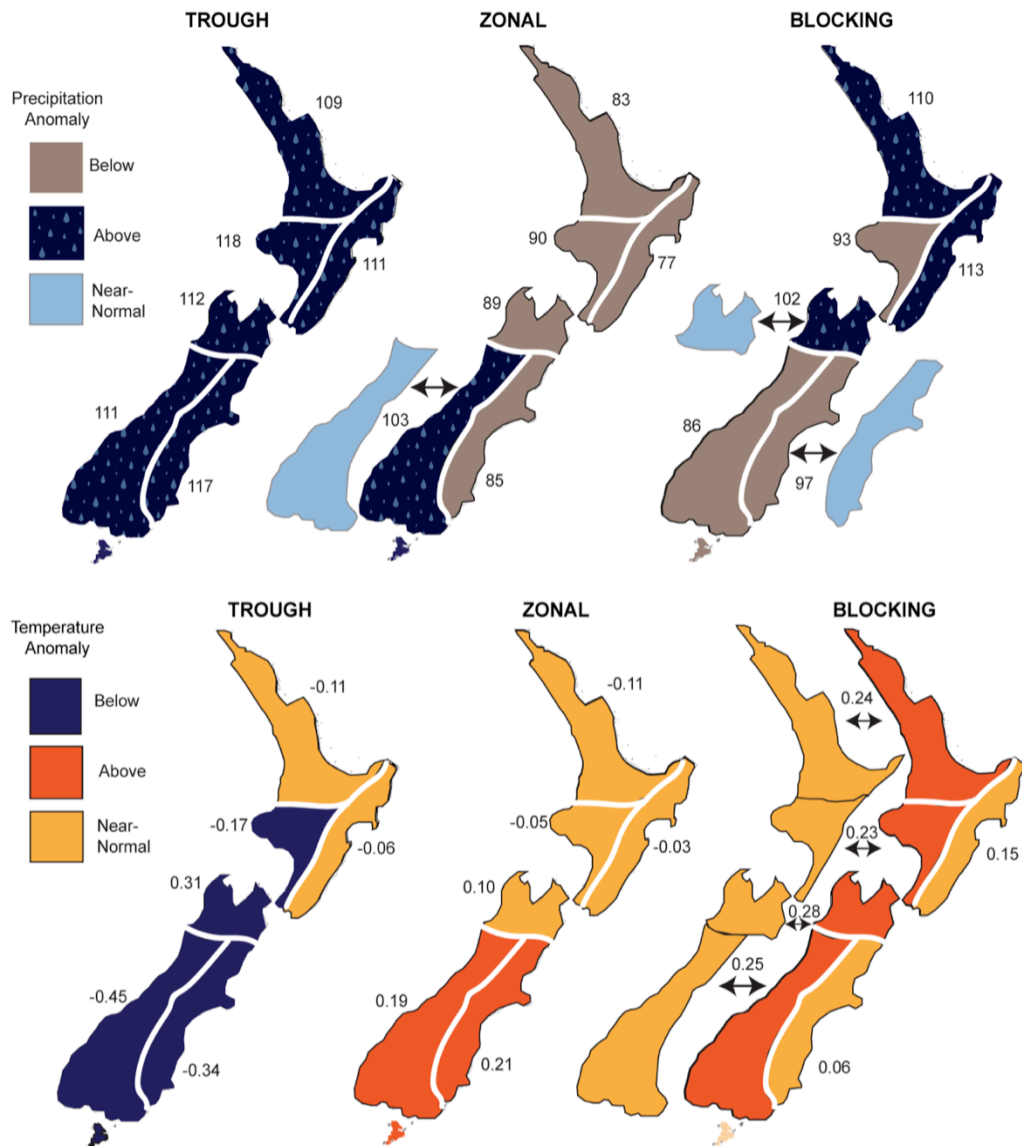


Fig. 6: Precipitation (%) and temperature (°C) anomalies for New Zealand’s climate districts (after Kidson, 2000). Anomalies are based on the analysis of Renwick (2011) for Trough, Zonal and Blocking regimes spanning the period of 1958-2010. Figure modified from Lorrey et al. (2014).

Table 2 Kidson regimes and types with occurrence over the instrumental record and relationship with Ohau inflow events and associated synoptic climate features over DJFMAM.

Kidson Regimes	Wind Direction/ WSI Conditions*	Occurrence (1948-2013)	Association with Ohau Inflow Events ($\geq 400 \text{ m}^3 \text{ s}^{-1}$)	Association with SOI*	Association with SAM*
Trough	Mixed/Wet, Cold	32.3%	57.6%	> during negative SOI (El Niño)	> during negative SAM
Zonal	Westerly & South-westerly/Wet-Normal, Warm	21.7%	24.7%	> during negative SOI (El Niño)	> during positive SAM
Blocking	Northerly & Easterly/Dry, Warm	46%	17.7%	> during positive SOI (La Niña)	> during positive SAM

*From Renwick, 2011

A similar scale was applied to the summer temperature tree-ring reconstruction from Oroko Swamp, which extends to 900 AD (Fig. 2A, 4C; Cook et al., 2002). Oroko Swamp is situated in the WSI where tree-ring width was determined to be most sensitive to changes in austral summer temperature, when maximum growth occurs (Cook et al., 2002). The Oroko temperature time-series was averaged with a 25-year running smooth, normalized to average 20th century air temperature (Cook et al., 2002 and references therein), and then linearly detrended (Fig. 4C). For the Oroko data, shifts to values above (below) one were assigned as warmer (colder) with shifts between 0 and 0.5 (-0.5) as average-to-above (-below) conditions. The results of the scaling for the Oroko time-series are presented in the third column of Table 3.

Indices of wet/dry and warm/cool in 25-year bins at both Lake Ohau and Oroko Swamp respectively can be assigned to characteristic RCRC regimes based on the precipitation and temperature anomalies described by Kidson (2000; Fig. 6). For example, in a period characterized by wet conditions at Ohau and cold conditions at Oroko equate to a Trough/Trough (T/T) regime because troughs are associated with both a positive precipitation anomaly and a negative temperature anomaly in the WSI (Fig. 6). Table 3 summarizes the combinations of Ohau/Oroko RCRC regimes spanning from 2010-900 AD.

Next, the different combinations of Zonal, Blocking and Trough regimes as indicated by both Ohau and Oroko time-series were weighted on a scale ranging from

2 to -2, with Zonal as the center point (Zonal = 0; Table 4). Additional regime combinations have a low probability of occurrence based on the analysis of Kidson (2000; Table 4). This 2 to -2 scaling scheme is used to infer synoptic conditions at both Ohau and Oroko with the average value of the two sites used to assess the agreement between the two locations. For example, during the 2010-1985 bin the average between the Ohau (T = -2) and Oroko (Z-B= 1) is -0.5, suggesting zonal to weakly trough conditions.

The regimes reconstructed for Oroko Swamp should agree, as they are in the same climate district, but differences can arise from issues with chronology, averaging effects, or heterogeneity within the climate district (Kidson, 2000). These sites also sit on opposite sides of the Southern Alps. To better assess the agreement between the regimes reconstructed from Lake Ohau and Oroko Swamp, uncertainty was calculated based on the standard deviation of the assigned regime scaling at each site and 1.25 (the standard deviation of the 2 to -2 scale; Table 4). Low uncertainty in the regime assignment is found when the combined synoptic types are similar, like ZB-B. This combination has an uncertainty of ± 0.52 (ZB-B uncertainty = standard deviation of 1 (ZB), 2 (B), and 1.25). The B/T combination results in greatest uncertainty (± 1.93). When there are combinations of climate regimes (e.g. Zonal-Blocking) a level of uncertainty is applied even if both sites agree. This uncertainty arises because a single, uniform regime cannot be assigned when conditions are average-to-above (-below) as the temperature and precipitation anomalies associated with these conditions can often be attributed to at least two different regimes (Fig. 6). Table 3 summarizes the synoptic conditions inferred from Ohau, Oroko and for the WSI as a result of the comparison of Ohau and Oroko. Overall, these scaling methods and the site comparison results in a WSI Circulation Index (WSI-CI), which characterizes synoptic conditions back to 900 AD (Fig. 4D).

Table 3 Twenty-five year time slices of inflow (Ohau) and temperature (Oroko) conditions, inferred synoptic regimes, and synoptic conditions (and error) based on the comparison between Ohau and Oroko. See Table 4 for Ohau-Oroko regime and uncertainty metric.

W=Wet; N=Normal; D=Dry; Avg=Average, Abv=Above, Blw=Below, Z=Zonal, B=Blocking, T=Trough and combinations thereof (e.g. N-D=Normal-Dry). Shaded area, interpreted as the ‘Little Ice Age’ is discussed in Section 4.3.2.

Year (AD)	Ohau Precip. Pattern	Oroko Temp. Pattern	Inferred Ohau Regime	Inferred Oroko Regime	Ohau Regime Scaling	Oroko Regime Scaling	Ohau-Oroko Regime	Uncertainty for Ohau-Oroko
2010	W	Avg-Abv	T	Z-B	-2	1	-0.5	1.62
1985	N	Avg-Abv	Z	Z-B	0	1	0.5	0.66
1960	N-D	Blw	Z-B	T	1	-2	-0.5	1.62
1935	N	Avg	Z	Z	0	0	0	0.00
1910	N-D	Avg	Z-B	Z	1	0	0.5	0.66
1885	N	Avg	Z	Z	0	0	0	0.00
1860	N-D	Avg-Abv	Z-B	Z-T	1	-1	0	1.31
1835	N	Abv	Z	B	0	2	1	1.01
1810	N-W	Avg-Abv	Z-T	Z-B	-1	1	0	1.31
1785	N-D	Avg-Abv	Z-B	Z-T	1	-1	0	1.31
1760	N-D	Avg-Abv	Z-B	Z-B	1	1	1	1.01
1735	N	Avg	Z	Z	0	0	0	0.00
1710	W	Avg	T	Z	-2	0	-1	1.01
1685	N	Avg-Abv	Z	Z-B	0	1	0.5	0.66
1660	N-B	Avg	Z-B	Z	1	0	0.5	0.66
1635	N-B	Avg-Abv	Z-B	Z-T	1	-1	0	1.31
1610	N-B	Avg-Abv	Z-B	Z-T	1	-1	0	1.31
1585	N	Avg	Z	Z	0	0	0	0.00
1560	N-W	Avg	Z-T	Z	-1	0	-0.5	0.66
1535	W	Blw	T	T	-2	-2	-2	0.43
1510	N-B	Abv	Z-B	B	1	2	1.5	0.52
1485	N-W	Avg-Abv	Z-T	Z-B	-1	1	0	1.31
1460	N-B	Avg	Z-B	Z	1	0	0.5	0.66
1435	N-W	Avg	Z-T	T	-1	-2	-1.5	0.52
1410	N	Blw	Z	T	0	-2	-1	1.01
1385	N	Avg-Abv	Z	Z-B	0	1	0.5	0.66
1360	N	Avg	Z	Z	0	0	0	0.00
1335	N	Avg	Z	Z	0	0	0	0.00
1310	N	Avg	Z	Z	0	0	0	0.00
1285	N-W	Avg-Abv	Z-T	Z-B	-1	1	0	1.31
1260	N	Avg-Abv	Z	Z-B	0	1	0.5	1.01
1235	N	Abv	Z	B	0	2	1	1.01
1210	W	Avg-Abv	T	Z-B	-2	1	-0.5	1.62
1185	N	Avg-Abv	Z	Z-B	0	1	0.5	0.66
1160	N	Abv	Z	B	0	2	1	1.01
1135	N	Avg-Abv	Z	Z-B	0	1	0.5	1.01
1110	N	Avg-Abv	Z	Z-B	0	1	0.5	0.66
1085	N	Blw	Z	T	0	-2	-1	1.01
1060	N	Avg-Abv	Z	Z-T	0	-1	-0.5	0.66
1035	N	Avg-Abv	Z	Z-T	0	-1	-0.5	0.66
1010	N-D	Blw	Z-B	T	1	-2	-0.5	1.62
985	N	Avg-Abv	Z	Z-B	0	1	0.5	1.01
960	N-D	Avg-Abv	Z-B	Z-B	1	1	1	1.01
935	N	Abv	Z	B	0	2	1	1.01

Table 4 The scale used for comparing and classifying the differences in regional climate regime classifications between Lake Ohau and Oroko Swamp. Uncertainty for each combination is calculated using the standard deviation of the regime scale and associated scaling for each regime, or combination of regimes. Regimes defined after Kidson (2000).

Regional Climate Regime Combinations	Regime Scaling	Uncertainty of Regime Assignment
Blocking	2	0.43
Blocking/Zonal-Blocking	1.5	0.52
Zonal-Blocking/Blocking	1.5	0.52
Zonal-Blocking	1	1.01
Blocking-Zonal	1	1.01
Zonal-Blocking/Zonal	0.5	0.66
Zonal/Zonal-Blocking	0.5	0.66
Zonal	0	0.00
Zonal/Zonal-Trough	-0.5	0.66
Zonal-Trough/Zonal	-0.5	0.66
Zonal-Trough	-1	1.01
Trough-Zonal	-1	1.01
Zonal-Trough/Trough	-1.5	0.52
Trough/Zonal-Trough	-1.5	0.52
Trough	-2	0.43
Additional Regime Combinations		
Blocking/Trough	0	1.93
Trough/Blocking	0	1.93
Zonal-Trough/Zonal-Blocking	0	1.31
Zonal-Blocking/Zonal-Trough	0	1.31
Zonal-Blocking/Trough	-1	1.62
Trough/Zonal-Blocking	-1	1.62
Blocking/Zonal-Trough	1	1.62
Zonal-Trough/Blocking	1	1.62
Zonal/Blocking-Trough	0	1.67
Blocking-Trough/Zonal	0	1.67

4.3 SYNTHESIS & DISCUSSION

4.3.1 RCRC Regimes, Lake Ohau Inflow and WSI Climate

Changes in the relative frequency of occurrence of motifs B and A at Ohau and summer temperature at Oroko during the ~1,000-year period of overlap between the two records allows for assignment of the dominant synoptic weather regime to each 25-year time interval. While New Zealand climate anomalies and the RCRC are well correlated (Fig. 5, Renwick, 2011), it is important to confirm that synoptic regimes (and types) are specifically representative of Lake Ohau inflow. A comparison between inflow events and RCRC regimes/types from 1948-2011 shows that Trough

and Zonal conditions are associated with 82% of inflow events $\geq 400 \text{ m}^3 \text{ s}^{-1}$ (Table 2), consistent with WSI precipitation anomalies. This, in addition to the correlation between Ohau inflow and regional precipitation demonstrated in Chapter 3 suggest that changes in the RCRC regimes can indeed be reconstructed from changes in the B/A ratio. Additional support for decadal to century scale changes in the predominant weather regime over WSI comes from temperature anomalies as represented by tree-rings from Oroko Swamp in the same climate district (Lorrey et al., 2008).

Importantly, the RCRC regimes and their association with synoptic climate drivers, including SAM and ENSO, are well established over the instrumental period, with pronounced differences in the austral warm period (December-May; Table 2; Renwick, 2011; Jiang et al., 2013). However, different combinations of hemispheric-scale climate drivers such as SAM and ENSO can result in similar responses in regional synoptic circulation patterns (Lorrey et al., 2014). For example, the combination of SAM and ENSO generates a significant response over the instrumental and paleo-records. A wetter and colder WSI occurs when both El Niño (positive SOI) and negative SAM occur in tandem (Table 2; Lorrey et al., 2007; 2014; Renwick, 2011). Estimates of the relative roles of these hemispheric-scale processes can be better resolved through comparison with other regional reconstructions of these circulation patterns (see Future Directions). Overall, the WSI circulation index (WSI-CI), paired with regional reconstructions of the SAM and ENSO (tropical SST), enables a meaningful discussion of these teleconnections and their potential variability over the last 1,000 years where proxy datasets overlap.

4.3.2 Paleocirculation History of the Western South Island

The assignment of RCRC to the 25-year binned inflow and temperature reconstructions results in the WSI-CI (Fig. 7A). This index shows distinct periods of dry, warm northerly (Blocking) and wet, cold southerly (Trough) conditions prevailing at different times over the past 1,000 years (Table 5). Regime shifts occur approximately every 50 to 75 years but can oscillate between Blocking (northerly) and southerly (Trough) conditions at 25-year intervals. The WSI-CI begins with a period of weakly southerly (Trough) to westerly (Zonal) conditions from 985-1085 (Fig 7A), followed by a period of predominately northerly (Blocking) conditions (1085-1260 AD). Westerly (Zonal) flow persists from 1260-1360 AD.

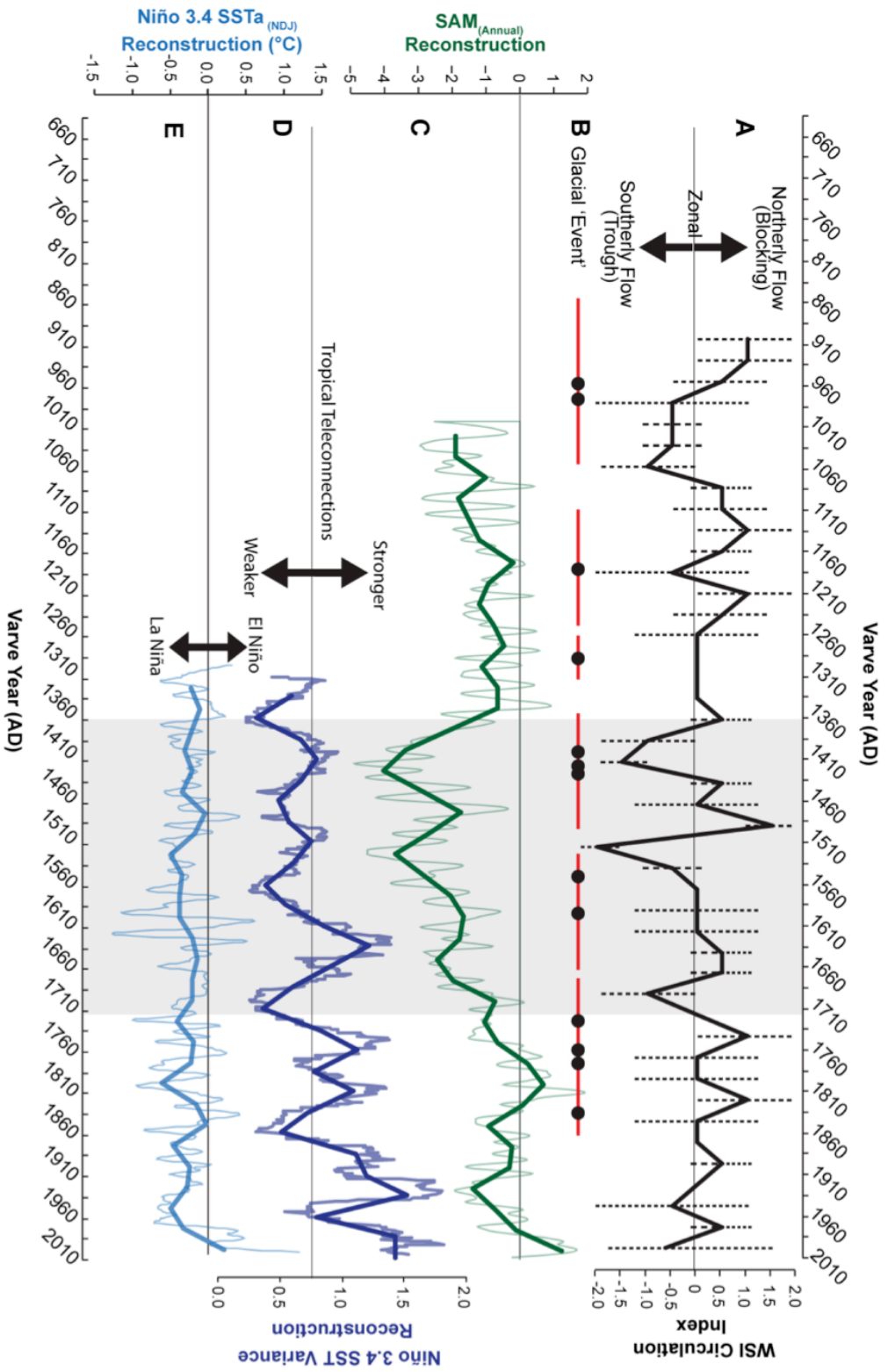


Fig. 7: A) WSI Circulation Index in 25 year bins; B) Glacial moraine ages (black dots with uncertainties shown in red) in the Mackenzie basin (from Alloway et al., 2014 and references therein); C) Southern Annular Mode reconstruction in 25 year bins treated with a 25 year LOESS filter (after Abram et al., 2014); D) Niño 3.4 SST variance in 25 year bins (solid) and a running 25 year variance as an indicator of the strength of tropical teleconnections (after Li et al., 2013); and E) Niño 3.4 SST anomalies (SSTa) treated as in D (Li et al., 2013).

At approximately 1385 AD there is a notable ‘mid-millennial’ shift from westerly (Zonal) conditions to predominately southerly (Trough) conditions, which then persist through to 1710 AD, with the exception of a 75-year period of westerly (Zonal) to northerly (Blocking) conditions between 1510-1585 AD (Fig. 7A). After 1585, shifts in climate state tend to occur every twenty-five years, with shifts to all of the three regimes but with northerly (Blocking) and westerly (Zonal) conditions being most common. Age uncertainties for each period are summarized in Table 5.

Based on the timing of this mid-millennial shift, we interpret 1385 AD as the onset of the Little Ice Age (LIA) in the WSI, with the core of the Southern Hemisphere LIA spanning 1385-1710 AD. The timing of this cooling is similar to that measured by a global proxy network, which points to the coldest conditions in the Northern Hemisphere persisting between 1400 and 1700 AD (Mann et al., 2009). This coincident timing supports the LIA potentially being a globally synchronous event. Comparison with surface exposure ages on LIA moraines primarily from the Mackenzie Basin (Fig. 2B; Alloway et al., 2014 and references therein) shows they were also deposited during with this period (Fig. 7B). Moraine ages are consistently aligned with periods of strong southerly (Zonal) flow (Fig. 7A and 7B; Table 5). The temperate glaciers of New Zealand have been shown to have a climate response rate as fast as 24 years, suggesting that advances coincident with a single 25-year bin of strongly trough or zonal conditions could be sufficient to force a glacial response (Oerlemans and Reichert, 2000).

While Schaefer et al. (2009) invoke shifts in the Interdecadal Pacific Oscillation (IPO) as a driver of glacier growth/persistence on the South Island. The WSI-CI generated here indicates shifts to predominately trough conditions, creating significant positive precipitation and negative temperature anomalies during the LIA in New Zealand. Based on the RCRC relationship with synoptic drivers, this points to negative SAM and El Niño (positive ENSO) conditions as key drivers of these anomalies for the WSI (Table 2). This interpretation is consistent with that of Lorrey et al. (2014) who utilized a similar RCRC approach and point to weak El Niño and negative SAM as the main synoptic drivers of Little Ice Age conditions in New Zealand.

Table 5 Reconstructed periods of northerly, southerly and zonal circulation from the combined Ohau and Oroko RCRC regime classification (based on Fig. 7). Age uncertainty in years is calculated as the average 2σ error of each time slice (calculated from the age model in Figure 3).

Northerly (Blocking)	Southerly-Mixed (Trough)	South-southwesterly (Zonal)
1960 – 1985 AD (± 7)	1985-2010 AD (± 6)	1835- 1885 AD (± 21)*
1885 – 1910 AD (± 14)	1910-1960 AD (± 8)	1760-1810AD (± 25)*
1810 – 1835 AD (± 26)	1685-1710 AD (± 18)	1710- 1735 AD (± 20)*
1735 – 1760AD (± 20)	1510- 1560 AD (± 16)*	1560 – 1635 AD (± 14)*
1635 – 1685 AD (± 14)	1385-1435 AD (± 11)*	1460-1485 AD (± 16)
1485 – 1510 AD (± 17)	1185-1210 AD (± 10)*	1285-1360 AD (± 6)*
1435 – 1460 AD (± 14)	985-1085 AD (± 24)*	
1360 – 1385 AD (± 8)		
1210 – 1260 AD (± 8)		
1085 – 1185 AD (± 15)		
910 – 985 AD (± 38)		

**Glacial ‘Advance’ (based on Alloway et al., 2014)*

Periods of more northerly flow (increased frequency of Blocking regimes) prevail during increased La Niña and positive SAM conditions (Renwick, 2011; Jiang et al., 2013), as during the period of 1085-1260 AD (Table 2). Zonal conditions leading into the mid-millennial shift between 1260-1360 AD suggest a period of transition with El Niño conditions and positive SAM as drivers. However, the relative role of these features cannot be determined without comparison to other regional and hemispheric-scale reconstructions of these indices.

4.3.3 Regional to Hemispheric Scale Drivers of Paleocirculation

To explore the relative role of ENSO and SAM in WSI-CI synoptic variability we compare the WSI-CI to a recently reconstructed annual SAM index generated from an ice core melt-layer sequence recovered from James Ross Island, Antarctica (Fig. 7C; Abram et al., 2014; data contributed by author), and use Niño 3.4 SST variance and SST anomalies (SSTa) as ENSO proxies (Fig. 7D and 7E; Li et al., 2013; data from <https://www.ncdc.noaa.gov/paleo/study/14632>). The Abram et al. (2014) SAM reconstruction was divided into 25-year bins and also smoothed using a LOESS filter (window equivalent to 25 years; Fig. 7C).

Li et al. (2013) reconstructed Niño 3.4 region SST (ENSO) over the past 700 years based on 2,222 tree-ring chronologies from the tropics and mid-latitudes of both the Northern and Southern Hemispheres. Li et al. (2013) use SST variance across the Niño 3.4 region to infer the relative strength of ENSO teleconnections outside of the

tropics. This Niño 3.4 SST reconstruction was converted to a 25-point running mean of variance and binned in 25-year intervals (Fig. 7D; after Li et al., 2013). The ENSO teleconnection to New Zealand shows significant fluctuation over the last 1,000 years, with periods of higher SST variance exhibiting strengthened tropical teleconnections (Li et al., 2013, their Fig. 2D). Following the interpretation of Li et al. (2013), we use SST variance as an indicator of ENSO teleconnection strength to New Zealand. This, paired with the Abram et al. (2014) SAM reconstruction over the same period, and the circulation index produced in this study, provides means by which to explore the relative roles of ENSO and SAM on New Zealand paleocirculation changes.

It is important to note that small offsets in reconstructions can be due to chronological error and varying seasonal sensitivity between proxies. However, the consistency between Niño 3.4 SST, SAM reconstructions (see below) and the WSI-CI suggest that chronologic errors and uncertainties are minor.

ENSO Teleconnections and the WSI Circulation Index

The ENSO-SST reconstruction does not extend back to the most notable period of persistent blocking in the WSI-CI (1085-1260 AD), but does show that increased northerly (Blocking) conditions in New Zealand are often paired with greater variance in SST, implying strengthened tropical connections to New Zealand's climate (Fig 7F). Based on the SST from Li et al. (2013) WSI-CI blocking periods are correlated with more La Niña like conditions, consistent with the instrumental record RCRC associations (Fig 7E; Table 2). Zonal (westerly) conditions also occur coincident with increased SST variance, when the ENSO teleconnection over the pan-Pacific region is enhanced (Li et al., 2013). Based on this relationship between WSI-CI and SST variance, it is evident that ENSO teleconnections to the mid-latitudes are strengthened during persistent Blocking (northerly) and Zonal (westerly) conditions.

The relationship between ENSO and SAM is also consistent with the RCRC associations, with Blocking (northerly) conditions typically aligning with the more positive phase of SAM. These periods suggest strong co-variability between SAM and ENSO, as observed over the instrumental record (Fogt et al., 2011; Ding et al., 2012). The most pronounced negative SAM as measured by Abram et al., (2014) between ~1410-1560 AD is coincident with low SST variance during the Little Ice

Age (Li et al., 2013), implying that this shift in SAM may be a dominant feature during this period.

SAM and the WSI Circulation Index

The Abram et al. (2014) SAM index is geographically representative of the Drake Passage region (Fig. 7C). While the SAM is effectively a measure of the annular structure of the circumpolar westerlies (as the name implies), it has a well-documented asymmetric spatial component, which results in variable localized climate impacts (Yeo and Kim, 2015). This changing spatial structure in the SAM can result in anti-correlation between New Zealand and the Drake Passage when the annular structure becomes more ‘wavelike’ and has an asymmetrical influence across the mid-latitudes (Yeo and Kim, 2015). Conversely, coincident negative SAM in the Drake Passage and WSI-CI Trough conditions over New Zealand (Southerly airflow, wet and cold) would suggest a strong annular structure to the SAM, causing such distant locations to experience similar climate anomalies.

Over the last 1,000 years, Abram et al. (2014) suggest the period of least melt on the Antarctic Peninsula (coolest temperatures) occurred circa 1410-1460 AD and was driven by a strong, negative-phase SAM lasting until ~1610. Over this period, the SAM is more persistently in its negative phase than during any other time in the last 1,000 years, coincident with some of the wettest and coldest conditions in southwestern New Zealand as recorded by the WSI-CI. Further, the oscillating pattern from southerly (Trough) to more northerly (Blocking) conditions during this phase of the ‘LIA’ (1560-1635 AD) is mimicked in the relative strength of the negative SAM (Fig. 7C). This suggests the LIA period in the Southern Hemisphere is characterized by strong, relatively persistent annular structure in the SAM with a potentially basin-wide response across the Pacific. Paired with low SST variance during the same period, this points to the SAM as a dominant feature of Little Ice Age climate in the Southern Hemisphere.

4.3.4 Future Directions

Modern observations suggest that SAM phase and magnitude play a strong role moderating the ENSO teleconnection to the high-latitudes (Fogt et al., 2011). However, identifying the drivers of the persistent and relatively abrupt shift to

strongly negative SAM and weak ENSO documented at Lake Ohau during the LIA requires further investigation and is beyond the scope of this study. The causes of these changes are likely to be complicated by wave-patterns and complex atmospheric dynamics, affecting the strength of tropical and polar teleconnections (Fogt et al., 2011). Identifying modern analog time slices, in addition to exploring other indices, such as the IPO (Vance et al., 2015), and the Madden-Julian Oscillation (MJO) may help to elucidate patterns of regional variability. Further, the CSIRO Mk3L modeled SAM Index shows promise for reconstructing SAM beyond the current 1 ka record (Abram et al., 2014) to the last 2 ka (S. Phipps, pers. comm.) The Lake Ohau record extending back to ~635 AD may provide a means for improved model-data comparison over the late Holocene.

Additional proxy records from different climate districts in New Zealand could be used to generate an additional circulation index representative of variability across the different climate districts. An attempt was made to incorporate records from different climate districts including Lake Tutira (Fig 2A; Gomez et al., 2011), Waitomo Caves (Fig 2A; Williams et al., 2005) and North Island Kauri tree-rings (e.g. Fowler et al., 2012), but issues with chronology, varying seasonal sensitivity and the resultant transfer functions means these records require additional work prior to being suitable for conversion into an high-resolution New Zealand circulation index. Future work aims to expand the WSI-CI index to annual and generate a New Zealand-wide circulation index. A NZ-wide index, particularly with North Island records, could provide important regional perspective for considering the temporal behavior of tropical to high-latitude teleconnections (Gomez et al., 2011; Fowler et al., 2012).

4.4 CONCLUSIONS

Utilizing the annually resolved Lake Ohau hydroclimate record in combination with the similarly resolved tree-ring record of summer temperature from Oroko Swamp (Cook et al., 2002), we generate a circulation index for the western South Island of New Zealand. This index utilizes the temperature and precipitation anomalies documented by the Regional Climate Regime Classification scheme for New Zealand originally generated by Kidson (2000) to assign synoptic scale circulation patterns to 25-year intervals from 900-2000 AD. This paleocirculation index shows strong co-variability with SAM and ENSO reconstructions, as well as during the instrumental record. Inferred dry, warm conditions are consistently associated with strengthened

tropical teleconnections to New Zealand and a positive SAM, while cold and wet conditions are driven by increased southerly airflow and negative phase SAM. The Little Ice Age (~1385-1710 AD) interval in western South Island of New Zealand is unique, with a climate system dominated by a significant and persistent negative, and strongly annular SAM combined with a weak tropical Pacific teleconnection. This same period coincides with core of the LIA in the Northern Hemisphere (1400 and 1700 AD; Mann et al., 2009) suggesting a globally synchronous LIA.

4.5 ACKNOWLEDGEMENTS

Project funding was provided by the GNS Science Global Change through Time Program, Sarah Beanland Memorial Scholarship, ANZICE Program (VICX0704), the Royal Society of New Zealand Marsden Fund (GNS1302), and KOPRI Project #PP151010. Many thanks to Hueng Soo Moon and Ho Il Yoon for assistance with the high-resolution x-radiographs and access to lab facilities; sincere thanks to James Renwick for numerous productive conversations about New Zealand climate. Many thanks to the staff at Meridian Energy Ltd., and the University of Otago Marine Sciences program and Geography Department for logistical support and core collection; and last but certainly not least, our gratitude to the Spiers and Inkersell families for their continuing support of our field-based research at Lake Ohau.

4.6 REFERENCES

Abram, N.J., Mulvaney, R., Vimeux, F., Phipps, S.J., Turner, J., and England, M.H., 2014. Evolution of the Southern Annular Mode during the past millennium. *Nature Climate Change* 4: 564-569.

Alloway, B., Almond, P., Augustinus, R., Barrell, D., Fuller, I., Golledge, N., Holt, K., Lorrey, A.M., Lowe, D., Mackintosh, A., McGlone, M., Newnham, R., Ryan, M., Stevens, R., Vandergoes, M.J., and Williams, P., 2014. New Zealand palaeoclimate and palaeoenvironmental change records for 60 ka – present: contribution to the Southern Hemisphere Assessments of Palaeoenvironments (SHAPE). Conference Proceedings, Australasian Quaternary Association Meeting, Mildura, June 29th-July 4th, 2014.

Blockley, S.P.E., Ramsey, C.B., Lane, C.S., and Lotter, A.F., 2008. Improved age modelling approaches as exemplified by the revised chronology for the Central European varved lake Soppensee. *Quaternary Science Reviews* 27(1): 61-71.

Blockley, S.P.E., Blaauw, M., Bronk Ramsey, C., and van der Plicht, J., 2007. Building and testing age models for radiocarbon dates in Late glacial and Early Holocene sediments. *Quaternary Science Reviews* 26: 1915–1926.

Bronk Ramsey, C., 2008. Deposition models for chronological records. *Quaternary Science Reviews* 27(1): 42-60.

Bronk Ramsey, C., 1995. Radiocarbon calibration and analysis of stratigraphy; the OxCal program. *Radiocarbon* 37(2): 425-430.

Bronk Ramsey, C., 2013. OxCal 4.2. *Web Interface Build 78*.

Ramsey, C. B., and Lee, S., 2013. Recent and planned developments of the program OxCal. *Radiocarbon* 55(2–3): 720-730.

Cook, E.R., Palmer, J.G., and D'Arrigo, R.D., 2002. Evidence for a 'Medieval Warm Period' in a 1,100 year tree-ring reconstruction of past austral summer temperatures in New Zealand. *Geophysical Research Letters* 29(14): 12-1.

Ding, Q., Steig, E.J., Battisti, D.S., and Wallace, J.M., 2012. Influence of the tropics on the Southern Annular Mode. *Journal of Climate* 25(18): 6330-6348.

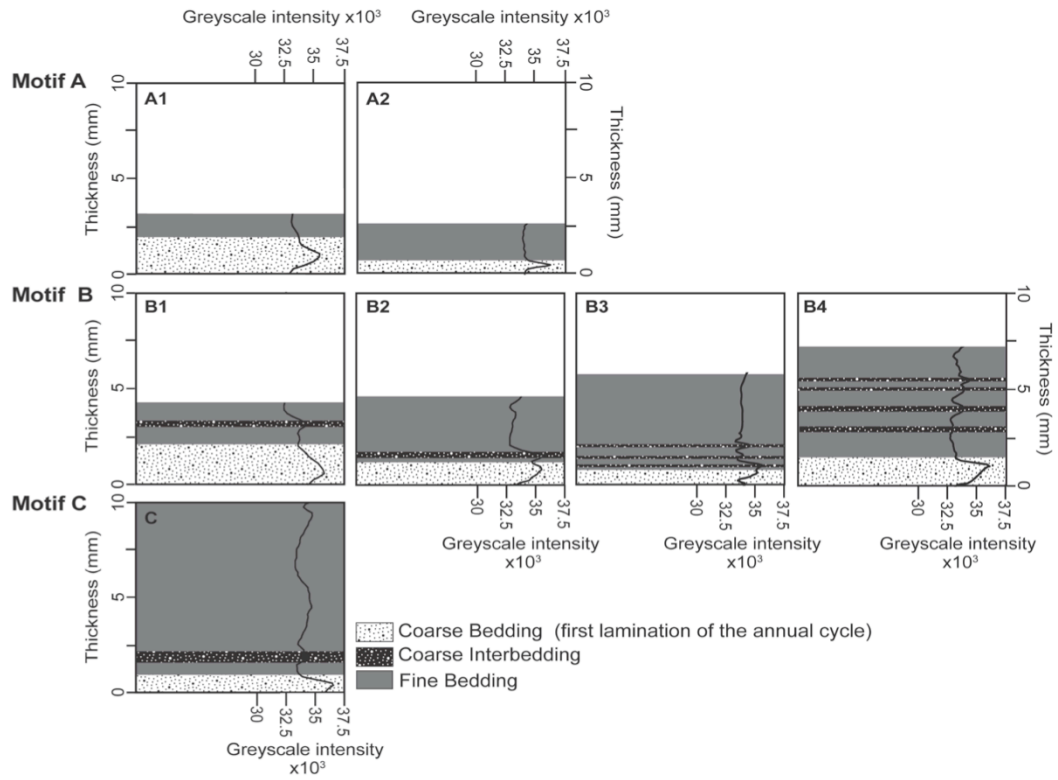
Fogt, R.L., Bromwich, D.H., and Hines, K.M., 2011. Understanding the SAM influence on the South Pacific ENSO teleconnection. *Climate Dynamics* 36(7-8): 1555-1576.

Fogt, R.L., and Bromwich, D.H., 2006. Decadal variability of the ENSO teleconnection to the high-latitude South Pacific governed by coupling with the Southern Annular Mode. *Journal of Climate* 19(6): 979-997.

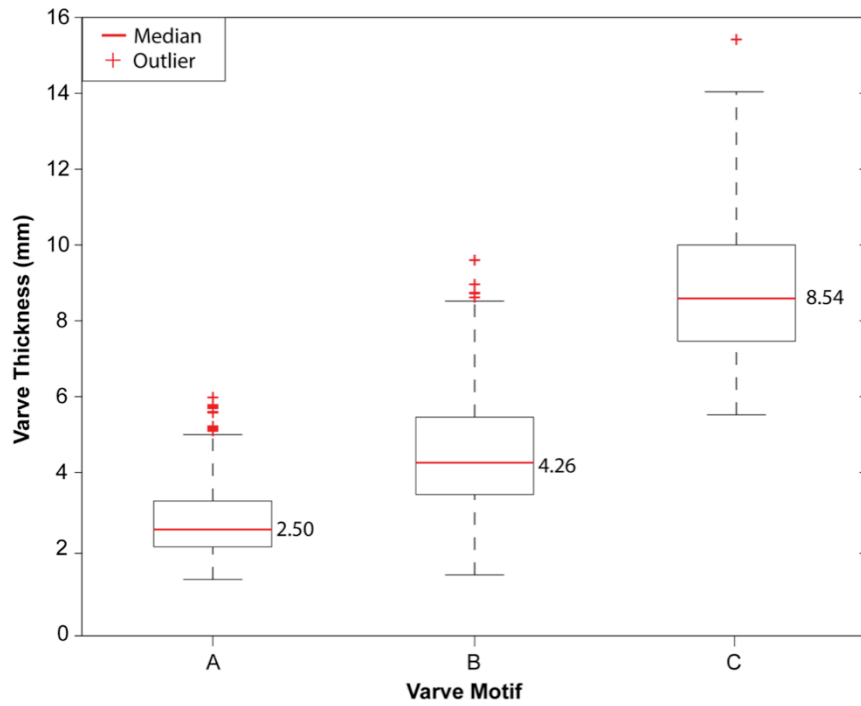
- Fowler, A.M., Boswijk, G., Lorrey, A.M., Gergis, J., Pirie, M., McCloskey, S.P., Palmer, J.G., Wunder, J., 2012. Multi-centennial tree-ring record of ENSO-related activity in New Zealand. *Nature Climate Change* 2(3): 172-176.
- Gomez, B., Carter, L., Trustrum, N.A., Page, M.J., and Orpin, A.R., 2013. Coherent rainfall response to middle-and late-Holocene climate variability across the mid-latitude South Pacific. *The Holocene* 23(7): 1002-1007.
- Grassi, B., Redaelli, G., and Visconti, G., 2005. Simulation of Polar Antarctic trends: Influence of tropical SST. *Geophysical Research Letters*, 32:L23806 doi:10.1029/2005GL023804.
- Griffiths, G.M., 2011. Drivers of extreme daily rainfall in New Zealand. *Weather and Climate* 31: 24-49.
- Hogg, A.G., Hua, Q., Blackwell, P.G., Niu, M., Buck, C.E., Guilderson, T.P., ... & Zimmerman, S. R.H., 2013. SHCal13 Southern Hemisphere calibration, 0–50,000 years cal BP. *Radiocarbon* 55(4): 1889-1903.
- Jiang, N., Griffiths, G., and Lorrey, A., 2013. Influence of large-scale climate modes on daily synoptic weather types over New Zealand. *International Journal of Climatology* 33(2): 499-519.
- Jiang, N., 2011. A new objective procedure for classifying New Zealand synoptic weather types during 1958–2008. *International Journal of Climatology* 31(6): 863-879.
- Kidson, J.W., 2000. An analysis of New Zealand synoptic types and their use in defining weather regimes. *International Journal of Climatology* 20(3): 299-316.
- Kidson, J.W., and Thompson, C. S., 1998. A comparison of statistical and model-based downscaling techniques for estimating local climate variations. *Journal of Climate* 11(4): 735-753.
- Kidson, J.W., 1994. Relationship of New Zealand daily and monthly weather patterns to synoptic weather types. *International Journal of Climatology* 14(7): 723-737.
- Kidston, J., Renwick, J. A., and McGregor, J., 2009. Hemispheric-scale seasonality of the Southern Annular Mode and impacts on the climate of New Zealand. *Journal of Climate* 22(18): 4759-4770.
- L'Heureux, M.L., Thompson, D.W.J., 2006. Observed relationships between the El Niño–Southern Oscillation and the extra-tropical zonal-mean circulation. *Journal of Climate* 19: 276-287.
- Li, J., Xie, S., Cook, E.R., Morales, M.S., Christie, D.A., Johnson, N.C., Chen, F., D'Arrigo, R., Fowler, A.M., Gou, X., and Fang, K., 2013. El Niño modulations over the past seven centuries. *Nature Climate Change* 3: 822-826.

- Lorrey, A.M., Fauchereau, N., Stanton, C., Chappell, P., Phipps, S., Mackintosh, A., Renwick, J., Goodwin, I., and Fowler, A., 2014. The Little Ice Age climate of New Zealand reconstructed from Southern Alps cirque glaciers: a synoptic type approach. *Climate Dynamics* 42(11-12): 3039-3060.
- Lorrey A.M., Williams, P., Salinger, J., Martin, T., Palmer, J., Fowler, A., Zhao, J., Neil, H., 2008. Speleothem stable isotope records interpreted within a multi-proxy framework and implications for New Zealand palaeoclimate reconstruction. *Quaternary International* 187(1): 52-75.
- Lorrey, A.M., Fowler, A. M., and Salinger, J., 2007. Regional climate regime classification as a qualitative tool for interpreting multi-proxy palaeoclimate data spatial patterns: A New Zealand case study. *Palaeogeography, Palaeoclimatology, Palaeoecology* 253(3): 407-433.
- Mann, M.E., Zhang, Z., Rutherford, S., Bradley, R.S., Hughes, M.K., Shindell, D., Ammann, C., Faluvegi, G., Ni, F., 2009. Global Signatures and Dynamical Origins of the Little Ice Age and Medieval Climate Anomaly. *Science* 326(5957): 1256-1260.
- Mann, M.E., Zhang, Z., Hughes, M. K., Bradley, R. S., Miller, S. K., Rutherford, S., and Ni, F., 2008. Proxy-based reconstructions of hemispheric and global surface temperature variations over the past two millennia. *Proceedings National Academy of Science* 105: 13252-13257.
- Mann, M.E. and Jones, P.D., 2003. Global surface temperatures over the past two millennia. *Geophysical Research Letters*. 30(1820): 15.
- Marshall, G.J., 2003. Trends in the Southern Annular Mode from observations and reanalyses. *Journal of Climate* 16(24): 4134-4143.
- McKerchar, A.I., Renwick, J.A., and Schmidt, J., 2010. Diminishing streamflows on the east coast of the South Island New Zealand and linkage to climate variability and change. *New Zealand Journal of Hydrology* 49: 1-14.
- Mullan, A.B. 1998. Southern Hemisphere sea-surface temperatures and their contemporary and lag association with New Zealand temperature and precipitation. *International Journal of Climatology* 18: 817–840.
- Neukom, R., and Gergis, J., 2012. Southern Hemisphere high-resolution palaeoclimate records of the last 2000 years. *Holocene* 22(5): 501-524.
- Oerlemans, J., and Reichert, B.K., 2000. Relating glacier mass balance to meteorological data by using a seasonal sensitivity characteristic. *Journal of Glaciology* 46(152): 1-6.
- Renwick, J.A., 2011. Kidson's synoptic weather types and surface climate variability over New Zealand. *Weather and Climate* 31: 3-23.

- Roop H.A., Dunbar, G.B., Levy, R., Vandergoes, M.J., Forrest, A.L., Walker, S.L., Upton, P. and Whinney, J., 2015. Seasonal controls on sediment transport and deposition in Lake Ohau, South Island, New Zealand: Implications for a high-resolution Holocene palaeoclimate reconstruction. *Sedimentology* 62(3): 826-844.
- Roop, H.A., Levy, R., Dunbar, G.B., Vandergoes, M.J., Howarth, J., Fitzsimons, S., Moon, H.S., Zammit, C., Ditchburn, R., Baisden, T., Yoon, H.I, in review. A hydroclimate-proxy model based on sedimentary facies in an annually laminated sequence from Lake Ohau, South Island, New Zealand. *Journal of Paleolimnology*.
- Salinger, J., Gray, W., Mullan, B., Wratt, D., 2004. Atmospheric circulation and precipitation. In: Harding, J., Mosley, P., Pearson, C., Sorrell, B. (Eds.), *Freshwaters of New Zealand*. The Caxton Press, Christchurch, New Zealand.
- Schaefer, J.M., Denton, G.H., Kaplan, M., Putnam, A., Finkel, R.C., Barrell, D.J., Andersen, B.G., Schwartz, R., Mackintosh, A., Chinn, T., and Schlüchter, C., 2009. High-frequency Holocene glacier fluctuations in New Zealand differ from the northern signature. *Science* 324(5927): 622-625.
- Sinclair, M.R., Wratt, D.S., Henderson, R.D., and Gray, W.R., 1997. Factors affecting the distribution and spillover of precipitation in the southern Alps of New Zealand-A case study. *Journal of Applied Meteorology* 36(5): 428-442.
- Thompson, D.W., Solomon, S., Kushner, P.J., England, M.H., Grise, K.M., and Karoly, D.J., 2011. Signatures of the Antarctic ozone hole in Southern Hemisphere surface climate change. *Nature Geoscience* 4(11): 741-749.
- Thompson, D.W.J., and Solomon, S., 2002. Interpretation of recent Southern Hemisphere climate change. *Science* 296: 895-899.
- Ummenhofer, C.C., Sen Gupta, A., and England, M.H., 2009. Causes of Late Twentieth-Century Trends in New Zealand Precipitation. *Journal of Climate* 22: 3-19.
- Ummenhofer, C., and England, M., 2007. Interannual extremes in New Zealand precipitation linked to modes of Southern Hemisphere climate variability. *Journal of Climate* 20: 5418-5440.
- Vance, T. R., Roberts, J. L., Plummer, C. T., Kiem, A. S., and van Ommen, T. D., 2015. Interdecadal Pacific variability and eastern Australian megadroughts over the last millennium. *Geophysical Research Letters* 42(1): 129-137.
- Williams, P.W., King, D.N.T., Zhao, J.X., and Collerson, K.D., 2005. Late Pleistocene to Holocene composite speleothem ^{18}O and ^{13}C chronologies from South Island, New Zealand did a global Younger Dryas really exist? *Earth and Planetary Science Letters* 230(3): 301-317.
- Yeo, S.R. and Kim, K.Y., 2015. Decadal changes in the Southern Hemisphere sea surface temperature in association with El Niño–Southern Oscillation and Southern Annular Mode. *Climate Dynamics* 1-16.



Supplementary Fig. 1: Sedimentary characteristics of the three different varve motifs and seven varve sub-types. Motif A lacks sublaminæ whereas motif B is characterized by one or more precipitation-induced coarse sublaminæ. Motif C laminæ form in response to significant inflow events (floods). Figure modified from Roop et al., (in review (Chapter 3).



Supplementary Fig. 2: Varve thickness (mm) distributions by varve motif. Varve thickness increases with varve type, consistent with Roop et al. (in review(Chapter 3)).

Supplementary Methods

Age model development

Full details of the dating and age model development for the 5.5-m Lake Ohau sedimentary sequence are being prepared for subsequent publication (Vandergoes et al., in prep); key details are summarized below. Direct and independent ages from ^{137}Cs analysis, pollen marker horizons (Supplementary Methods Fig. 1), radiocarbon dating of terrestrial plant macrofossils and *Cladocera* Spp. concentrates are used to provide age control for the sequence. Supplementary Methods Table 1 outlines the age marker horizons used and the AMS dates obtained from the Lake Ohau sequence. The resulting age model is presented in Figure 3 (Chapter 4). All depths reported below are depth adjusted to OH6m1c (Supplementary Methods Table 1).

Pollen marker horizons identified in the core were utilized as independent age tie points for the sequence (Supplementary Methods Fig. 1). In the European historical period, increases in pollen from exotic plant species *Rumex* (sorrel), *Pinus* (pine) and *Salix* (willow) provide age tie points. References to the arrival and distribution of these species in New Zealand have been sourced from the Global Invasive Species Database (<http://www.issg.org>) and appropriate references therein.

Rumex acetosella (Sheep Sorrel), the main common introduced weed species of abandoned cultivated land in New Zealand was first recorded in 1867, although it is thought to have arrived some time earlier (Moore, 1955). We, therefore, assign an age of 1865 with a probability density function (PDF) of ten years to its first increase in the sediment/pollen record (64 cm). Pine (*Pinus*) species were first introduced in New Zealand shortly before 1830 with state forestry beginning in 1896 (Webb et al., 1988; Wardle, 1991). The natural spread of pines was first noted in the late 1890s, with a rapid increase in invasions in the first two decades of the 20th century, and especially after the 1940s (Hunter and Douglas, 1984). Historical pictures of the Lake Ohau region in 1899 show conifer (pine) trees growing locally around Lake Ohau valley homesteads (McMillan, 2012). The first increase of *Pinus* in the sedimentary/pollen record (46cm) has been assigned an age range of 1890 to 1920 calendar years. A second combined rise in *Pinus* and *Salix* at 39 cm is considered to represent increases in these species throughout the landscape during the 1940's (post war era) and is assigned an age range of 1920 to 1950 calendar years. These pollen marker horizons compare well with the results of ^{137}Cs dating of the core, which show

the onset of and peak ^{137}Cs concentrations at 30.5 cm and 23.4 cm in which represent 1954 and 1964, respectively (Roop et al., in review (Chapter 3)).

Two other pollen marker horizons used as age tie points for the sedimentary sequence are the increase of *Pteridium* (Bracken fern) pollen and charcoal (279 cm) and the peak of Grass pollen (249 cm). Well dated charcoal records from South Island New Zealand and, in particular, sites closest to the Lake Ohau region (Diamond Lake, Dingle Burn; McWethy et al. 2010) indicate that significant increases *Pteridium* pollen and charcoal abundance occurred between 1320-1340 AD as a result of Polynesian burning and land clearance. Polynesian (Maori) arrived in New Zealand circa 1280 AD (McWethy et al., 2010). The peak in Grass pollen at many of the sites closest to Lake Ohau is seen to have occurred in the late 1300's, slightly later than the 1280 AD arrival. The timing of these changes in the records presented by McWethy et al. (2010) show some regional variability, highlighting the dangers of aligning proxy archives and chronologies on the basis of palynostratigraphy (Blaauw, 2012). However, we feel confident that at a regional level for central South Island, New Zealand, these changes would have occurred within a 20-40 year time frame (McWethy et al. 2014). Base on this data, we assign age ranges of 1340-1360 AD to the *Pteridium* and charcoal rise and 1390-1430 AD to the peak in grass pollen in the Lake Ohau sequence.

Terrestrial leaf macrofossil remains provided the primary target for age control in pre European period of the sequence. Full and partial non-degraded remains of two *Fuscospora cliffortioides* (previously *Nothofagus solandri* var. *cliffortiodies*; Mountain Beech) leaves at 188 and 322 cm, respectively, provide key age tie points. Investigation of other organic remains within the sediment (e.g., pollen, charcoal, bark fragments, bulk algal remains) have proven to be less reliable for providing age control in this depositional setting, primarily due to lack of abundance, reworking of older catchment material or inconsistent incorporation of the in-lake reservoir effect.

The sub fossil remains of *Cladocera* were identified as an additional dating target due to their abundance in the Lake Ohau sediments. These were concentrated through a variety of steps that comprised of repeated sieving at 150 μm mesh interspersed with warm washes of HCl, NaOH and ultrasonic disaggregation. Dating of the *Cladocera* concentrates yielded consistently older ages than those based on leaf macrofossils and pollen marker horizons from the same/similar depth horizons. The

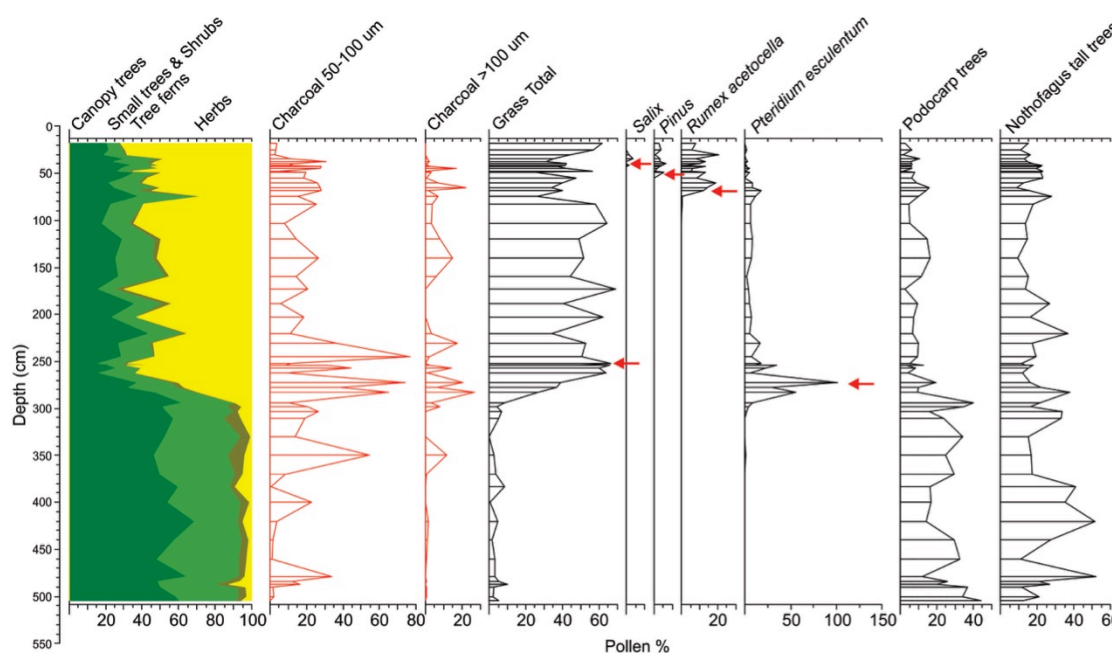
age discrepancy remains constantly offset throughout the core and indicates that it is appropriate to subtract a constant age correction from each *Cladocera* age relative to its respective macrofossils and pollen marker horizon; therefore deriving a Delta-R (ΔR , localized reservoir correction) for the *Cladocera* ages from the Lake Ohau sedimentary sequence.

Weighted Mean (n=4) derived from the difference *Cladocera* ages associated with the horizons incorporating the two leaf macrofossils, the rise in Grass pollen in the core, and immediately pre-1952 A.D. (*in Supplementary Methods Table 1) provide a $\Delta R = 1082$ (Ward and Wilson, 1978), with a Standard Deviation (square root of variance) of 52. The resulting ΔR is then incorporated into the Bayesian P_sequence model within Oxcal v4.2.4 (Bronk Ramsey, 2013) to develop the resulting age model.

The independent chronology from ^{137}Cs , ^{14}C and palynostratigraphy was integrated using the P_Sequence model in OxCal 4.2.4 (Bronk Ramsey and Lee, 2013). Using the P_Sequence algorithm to model layer counts requires the model parameter “k” to be defined and the assumption that anomalous layers are randomly distributed (Bronk Ramsey 2008). When using the P_sequence prior to model layer counts in Lake Ohau, k is the ratio of years to counted layers. In simple terms it defines the uncertainty in the layer counts and is set to 1 here because this is the highest value that provides acceptable model agreement index. i.e. agreement between the independent chronology and layer counts (cf. Blockley et al. 2007; 2008, Bronk Ramsey, 2008).

The distribution of anomalous layers is unlikely to be random across the entire length of Ohau 6m1c because their abundance correlates with complex varve motifs (Roop et al., in review). However, it is reasonable to infer that anomalous layers are randomly distributed within sections of the core that contain similar facies assemblages characterized by the relative frequency of occurrence of motif A (low complexity, low number of anomalous layers) and motif B (higher complexity, higher number of anomalous layers). These core sections (n=5) have been parameterized in the model using four boundaries (Bronk Ramsey, 2001); Fig. 3 (in text)). The boundaries allow the structure of the model to fulfill the underlying assumption that within core sections the distribution of anomalous layers is random.

One of the major benefits of the Bayesian age modelling approach is its ability to integrate and collapse age estimate uncertainties from multiple sources of chronological data. As with any modelling approach it is important to assess how accurately the model outputs reflect the input data. OxCal 4.2.4 achieves this comparison using an agreement index which is a measure of fit between the resultant (posterior) age probability density functions (PDFs) given the prior model and the original chronological data and their (likelihood) age PDFs (Bronk Ramsey and Lee, 2013). An agreement index (A.I.) threshold of 60% is widely regarded as an acceptable level of fit because it provides an equivalent level of discrimination to a Chi squared test at 5% (Bronk Ramsey, 1995). The Ohau6m1c P_Sequence model provided an agreement index of 64.5% demonstrating that the age model is representative of the chronological data. The chronologic model provides an average precision of ± 25 years (2σ) and a basal age of 646 ± 86 A.D (2σ).



Supplementary Methods Fig. 1: Pollen and charcoal changes from the Lake Ohau sedimentary sequence. Coloured panels show a summary of change in percent of total terrestrial pollen for native trees and disturbance-associated taxa (e.g., Poaceae, *Pteridium*) related to Polynesian burning and non-native taxa (Pinaceae, *Rumex*, *Salix*) introduced by Europeans. Red curves show charcoal accumulation and black curves changes in key pollen taxa used to identify time horizons. Red arrows indicate depths for key pollen chronostratigraphic horizons (see text).

Table 1 AMS radiocarbon ages and age tie points from Lake Ohau sediments. All radiocarbon dates are derived from core OH6m1c. Pollen chronostratigraphic horizons are derived from core OH6m1. ¹³⁷Cs tie points derived from core OH1m1. Correlation between these cores was conducted visually in Corelyzer (<http://andrill.org/~jareed/corewall.org/>) to allow integration of these results on a common depth scale. Core surface represents year 2010 (Roop et al., in review (Chapter 3)).

OH6m1c Depth Below Lake Floor (cm)	Sample type/ chronostratigraphic horizon	¹⁴ C Lab ^a	Uncalibrated ¹⁴ C age (¹⁴ C yr BP)	+/-1σ	ΔR Corrected age	Calibrated age range 2σ AD ^b
() = mid-point						
0	Core surface		2010	0		2008-2012
23.4	¹³⁷ Cs peak		1964	5		1959-1969
30.5	¹³⁷ Cs Int		1952	3		1949-1955
39	Pollen: <i>Pinus/Salix</i>					1920-1950
46	Pollen: <i>Pinus</i>					1890-1920
64	Pollen: <i>Rumex</i>		1865	10		1845-1885
160-175 (167)	Cladocera	NZA58300	1569	18	487±18	1396-1624
188.1	<i>Fuscospora</i> leaf	NZA53415	448	18		1444-1607
195-215(205)	Cladocera*	NZA55429	1505	19	423±19	1438-1633
249	Pollen: Grass peak					1390-1430
245-260(253)	Cladocera*	NZA58292	1641	18	559±18	1307-1464
279	Pollen: <i>Pteridium</i> /charcoal					1340-1360
287-305(295)	Cladocera	NZA58032	1757	12	675±12	1280-1409
322.4	<i>Fuscospora</i> leaf	NZA53418	679	17		1297-1392
314-334(325)	Cladocera*	NZA55109	1786	17	704±17	1266-1405
340-360(350)	Cladocera	NZA58293	2001	18	919±18	1034-1265
425-440(437)	Cladocera	NZA58291	2195	18	1113±18	861-1145
475-495(485)	Cladocera	NZA58033	2265	12	1183±12	771-1015
499-519(500.5)	Cladocera	NZA- 556090	2477	22	1395±22	585-843
519-539(519.3)	Cladocera	NZA- 556091	2384	13	1302±23	655-890

^a Radiocarbon laboratories: Rafter Radiocarbon Laboratory, GNS Science, Lower Hutt, NZ (NZA)

^b Calibrations were made using OxCal v4.2.4 (Bronk Ramsey, 2013) using the SHCal 13 calibration curve (Hogg et al., 2013).

^c *Cladocera* ages used to develop ΔR, localized reservoir correction *.

References

- Blaauw, M., 2012. Out of tune: the dangers of aligning proxy archives. *Quaternary Science Reviews* 36: 38-49.
- Bronk Ramsey, C., 2013. OxCal 4.2. *Web Interface Build 78*.
- Hogg, A.G., Hua, Q., Blackwell, P.G., Niu, M., Buck, C.E., Guilderson, T.P., ... & Zimmerman, S. R.H., 2013. SHCal13 Southern Hemisphere calibration, 0–50,000 years cal BP. *Radiocarbon* 55(4): 1889-1903.
- Hunter, G.G. and Douglas, M.H., 1984. Spread of exotic conifers on South Island Rangelands. *New Zealand Journal of Forestry* 29(1): 78-96.
- McMillan, E., 2012. Frugal Country and Hard on the Boots. *Eileen McMillan* pp. 508.
- McWethy, D.B., Wilmshurst, J.M., Whitlock, C., Wood, J.R., and McGlone, M.S., 2014. A high-resolution chronology of rapid forest transitions following Polynesian arrival in New Zealand. *PloS one* 9(11): e111328.
- McWethy, D.B., Whitlock, C., Wilmshurst, J.M., McGlone, M.S., Fromont, M., Li, X., Dieffenbacher-Krall, A., Hobbs, W.O., Fritz, S.C., and Cook, E.R., 2010. Rapid landscape transformation in South Island, New Zealand, following initial Polynesian settlement. *Proceedings of the National Academy of Sciences* 107(5): 21343-21348.
- Moore, L.B., 1955. The ecology of tussock grasslands. In *Proceedings of the New Zealand Ecological Society* 3:7-8
- Roop, H.A., Levy, R., Dunbar, G.B., Vandergoes, M.J., Howarth, J., Fitzsimons, S., Moon, H.S., Zammit, C., Ditchburn, R., Baisden, T., Yoon, H.I, in review. A hydroclimate-proxy model based on sedimentary facies in an annually laminated sequence from Lake Ohau, South Island, New Zealand. *Journal of Paleolimnology*.
- Vandergoes, M.J., Howarth, J., Turnbull, J., Li, X., Keller, L., Roop, H.A., Dunbar, G., Levy, R., Proir, C., Fitzsimons, S., Baisden, T., Norris, M., Ditchburn, B., (in preparation). Developing robust chronologies for laminated lake sediments using multi-macrofossil ¹⁴C dating and layer counting in a Bayesian modelling framework.
- Wardle, P., 1991. *Vegetation of New Zealand*. Cambridge University Press, London pp 672.
- Webb, C.J.; Sykes, W.R.; Garnock-Jones, P.J. (1988) *Flora of New Zealand, volume IV. Naturalised Pteridophytes, Gymnosperms, Dicotyledons*. Botany Division, Department of Scientific and Industrial Research. pp 672.
- Ward, G.K., and Wilson, S.R., 1978. Procedures for Comparing and Combining Radiocarbon Age-Determinations- Critique. *Archaeometry* 20: 19-31.

CHAPTER 5

Project Summary and Future Research

5.1 RESEARCH MOTIVATIONS

The initial concept of utilizing the glacial lakes in the Mackenzie Basin as paleoclimate targets extends back to the pioneering efforts of R. Pickrill and J. Irwin in the early 1980's, when they studied the complex depositional system of Lake Tekapo (Pickrill and Irwin, 1983). More recently, an Institute of Geological and Nuclear Science (GNS Science) project again examined sediment from Lake Tekapo to develop a high-resolution paleoclimate record (Graham, 2005). However, complications with geochronology and difficulties in interpreting the lamination stratigraphy led researchers to focus efforts on Lake Ohau, the smallest and least glaciated catchment of the three large glacial lakes in the Mackenzie Basin. The research discussed in this thesis is the 'tip of the iceberg' for the Lake Ohau research team. A deep drilling project will take place at Lake Ohau in early 2016, with ambitions to collect multiple 80 m sediment sequences extending back ~17,000 years. The hope is that the work presented here serves as a robust foundation upon which future research efforts can build.

5.2 PROJECT SUMMARY

This project had one overarching research objective: to develop a high-resolution paleoclimate reconstruction for Southern New Zealand. To generate a robust, high fidelity paleoclimate reconstruction from Lake Ohau, this work was structured in three separate but synergistic parts with the aim of addressing the following questions:

- (1) How does sedimentation in Lake Ohau vary temporally and spatially, and how do the dark and light laminations preserved in the sediment cores relate to seasonal changes in terrigenous sediment input?
- (2) Over the instrumental period, what are the primary hydrological and meteorological drivers impact on the amount and timing of sediment discharge into Lake Ohau? Can we develop a reliable climate-proxy model for interpreting down-core variability in the physical character of the lamination stratigraphy?
- (3) Can the controls on sediment deposition into Lake Ohau and the resultant sedimentary sequence be reliably utilized to reconstruct climate over the past 1,350 years? If so, what climatic variations have occurred in the Lake Ohau

catchment and, by extension, the South Island and Southern Hemisphere mid-latitudes over the late-Holocene?

Addressing these questions, this research led to the following conclusions:

(1) Depositional Environment (Chapter 2)

Contemporary monitoring of the Lake Ohau system demonstrates that sediment dispersal and deposition are controlled by pronounced basin-wide seasonality in precipitation, river inflow, lake water temperature, and the resultant response in internal lake dynamics. In general terms, the thermal stratification in summer enables the propagation of fine silt particles to the distal end of the lake. In winter, isothermal conditions result in persistent underflows with only sufficient lateral momentum for the transport and subsequent deposition of very fine silt. This coarse/fine accumulation near the lake outflow reflects summer and winter deposition and, thus, the laminae are interpreted as varves. Observations during the monitoring period included accumulation of simple laminae in addition to complex laminae and thick (≥ 9 mm) event layers, which result from precipitation-induced inflow events and floods, respectively. This variety of varve types provides an important tool for gaining insight into the climatic and hydrologic drivers of sediment accumulation discussed in Chapter 3.

(2) Climate-proxy development (Chapter 3)

Sedimentary analysis for the Lake Ohau core identified three primary varve motifs (simple (A), complex (B) and event layers (C)) which form the basis for developing a hydroclimate-proxy model that qualitatively links inflow patterns to varve accumulation. Using a model accuracy statistic, it is clear that each varve motif forms in response to a different annual hydrograph, with peak sensitivity to summer and autumn precipitation-driven inflow events. These inflow events create additional coarse laminae to the annual couplet and result in complex varve stratigraphy (Motif B). Motif A represents decreased summer inflow or drier conditions while Motif B represents austral warm periods with normal-to-wet conditions. Utilizing these instrumental period observations, varve characteristics are used to infer the hydrology and storm event frequency for the pre-instrumental record (as highlighted in Chapter

4), resulting in one of the first continuous reconstructions of paleohydrology in southern New Zealand.

(3) Paleoclimate Reconstruction (Chapter 4)

Employing the hydroclimate-proxy model, the distribution of different facies over the 1,350-year record was used to generate a wet/dry index for Lake Ohau. This index, paired with a complementary tree-ring reconstruction from the same climate district, was used to create a paleocirculation index based on temperature and precipitation anomalies from the New Zealand Regional Climate Regime Classification developed by Kidson (2000).

This Western South Island Circulation Index indicates several multi-decadal periods of either persistently wet/cold or warm/dry conditions over the past ~1,000 years (period of proxy record overlap). These changes are driven by the persistence of regional synoptic types, which are closely associated hemispheric scale climate drivers including SAM and ENSO. Comparison of the WSI Circulation Index with complementary records from the tropics and high southern latitudes provides a means for interrogating the relative role and strength of ENSO and SAM as drivers on New Zealand's climate. While there is evidence for changing strength in the interplay and teleconnections of these features, the most notable shift occurs at 1385 AD. At this time, tropical teleconnections weaken, and the SAM acts as a dominant driver of what is interpreted to be the onset of the Little Ice Age. The coldest and wettest conditions at Lake Ohau persisted from ~1385-1710 AD, consistent with the coldest LIA temperatures in Northern Hemisphere, pointing to a globally synchronous LIA. Further, the consistent indication of SAM as a driver of colder climate in paleoclimate records from New Zealand to the Drake Passage points to a strong annular structure of the SAM and suggests an equator-ward shift of the circumpolar westerlies was a primary driver of trans-Pacific cooling.

In summary, the research contributes the following:

- a. An improved understanding of the depositional environment of Lake Ohau and confirmation of the site as an important Southern Hemisphere mid-latitude paleoclimate archive.

- b. One of the first annually laminated and continuous record of paleohydrology in southern New Zealand.
- c. A unique methodology to generate a paleo-atmospheric circulation index for southern New Zealand that shows promise for better understanding large scale drivers of Southern Hemispheric climatic changes, including those with Northern Hemisphere analogs such as the Little Ice Age.

5.4 FUTURE DIRECTIONS

As with any scientific research endeavor, one set of research questions undoubtedly leads to additional lines of inquiry. Outlined below are ongoing and future areas of research:

(1) Depositional Environment

- Continued and improved monitoring will help to better document the range of variability in, and complexities of, this temperate depositional environment.
- Hydrodynamic and sediment fate modeling using a three-dimensional lake model could help to test depositional changes resulting from particular climatic or geological drivers (e.g. earthquakes and slope failure).

Following the publication of Chapter 2, the Lake Ohau process-network monitoring has expanded and remains a key component of the current research effort. Collaboration with hydrodynamics experts has resulted in a subsequent publication focused on the internal lake dynamics leading to sediment deposition in Lake Ohau (Cossu et al., in review; Appendix A).

One future work direction is hydrodynamic and sediment fate modeling using the three-dimensional Si3D lake model (in collaboration with the UC Davis Tahoe Environmental Research Center). With a robust multi-year dataset of internal lake dynamics and sedimentation, modeling efforts could help to test depositional changes resulting from particular climate or geological drivers (e.g. earthquakes and slope failure). Ongoing monitoring will improve our understanding of the range of variability in, and complexities of, this temperate depositional environment. At a minimum, monitoring will continue until drilling operations in 2016.

(2) Hydroclimate-proxy development

- Additional statistical analyses in order to develop a quantitative association between varve facies and instrumental period climate.
- Exploring rain intensity and frequency as a factor in sediment generation/mobilization. Are there catchment thresholds in precipitation or soil moisture that can be linked to sediment accumulation?
- Develop further automation of layer counting and identification of physical or geochemical properties that are indicative of either annual accumulation or varve facies.

Work is ongoing for finding quantitative links between sediment accumulation, varve characteristics and hydrometeorological datasets. At present, the application of additional statistical methods (e.g. Elbert et al., 2015) have yet to yield significantly different results from those presented in Chapter 3. Additional parameters such as rain intensity/frequency and soil moisture may be useful metrics for comparing to varve stratigraphy or inflow patterns. Unfortunately, TopNet outputs, our primary source of catchment-wide data, cannot yet be interrogated on sub-daily timescales. Lower resolution (e.g. weekly) investigations may provide a good starting point.

Initial investigation of high-resolution ITRAX μ -xrf data collected at the GEOPOLAR Institute at the University of Bremen as part of the research have yielded few conclusive associations between geochemistry and the coarse/fine laminae. While millimeter scale geochemical signatures may not be evident, multi-decadal to centennial scale trends may be indicative of environmental changes in the Ohau catchment. These data are currently being investigated in collaboration with researchers in Bremen.

(3) Paleoclimate Record

- The generation of a New Zealand Circulation Index through the integration of additional high-resolution proxies from different New Zealand climate districts.
- Data-model comparisons using regional synoptic model approaches and climate system models.

- Distribution of floods (Motif C) relative to climatic shifts and known periods of human-driven landscape disturbance (e.g. Polynesian and European arrival).
- Geochemical and physical property variations as a tool for interpreting paleoclimate changes.

As discussed in Chapter 4, additional work on New Zealand high-resolution proxies could lead to the generation of a more regionally representative Circulation Index. Through the addition of more proxy sites, we can further interrogate the initial findings of this work. Utilizing new tools such as the Past Climate Interpretation of Climate (PICT; pict.niwa.co.nz; Lorrey et al., 2014) could help to identify modern analogs for inferred atmospheric circulation changes in the past and would enable hypothesis testing about ENSO/SAM teleconnections and the potential drivers of these variations. PICT requires a minimum of three proxies for ensemble work. An ideal North Island target for comparison in a proxy ensemble is Lake Tutira (e.g. Gomez et al., 2012; Page et al., 2010). Further work to enhance the chronology and determining the seasonal sensitivity of this site would facilitate this type of comparison.

Model-data comparisons with climate models such as the CSIRO Mk3L climate system model may help to further elucidate and test the mechanisms driving changing circulation over the last 1,350 years. Model-generated paleo-SAM and -ENSO indices that extend back 2 ka and improve on upon the existing 1 ka simulations (discussed in Abram et al. 2014) are currently under development and will facilitate a more robust model-data comparison with Lake Ohau record (S. Phipps, pers. comm.).

Additional work on time series analysis and data consolidation for the Lake Ohau record (e.g. different bin resolutions at 5 and 10 year instead of 25) in combination with geochemical and physical property data may provide additional information about land use changes, rates of climatic change, and other geomorphic drivers, including Alpine Fault earthquakes, which in the current analysis show no notable change on sediment character or accumulation over the last 1,350 years (based on dates of earthquakes in Wells et al. 1999). To that end, ongoing investigation of recently recovered cores from the lake depocenter may help to

explore some of these geomorphic and hydrodynamics questions, which were beyond the scope of this research project.

Continuing these efforts will help to advance our understanding of the Lake Ohau depositional environment and can provide additional tools for interpreting the potential ~17 ka sequence to be collected from Lake Ohau in 2016.

5.4 REFERENCES

- Abram, N.J., Mulvaney, R., Vimeux, F., Phipps, S.J., Turner, J., and England, M.H., 2014. Evolution of the Southern Annular Mode during the past millennium. *Nature Climate Change* 4: 564-569.
- Cossu, R., Forrest, A., Roop, H.A., Dunbar, G.B., Vandergoes, M.J., Levy, R., Stumpner, P., Schladow, G., in review. The role of Limnological processes for sedimentation in Lake Ohau, New Zealand. *Marine and Freshwater Research*.
- Elbert, J., Jacques-Coper, M., Van Daele, M., Urrutia, R., and Grosjean, M., 2015. A 600 years warm-season temperature record from varved sediments of Lago Plomo, Northern Patagonia, Chile (47° S). *Quaternary International*.
doi:10.1016/j.quaint.2015.01.004
- Graham, I.J., Alloway, B.V., Cochran, U., Cook, R.A., Ditchburn, R.G., Mildenhall, D.C., Morgenstern, U., and Prior, C.A., 2005. Sedimentology, Geochronology and Micropalaeontology of Post- and Immediately Pre-European Lake Tekapo Sediment (Based on analysis of Core L1395). *Institute of Geological and Nuclear Sciences*, Lower Hutt, New Zealand.
- Gomez, B., Carter, L., Orpin, A.R., Cobb, K.M., Page, M.J., Trustrum, N.A., and Palmer, A.S., 2011. ENSO/SAM interactions during the middle and late Holocene. *The Holocene* 0959683611405241.
- Lorrey, A., Fauchereau, N., Stanton, C., Chappell, P., Phipps, S., Mackintosh, A., Renwick, J., Goodwin, I., and Fowler, A., 2014. The Little Ice Age climate of New Zealand reconstructed from Southern Alps cirque glaciers: a synoptic type approach. *Climate Dynamics* 42(11-12): 3039-3060.
- Page, M.J., Trustrum, N. A., Orpin, A.R., Carter, L., Gomez, B., Cochran, U.A., Mildenhall, D.C., Rogers, K.M., Brackley, H.L., Palmer, A.S., Northcote, L., 2010. Storm frequency and magnitude in response to Holocene climate variability, Lake Tutira, North-Eastern New Zealand. *Marine Geology* 270(1): 30-44.
- Pickrill, R.A., and Irwin, J., 1983. Sedimentation in a deep glacier-fed lake—Lake Tekapo, New Zealand. *Sedimentology* 30(1): 63-75.
- Wells, A., Yetton, M.D., Duncan, R.P., and Stewart, G.H., 1999. Prehistoric dates of the most recent Alpine fault earthquakes, New Zealand. *Geology* 27(11):995-998.

Appendix A

This manuscript was accepted for publication in *Marine and Freshwater Research*. Postdoctoral researcher Remo Cossu and his mentor, Dr. Alexander Forrest, led this work. The author contributed data, multiple rounds of comments and interpretive help to this manuscript. This work builds directly on the content presented in Chapter 2.

CITATION

R. Cossu, R., Forrest A.L., Roop, H.A., Dunbar, G., Vandergoes, M.J., Levy, R.H., Stumpner, P., & Schladow, S.G., accepted. Seasonal variability in turbidity currents in Lake Ohau, New Zealand and their influence on sedimentation. *Marine and Freshwater Research*.

Seasonal variability in turbidity currents in Lake Ohau, New Zealand and their influence on sedimentation

Remo Cossu

Australian Maritime College, University of Tasmania, Launceston, TAS, Australia
remo.cossu@utas.edu.au

Alexander L. Forrest

Australian Maritime College, University of Tasmania, Launceston, TAS, Australia
Environmental Research Center, Department of Civil and Environmental Engineering, University of California, Davis, CA

H.A. Roop

GNS Science, Department of Paleontology, Lower Hutt, Wellington, NZ
Antarctic Research Centre, Victoria University of Wellington, Wellington, NZ

G.B. Dunbar

Antarctic Research Centre, Victoria University of Wellington, Wellington, NZ

M.J. Vandergoes

GNS Science, Department of Paleontology, Lower Hutt, Wellington, NZ

R.H. Levy

GNS Science, Department of Paleontology, Lower Hutt, Wellington, NZ

Paul Stumpner

Environmental Research Center, Department of Civil and Environmental Engineering, University of California, Davis, CA

S.G. Schladow

Environmental Research Center, Department of Civil and Environmental Engineering, University of California, Davis, CA

Abstract

Layers of sediment that are deposited on the floor of Lake Ohau, New Zealand offer a means to reconstruct past climate conditions in the Southern Hemisphere at sub-decadal and annual resolution. A robust understanding of the modern physical processes that control the influx and dispersal of sediment in the lake is required to reconstruct climate from these sedimentary archives. In this study, water temperature and velocity measurements collected between 2012/2013 were analyzed to determine the primary physical processes that influence sediment transport in the lake. Sediment input from river inflow occurs throughout the year but exhibits strong seasonal variation. Large inflow events ($Q > 500 \text{ m}^3 \text{ s}^{-1}$) that follow strong summer rainstorms trigger high-concentration turbidity currents, which are the main agents for sediment delivery and deposition. During winter, smaller turbidity currents also occur after rain events and contribute to annual sediment accumulation. In addition, large internal waves were observed during the summer and may influence sedimentation. In conclusion, several processes including river inflow, internal waves and convectively driven flows control sediment deposition and accumulation in the Lake Ohau system. We utilize these observations to establish a conceptual model to explain the observed infill stratigraphy in Lake Ohau and guide interpretation of the longer sedimentary record.

1. Introduction

Sedimentation patterns in alpine and temperate lakes can be strongly influenced by the magnitude and physical properties of river inflows (Hamblin and Carmack, 1978; Alavian *et al.* 1992; De Cesare *et al.* 2006). In particular, increased river inflow in response to rainfall and/or the spring freshet can form gravity currents carrying large sediment loads into lakes (Weirich, 1986; Desloges and Gilbert, 1994, Gilbert *et al.*, 2006; Amann *et al.* 2014). Seasonal variability in river-fed lakes can influence sedimentation and produce clastic varves, e.g. relatively thick layers of coarse sediment during summer and thinner layers of fine sediments during winter (e.g. Leemann and Niessen, 1994; Gilbert and Butler, 2004). In order to use clastic varves to reconstruct past climate, establishing the linkages between meteorological, limnological, and sedimentary processes in lakes is required (e.g. Leemann and Niessen, 1994; Hardy 1996). Lake monitoring programmes provide measurements of physical properties in the water column (e.g. temperature, river inflow, velocities etc.) and sediment characteristics (e.g. turbidity, particle concentration, particle size etc.) that can help identify the control processes on sedimentation and to accurately interpret the sedimentary record preserved in the lake bed (Leeman and Niessen 1994; Tylmann *et al.* 2012; Ojala *et al.* 2012).

Many lake systems and their associated sedimentation regimes have been studied in the Northern Hemisphere (e.g. Pharo and Carmack, 1979; Mulder and Syvitski, 1995; Gilbert and Crookshanks, 2008) and have been used to generate annually resolved paleoclimate reconstructions (e.g. Gilbert 1975; Desloges 1994, Leemann and Niessen, 1994; Hardy 1996; Gilbert *et al.* 2006; Amann *et al.* 2014; and many others). Similar studies are largely absent from the Southern Hemisphere (Ojala *et al.*, 2012) despite the potential to gain insight into Pacific and Southern Hemisphere climate modes including El Niño Southern Oscillation (ENSO) and the Southern Annular Mode (SAM), which regulates the Southern Hemisphere westerly winds (Thompson and Salomon, 2002; Ummenhofer *et al.* 2009).

Located on the South Island of New Zealand, Lake Ohau offers a prime target to address this gap in global climate records as it sits near the northern boundary of the westerly winds that dominate atmospheric circulation. A 70 m thick sequence of sediments in the lake basin offers the potential to examine climate evolution in the Southern Hemisphere since the end of the last glacial maximum (~17 kyr BP). Fine-scale (mm) laminations preserved in lake floor sediment likely form in response to seasonal variability in hydroclimate (Roop *et al.*, 2015). However, detailed examination of hydrodynamic conditions through the seasonal variations is required to improve our understanding of sediment dispersal within the lake and identify the cause(s) of mm-scale varves.

In this paper we examine temperature, current velocity, and turbidity data acquired near the dominant inflow of Lake Ohau to explore the impact of changing physical properties in the water column on sedimentation over an annual cycle. Constraining the role of large flood events is a particular focus as heavy rainstorms can trigger sedimentation rates on the order of 15 mm y^{-1} at the distal end of the lake and $>200 \text{ mm y}^{-1}$ near the river delta (Roop *et al.* 2015). Clearly, flood-related large turbidity currents, internal waves and convectively driven density currents have an impact on long-term sedimentation patterns in the Lake Ohau system. The development of a conceptual model that integrates these elements is a primary aim of this research.

2. Material and Methods

Site description

Lake Ohau (44° 14.040'S, 169° 51.240'E; 520 masl) is one of three north-south trending lakes formed during the rapid glacial retreat between 17.9 and 17.4 kyr BP following the last glacial maximum on the South Island of New Zealand (Figure 1b; Putnam *et al.* 2013). The lake lies in the intermontane Mackenzie Basin, is 18.5 km long, up to 5 km wide with a total area of approximately 54 km². The lake has a mean depth of 74 m but reaches a maximum depth of 129 m along its central axis. Important bathymetric features are the steep delta front near the head of the lake where the depth increases rapidly to > 100 m (with a slope of approx. 5%) and a sharp 90° turn to the east located in the southern portion of the lake, which separates the main basin and the eastern end of the lake (Figure 1).

Water inflow into the lake is mainly controlled by the Hopkins and Dobson Rivers, which drain a combined area of 924 km² before converging just upstream of the lake and contributing ~85% of the total annual inflow (Woods *et al.*, 2006). The inflow rates into Lake Ohau predominantly depend on summer precipitation and summer snowmelt (17% of total annual flow; Kerr, 2013) with an increase in discharge during the spring freshet (October-November) and typically lower inflow rates during the winter period (Roop *et al.* 2015 and references therein).

Instrument deployment and data acquisition

Two arrays of instruments were deployed between January 2012 and January 2013 near the head of the lake at 25 m water depth (44° 11.069'S, 169° 51.680'E) and at 50 m water depth (44° 11.368'S, 169° 51.718'E). Each of the two moorings consisted of one thermistor chain and one Acoustic Doppler Current Profiler (ADCP; Figure 1). The thermistor chains had seven individual temperature loggers (TR-1060, RBR), which were located at 5, 10, 20, 25, 30, 35 and 45 m water depth. The loggers had an accuracy of 0.002 °C (resolution of < 0.00005 °C) and a sampling interval of 5 seconds. All loggers were

calibrated and synchronized before the start of the instrument deployment. Additional temperature information was recorded using Onset HOBO Water Temperature Pro v2 data loggers with an accuracy of 0.2 °C (resolution of 0.02 °C). Temperature data with the HOBO loggers were collected at 5-minute intervals at 2.5, 7.5, 13, 17, 22, 27.5, 32.5, 37.5 and 42.5 m water depth. An additional Onset HOBO thermistor chain was located near the outflow (44° 16.782'S, 169° 55.480'E) with loggers at 5, 21, 36 and 51 m water depth, which recorded at 5 min intervals (positions of all instrumentation shown in Figure 1c).

Density was computed using the linear freshwater equation of state (Chen and Millero, 1986). The position, h , of the height of the seasonal thermocline above the lakebed was established by determining the location of maximum density gradient by using the first moment of the density gradient (Patterson *et al.* 1984):

$$h = \int_0^H z \frac{\partial \rho}{\partial z} dz \bigg/ \int_0^H \frac{\partial \rho}{\partial z} dz \quad (1)$$

where ρ is the density of water, H the entire thickness of the water column and z is the depth measured from the surface.

Velocity data were collected using a RDI 1200 kHz, 4 beam ADCP moored on the bottom near the thermistor chain at a depth of 25 m and a RDI 600 kHz, 4 beam ADCP at depth of 50 m respectively (Figure 1). The ADCP recorded velocities of the 4 beams (Mode 1) every 30 minutes in bins of 1 m starting from 1 m above the lake bottom. For both instruments, the resolution and accuracy was 0.001 m s⁻¹ and ±0.0003 m s⁻¹, respectively. A total of 240 pings were averaged per sample. Horizontal velocity data were calculated using $v_{hor} = \sqrt{v_{east}^2 + v_{north}^2}$ where v_{east} and v_{north} are the directional velocity

components. ADCP data were only available until early January 2013 as both ADCPs were covered with sediment, and one was lost completely, during a large flood event.

River inflow data are estimated using a mass balance approach using a combination of measured outflow and lake level records collected by Meridian Energy Ltd. Weather data, including temperature (HP35C Campbell Scientific, UT, USA), solar radiation (Li-200 pyranometer Li-Cor, NE, USA) and wind speed and direction (3002 RM Young, MI, USA; 3 m height), were obtained at 10-minute intervals from the automated Killin Barn weather station located southwest of the lake (44° 11.274'S, 169° 51.841'E) and precipitation data was collected at the Elcho Flats station (43° 11.924'S, 169° 51.838' E; managed by Meridian Energy Ltd.), upstream of Lake Ohau (both sites labeled in Figure 1). Using these meteorological data along with the measured surface water temperatures, the four main heat flux components, net shortwave irradiance (SW), net longwave radiation (LW, determined after the Tennessee Valley Authority 1972), sensible heat (H), and latent heat (kE) can be used to estimate net heat flux using a similar approach and assumptions as detailed in Forrest *et al.* (2008).

An additional data set of suspended sediment concentration and particle size distribution was measured in June 2012 with a Laser In Situ Scattering and Transmissometry 100X type B instrument (LISST-100X) from Sequoia Scientific, Inc. The LISST-100X was used to take vertical profiles at 6 different location along the thalweg of the lake (see Figures 1a and 1c) during a winter flood event at DOY 175. The sampling rate was 1Hz and the particle size range detectable with the instrument is 1.25 μm to 250 μm .

3. Results

Annual meteorological cycle

Figure 2 summarizes the meteorological observations made during the on-site measurements. Air temperature records reveal large seasonal and diurnal variability (Figure 2a), consistent with the

intermontane setting. Precipitation at the Elcho Flats Station shows strong rain events throughout the year (Figure 2b). Average wind speeds are generally smaller in autumn and winter (Figure 2c). However, strong wind events ($>8.0 \text{ m s}^{-1}$) prevail throughout the entire year (Figure 2c) and consistently originate from the north-northeast as down-valley winds. During winter, the average river discharge Q_{av} is approximately $60 \text{ m}^3 \text{ s}^{-1}$ with several flood events exceeding $200 \text{ m}^3 \text{ s}^{-1}$ (Figure 2d). There is an increase in the average discharge $Q_{av} = 105 \text{ m}^3 \text{ s}^{-1}$ during summer with two peak discharge events ($Q \sim 1000 \text{ m}^3 \text{ s}^{-1}$) on January 4th and January 10th, 2013. Generally these discharge measurements are congruent with records dating back to 1926, with flow peaks in December or January. However, large flood events of the magnitude recorded in January 2013 have occurred less than 10 times since the beginning of the historical record in 1926 (Roop *et al.* 2015). In this paper we distinguish between average discharge for $Q < 100 \text{ m}^3 \text{ s}^{-1}$, flood events with $Q > 100 \text{ m}^3 \text{ s}^{-1}$ (marked by dashed line in Figure 2d) and large flood events which have $Q > 500 \text{ m}^3 \text{ s}^{-1}$. As shown in all panels of Figure 2, weather data correlate well with estimates of river inflow as peak inflow rates directly follow episodic storm events and associated periods of rain.

As highlighted in Figure 2 with the grey bars, we focus on two significant thermal regimes occurring in winter (Period 1) associated with a weakly stratified water column and in summer (Period 2) associated with a stratified water column. These two periods, as defined in Roop *et al.* (2015), are hypothesized to significantly contribute to intra-annual variations in lake floor stratigraphy.

Winter-period (Period 1: DOY 160 - 260)

Figure 3 depicts weather data, temperature and velocities in the water column at site 2 during Period 1 (DOY 160 – 260). Air temperatures reveal a diurnal variability with a mean temperature around $4 \text{ }^\circ\text{C}$ (Figure 3a). There are several rain events where precipitation exceeds 10 mm day^{-1} (Figure 3b) followed by significant flooding (Figure 3c). The most prominent flood event was observed between

DOY 195 and DOY 200 where inflow rates peaked at values $Q = 250 \text{ m}^3 \text{ s}^{-1}$. Predominantly calm or light winds prevail with a mean wind speed $U_{wind} = 3 \text{ m s}^{-1}$. This value was only exceeded on three occasions when wind speeds were $> 5 \text{ m s}^{-1}$ (Figure 3d).

The temperature in the water column was around $10 \text{ }^\circ\text{C}$ on DOY 160 and dropped down to minimum values of $7\text{-}8 \text{ }^\circ\text{C}$ by DOY 240 (Figure 3e). Temperature variability was very small throughout the water column with largest differences occurring near the bottom. In particular, periodic temperature variations of $1\text{-}2 \text{ }^\circ\text{C}$ were present within 5 m off the lakebed between DOY 200 and 250 (delimited by the black dashed arrow). Horizontal velocities in the water column are illustrated in Figures 3f. Close to the bottom, the horizontal velocities were observed to fluctuate between 0.02 and 0.1 m s^{-1} with episodic increases of up to $0.25 - 0.3 \text{ m s}^{-1}$ when river inflow rates are large (e.g. on DOY 195 to DOY 200 and DOY 214 to DOY 216). Although not shown, periods of large velocities have a flow direction consistently towards south and south-east. In contrast, small velocity fluctuations of $0.02 - 0.05 \text{ m s}^{-1}$ during periods of low inflow correlate well with small periodic temperature variations near the bottom (e.g. between DOY 200 and DOY 230). The recorded Echo intensity (EI) of the four ADCP beams at 5 m above the bed is shown in Figure 3h and has a mean value of EI $\sim 100 \text{ dB}$ (horizontal line) during Period 1. We interpret this EI count as a relative estimate of acoustic backscatter, inferring an increased sediment load being present in the water column (Kim and Voulgaris, 2003). Significant increases of up to EI = 170 dB occurred during periods from DOY 175 to 178, DOY 195 to 200 and DOY 245 to 255 which correlates well with periods of increased river inflows and larger horizontal and vertical velocities respectively.

Figure 4 shows measured sediment concentration profiles at six locations (see Figure 1a) collected during an inflow event with $Q > 180 \text{ m}^3 \text{ s}^{-1}$ at DOY 175 (marked by arrow in Figure 3). This inflow was characterized with maximum velocities of 0.2 m s^{-1} and EI values of 180 dB . At most

locations, the largest concentrations ($\mu\text{L/L}$) were close to the lakebed and Figures 4c to 4f exhibit typical underflow profiles similar to the observed velocity distribution in Period 1. Interestingly, the distribution of particles in the deepest part in the lake (Figure 4e) display highest concentrations between $z = 80$ and $z = 100$ m . Nonetheless, near the outflow, the water column reveals the highest concentrations in the lake with a typical nose-shaped profile of an underflow (Middleton, 1993). This sediment underflow is attributed to accumulation of sediments between $z = 50 - 60$ m after the flow has passed through the deepest part of the lake (Figure 4e) and runs into the eastern basin with shallower bathymetry. It is proposed that this event typifies underflow conditions during Period 1 (see discussion).

Spring - summer period (Period 2: DOY 300 in 2012 – 35 in 2013)

Figure 5 depicts weather data and corresponding processes in the water column at site 2 between DOY 300 in 2012 to DOY 35 in 2013. Air temperatures reveal a large seasonal and diurnal variability but also a constant increase of temperatures from $+8$ °C to $+14$ °C (Figure 5a). There are several large rain events (> 20 mm day⁻¹, Figure 5b), which correlate well with inflow rates shown in Figure 5c. The average discharge rates remain relatively constant ($Q \sim 80$ m³ s⁻¹) but show episodic, rapid increases of up $Q = 150 - 200$ m³ s⁻¹ lasting for several days (Figure 5c). The two most significant events occurred between DOY 3 - 7 and DOY 10 - DOY 15 in 2013 when inflow rates peaked at 1000 m³ s⁻¹ and were associated with heavy rain events. Wind data strongly fluctuate with the mean wind speed being 4 m s⁻¹ and peak wind speeds exceeding 8 m s⁻¹ on numerous occasions (Figure 5d).

During Period 2, epilimnetic water temperatures range from 8 °C to approximately 14 °C in the bottom waters (Figure 5e). The epilimnion deepens continuously from an average depth of 20 m at DOY 320 to 30 m at DOY 35 in 2013. The thermocline shows strong excursions with a maximum depth at 35 m (DOY 10, 2013) and a minimum depth of 3 m (DOY 3, 2013). Horizontal velocities show episodic, large increases near the bottom with peak velocities of up to 0.4 m s⁻¹ (DOY 10, 2013). These increased

velocities are in close agreement with increased river inflow rates into the lake (Figures 5c and 5g) and have flow direction towards south and south-east similar to Period 1. Figure 5g shows the averaged EI taken 5 m above the bottom which ranges between EI = 100 dB to EI = 200 dB. In the same way that EI was interpreted for Period 1, the intensity peaks correlate well with increased horizontal and vertical velocities near the bottom, and are suggestive of high sediment transport during times of large inflows into the lake.

4. Discussion

For a climate-proxy site it is crucial to understand the significance of processes prevalent in the lake influencing deposition. The data from 2012/2013 suggest a complex interaction of several limnological factors, such as sediment-laden density currents, internal wave action and convectively driven currents at play.

Turbidity density currents

Figure 6a shows the vertical velocity profile of a turbidity current obtained by averaging 3h-period of quasi-steady flow conditions during an inflow event of $Q > 300 \text{ m s}^{-1}$ at DOY 250. At the 25 m-mooring (closed circles), maximum horizontal velocities reach 0.2 m s^{-1} near the bottom, which decrease to $< 0.05 \text{ m s}^{-1}$ at 5 m above the bottom. The vertical velocity profile in Figure 6b displays a similar shape with maximum downward directed velocities of 0.02 m s^{-1} near the bed, which then reach background velocities by a height of 5-6 m above the bottom. Additionally, EI reduces from its maximum value of 200 dB near the lakebed to less than 50 dB at 8 m above the bed (Figure 6c).

The same underflow was monitored at the 50 m-mooring (open circles) where maximum horizontal flow velocities reached 0.25 m s^{-1} near the bed which reduce to less than 0.05 m s^{-1} at 15 m above the bottom (Figure 6d). In contrast, vertical velocities showed no significant change indicating that the flow was almost horizontal by this stage (Figure 6b). EI values in Figure 6c revealed an identical

profile with maximum intensities near the bed (EI = 160 dB) and significantly less intensities (EI = 50 dB) at 20 m above the bed. Thus, a turbidity current with a height of approximately $h = 5 - 10$ m passed site 1 over a period of 3 hours. Due to entrainment of ambient fluid the height of the current increased to $h = 20$ m and passed site 2. Furthermore, the reduced EI near the bottom suggests that sediment particle concentration decreased due to entrainment of ambient water along the slope (e.g. Best *et al.* 2005 and references therein). A simple one-dimensional approximation where the entrainment is approximated by $E \sim dh/dx$, with x being 1km between the two sites, yields $E = 0.005 - 0.015$ which is found in many laboratory and field studies (Dallimore *et al.* 2001; Baringer and Price 1997; Cenedese *et al.* 2004) summarized in Wells *et al.* (2010).

Figures 6d to 6f show the first large flood event during the summer at DOY 1-3 in 2013. Data were averaged over 3h-period of quasi-steady flow conditions at site 2 and there were no ADCP data available from site 1. The velocities show the typical nose-shaped profile of turbidity currents (e.g. Middleton, 1993) with velocities of up to 0.25 m s^{-1} near the bed, before reaching the maximum velocities of 0.3 m s^{-1} at $z = 4$ m which eventually reduce to 0.05 m s^{-1} at 15 m above the bottom (Figure 6d). Vertical velocities reveal a constant upward direction of flow of 0.01 m s^{-1} between the bottom and a height of $z = 15$ m (Figure 6e). Additionally, the EI profile has a maximum near the bottom (200 dB) and continuously decreases to 80 dB at approximately $z = 20$ m (Figure 6f).

We found similar velocity and EI profiles at seven times (not shown here) during increased river inflow providing irrevocable evidence of turbidity currents near the bottom (50 m) being generated by river discharges in Lake Ohau. Moreover, increased EI values support the hypothesis that turbidity currents can be associated with increased sediment transport and that they occur mainly near the bottom of Lake Ohau at the measuring sites.

Figure 7a shows the recorded temperature measured 5 m below the surface and 5 m above the lake bed during the large floods (DOY 360 2012 to DOY 15 2013) while Figure 7b depicts corresponding horizontal velocities within the bottom 15 m. Interestingly, at DOY 365, DOY 1-3, DOY 11 and DOY 14 bottom temperatures increase rapidly by up to 2°C, indicating that warmer water is descending down the slope. During two events of increased velocities near the lake bed (on DOY 1-4 and DOY 10-11) temperatures were observed to be greater near the lakebed than at the surface (Figure 7b). Velocities and height of the gravity current are at the same order of magnitude as an inflow event observed in Lillooet Lake (Best *et al.* 2005). Temperature inversions over such a large depth range are only possible if the underflow had a large sediment concentration to overcome the buoyancy arising from the warmer water when it is dragged downslope by the current. For instance, De Cesare *et al.* (2006) found warm density currents piercing through the 20 m thermocline and intruding down to a depth of > 200 m in Lake Lugano owing to high sediment concentrations. Similar riverborne turbidity currents with temperature anomalies of up to 3.5 °C were reported in Lambert and Giovanoli (1988) where warm temperatures indicated that river water moved as an underflow through Lake Geneva due to short-term increases in sediment concentration.

Additional temperature anomalies between the top and the bottom waters were also observed in the winter (Figure 7c). Sudden increases of horizontal velocities (Figure 7d) correlate well with these inversions and are again attributed to turbidity currents that descend along the lakebed. Compared to summer inflow events the temperatures rise only by 0.5 °C owing to nearly isothermal conditions. Nonetheless, the density difference required to overcome the buoyancy of warm water plunging down a slope with colder ambient water can only stem from suspended sediment particles in turbidity currents. Thus, these flows in Period 1 underline the importance of turbidity currents as an agent for sediment transport in the lake during winter.

Convection currents

Recall how Figure 3 shows diurnal changes in water temperature and velocity near the bottom suggestive of the presence of another forcing mechanism, other than increased river inflow, during the destratified Period 1. The temperature in shallow, well-mixed waters at the edges of lakes can cool more rapidly than that of adjacent deeper waters, in particular during periods of winter cooling. The resulting differential heating between the pelagic and littoral waters have been found to form relatively cold, dense gravity currents along lake boundaries from shallow to deeper parts. For instance, cold-water plumes with a thickness of 10 m adjacent to the lake boundary were generated in the near-surface convective mixed layer when air temperatures were 7 °C below the surface water temperature (Thorpe *et al.* 1999). Similar observations have been reported in other lakes (Fer *et al.* 2002; Jonas *et al.* 2003; Forrest *et al.* 2008). Consistent in these studies was a net heat flux, which demonstrated cooling during the night (heat loss) so that dense cold-water plumes eroded the stratification that had developed during daytime.

Figure 8 compares air temperature (Figure 8a), wind speed (Figure 8b), inflow rates (Figure 8c), the estimated heat flux (Figure 8d) as well as the observed temperature (Figure 8e) and horizontal velocities (Figure 8f) in the water column at site 2 between DOY 215 to DOY 235. Periodic temperature fluctuations of ~ 1 °C and velocities near the bottom up to 0.1 m s⁻¹ correspond to air temperature changes but they do not correlate well with the low, constant inflow rates ($Q < 60 \text{ m}^3 \text{ s}^{-1}$) or relatively low wind speeds ($< 3 \text{ m s}^{-1}$). On the other hand, the estimated heat flux of 150 W m⁻² from the lake to the atmosphere is at the same order of magnitude as has been documented in other lakes (e.g. Jonas *et al.* 2003; Forrest *et al.* 2008) where sufficient heat loss at night drives the formation of cold density plumes. Furthermore, the constant periodicity of roughly 24h-period supports the idea that downslope flows of cold dense water plumes occur at the head of the lake in response to diurnal heating and cooling.

Internal waves

One of the major controls on hydrodynamics in temperate lakes is the density stratification of the water column due to solar heating in the summer. Figure 5 compares the inflow rates (Figure 5a), wind velocities (Figure 5b) and the thermal variability near the inflow (Figure 5e) and outflow (Figure 5f) for Period 2. Lake Ohau starts to stratify after DOY 320 when a strong temperature gradient (thermocline) develops. The thermal regime reveals up to 4 °C colder temperatures near the inflow compared to the outflow, which can most likely be attributed to cold river inflow.

The mean depth of the thermocline near the inflow is about $z_{Th} = 20$ m but the depth varies greatly as demonstrated by excursions close to the water surface and bottom during peak inflow (DOY 3 or DOY 10 in 2013). However, similarly rapid changes occur during periods of low inflow rates (DOY 340 to DOY 365) so that thermocline movements are partly independent of river inflow. The temperature difference between bottom and surface layers is relatively small. For instance, a maximum observed temperature difference between $z = 10$ m and $z = 40$ m is $\Delta T = 2$ °C so that the seiche period, T_{Seiche} , can be estimated using the common formation, $T_{Seiche} = \frac{2L}{\sqrt{g'z_{Th}}}$ (e.g. Fischer, 1979) to be on the order of 36 – 48 hours (with L being 10 km in Lake Ohau, g' is the reduced gravity due to temperature difference and $z_{Th} \sim 20$ m is the depth of the thermocline). The amplitudes during this period are large (on the order of O(10) meters (Figures 5e and 5f). Seiches with such amplitudes can cause velocities of 0.05 – 0.10 m s⁻¹ and could be responsible for increased velocities during this period (Fischer et al., 1979).

Figure 9a demonstrates the estimated depth of the thermocline and Figure 9b shows the frequency and magnitude of thermocline excursions (Δz_{Th}). It is evident that about 40% of the time Δz_{Th} is larger than 5 meters. Furthermore, the distribution is almost symmetrical indicating that the

thermocline is equally subjected to up- or downwelling and that a periodic motion in form of an internal wave is driven by a mechanism unrelated to river inflow.

Figure 10 shows the Power Spectra Density (PSD) of wind velocities and the estimated position of the thermocline. The dominant frequencies in the spectra (12h and 48h intervals) compare favorably well. The offsets of the peaks could be attributed to the location of site 3 which is not the downwind end but at the east end of the eastern basin (Figure 1). Additionally, the thermocline was identified based on four thermistor loggers over a depth of 50 meters, which allows only for a rough estimate of the thermocline position in the water column. Nonetheless, Figure 10 indicates that thermocline movements near the outflow can be linked with the wind-induced stress whilst the thermal regime near the inflow suggests that internal wave climate is greatly influenced by river inflow.

Conceptual model for seasonal changes in Lake Ohau

Lake Ohau is subjected to varying climate conditions and rainfall events manifested in strongly fluctuating river inflow rates which frequently trigger turbidity currents over an annual cycle. The critical suspended sediment concentration required to trigger turbidity currents for freshwater lakes is relatively low with $\ll 1 \text{ kg m}^{-3}$ (Mulder and Syvitski, 1995). Although the sediment concentration of the inflow during floods is not known it can be easily concluded that the size of Lake Ohau's drainage area ($\sim 1200 \text{ km}^2$) and elevation (500 m – 3000 m) produces average concentrations of at least 1 kg m^{-3} (Figure 7 in Mulder and Syvitski, 1995). It can be further concluded that floods clean the catchment area and river bed and yield even higher sediment concentrations at the head of the lake than during average discharge rates. Thus, based on meteorological and hydrological forcing the sediment supply and deposition has to be differentiated into several stages representing different discharge rates and correlated sediment concentration.

Figure 11 presents a conceptual model of the observed processes that contribute to sedimentation and ultimately varve formation in Lake Ohau. In addition, Figure 11 sketches further processes known from other lake studies which may add to the sedimentation regime but require further monitoring in Lake Ohau. Figure 11a shows the conditions during Period 1 in which several flood events of $Q > 200 \text{ m}^3 \text{ s}^{-1}$ were observed. Historically, inflows of this magnitude are relatively common with 641 occurrences from 1926 - 2013. Over our monitoring period these flows showed increased acoustic back-scatter data and had warmer temperatures than the ambient fluid indicating significant sediment concentration to overcome the buoyancy force. Due to the density difference between inflow and lake water they propagate through the lake as underflows and reach the distal part of Lake Ohau, depositing fine ($\sim 5 \mu\text{m}$) particles as measured in sediment traps by Roop *et al.* (2015) and also in accord with data obtained from LISST profiles (Figure 4).

In addition, periodic cold water plumes ($1 \text{ }^\circ\text{C}$ colder than ambient water temperature) during regular inflow conditions were found to descend down the lake slope in the winter. Diurnal temperature fluctuations were still noticeable near the outflow with variations of up approximately $0.2 \text{ }^\circ\text{C}$ (Roop *et al.* 2015) suggesting that these currents also reach the distal part of the lake or occur around the periphery of Lake Ohau. Cold water plumes could also develop from cold river inflow, which is cooled down by cold air temperatures at night. Though their origin is unclear, the driving force for periodic cold water bursts in Period 1 seems to be convectively driven density plumes which are an effective driver for flushing near-shore regions (e.g. Fer *et al.* 2002). The observed velocities associated with cold water plumes of 0.1 m s^{-1} are strong enough to erode and transport suspended sediment into more distal parts. Such density plumes could potentially contribute to the total annual sediment deposition in Lake Ohau but based on the low backscatter data they are less significant than sediment supplied by increased river discharge ($Q > 100 \text{ m}^3 \text{ s}^{-1}$) in Period 1.

The majority of sediment flux occurs during spring and summer and the corresponding thermal regime is depicted in Figures 11b (moderate flood events with $Q \sim 100 - 500 \text{ m}^3 \text{ s}^{-1}$) and Figure 11c (large flood events $Q > 500 \text{ m}^3 \text{ s}^{-1}$), respectively. Flood events of $Q > 500 \text{ m}^3 \text{ s}^{-1}$ occurred 37 times during the last 87 years, implying that Lake Ohau receives greatly enhanced influxes of sediment several times a decade. The presence of steep temperature gradients during the summer is significant but its impact on the sedimentation regime remains speculative. The thermocline could act as a barrier to prevent finer particles from immediate settling. Rapid, periodic temperature fluctuations up to 5-6 °C around the depth of 20 m near the outflow are either wind-induced or river-inflow-induced seiches which cause thermocline excursions near the outflow. However, breaking of internal waves could also cause sediment slumps and resuspension of particles leading to further sedimentation (Pharo and Carmack, 1979). The internal wave climate is not entirely clear from this one year record. For instance, the presence of Kelvin waves associated with large bottom velocities as observed in Lake Geneva (Lemmin et al., 2005) could be present but to detect such waves more thermistor chains around the periphery of Lake Ohau are required.

It is noteworthy that the 2012/2013 summer season was relatively cold compared to other years and that flood events had a significant impact on the thermal variability of the lake. During warmer summers the thermal stratification would be much stronger which puts more emphasis on the internal wave climate and related resuspension events in the wash-zone of the thermocline (Pharo and Carmack, 1979; Peeters and Kipfer, 2009). An additional source of sediment could stem from sediment resuspension caused by surface waves as observed in Sunwapta Lake (Gilbert and Shaw, 1981) and more recently in Lake Tahoe (Reardon *et al.* 2014). Generally, Lake Ohau has steep slopes and only small parts are shallow shelf areas, but due to the wind and wave climate along the north-south axis

additional sediment could get resuspended near the south shore. For instance, this could explain the high sediment concentration near the bottom in the eastern basin depicted in Figure 4f.

A strong thermal gradient also has an impact on river plumes and how they intrude in the lake system (Alavian *et al.* 1992). Inter- and overflows could play a bigger role during moderate floods, for instance when the thermocline is not eroded and a strong thermal gradient prevails or when inflows carry less sediment and are unable to pierce through the thermocline. This could cause the distribution of finer sediments across the lake (Figure 11b) as seen in many other studies (e.g. Pharo and Carmack, 1979; Lambert and Giovanoli 1988; Gilbert *et al.* 2006). Another mechanism which has been observed in several lakes is that underflows become buoyant after the coarse sediment has settled out of suspension and detach from the lake bed further away from the delta (Figure 11b). This mechanism could also explain the presence of coarse sediment near the inflow and continuous fining of sediment towards the distal end of the lake.

On two occasions after heavy rainfall large floods with $Q > 900 \text{ m}^3 \text{ s}^{-1}$ triggered turbidity currents which reached heights of tens of meters and velocities of up to 0.4 m s^{-1} in early 2013. Such large floods have only been reported 7 times within the last 87 years. Near the inflow the thermal stratification is temporarily destroyed (Figure 5e) but the lake still exhibits a thermal stratification at the outflow (Figure 5f). Optical back-scatter data (Figure 6f) and turbidity measurements ($\text{NTU} > 31$) observed by Roop *et al.* (2015) and temperature inversions (Figure 8b) indicate that the sediment load during these inflow events was very high. These flows produced large sediment fluxes into the lake with rates of $\sim 100 \text{ mm}$ lake bottom equivalent near the inflow and $\sim 5 \text{ mm}$ lake bottom equivalent near the outflow, respectively (Roop *et al.* 2015). These values are comparable to maximum deposition rates in other intermontane lakes, for instance, in Kamloops Lake (Pharo and Carmack, 1979). or in Lake Lillooet (Gilbert *et al.* 2006). Very large floods occur at least once a decade in Lake Ohau and we

hypothesize that distinctly thicker sediment layers associated with these events should be found near the delta and near the outflow. The sediment regime displays a strong seasonality and large floods cause the largest sediment input in late spring and summer when most sediment is available from the catchment area. However, floods with $Q > 200 \text{ m}^3 \text{ s}^{-1}$ occur several times throughout the year. Turbidity currents arise from these floods and operate mainly as underflows contributing to accumulation rates during the annual cycle.

5. Conclusions

Lake Ohau exhibits an extreme turbidity current regime with varying seasonal intensity. Sedimentation is mainly controlled by high sediment loads from river floods in the summer but these persist at lower frequency throughout the year. The processes sketched in Figure 11 can occur independently, simultaneously, or even interact with each other, underlining the complexity of this lake system. To examine the interplay of these mechanisms on an interannual basis, a long-term monitoring program is required for Lake Ohau, ideally with a larger spatial and time step resolution of thermistor chains near the inflow, at the downwind end of the lake and in the eastern basin. Moreover, ADCP instruments located further away from the inflow could provide information whether bottom currents, inter- or surface flows dominate over the course of the year. The use of sediment traps, turbidity measurements at the inflow and monitoring of meteorological factors is in progress and will be required to understand the sedimentation regime. The development of numerical models is desirable to improve understanding of the system response external surface forcing. Field measurements, with the aim to understand the importance of internal waves for sedimentation regime, characteristics of turbidity currents and sediment density surges at the delta will be the focus of future work in Lake Ohau and lead to a holistic model on varve formation.

Acknowledgements

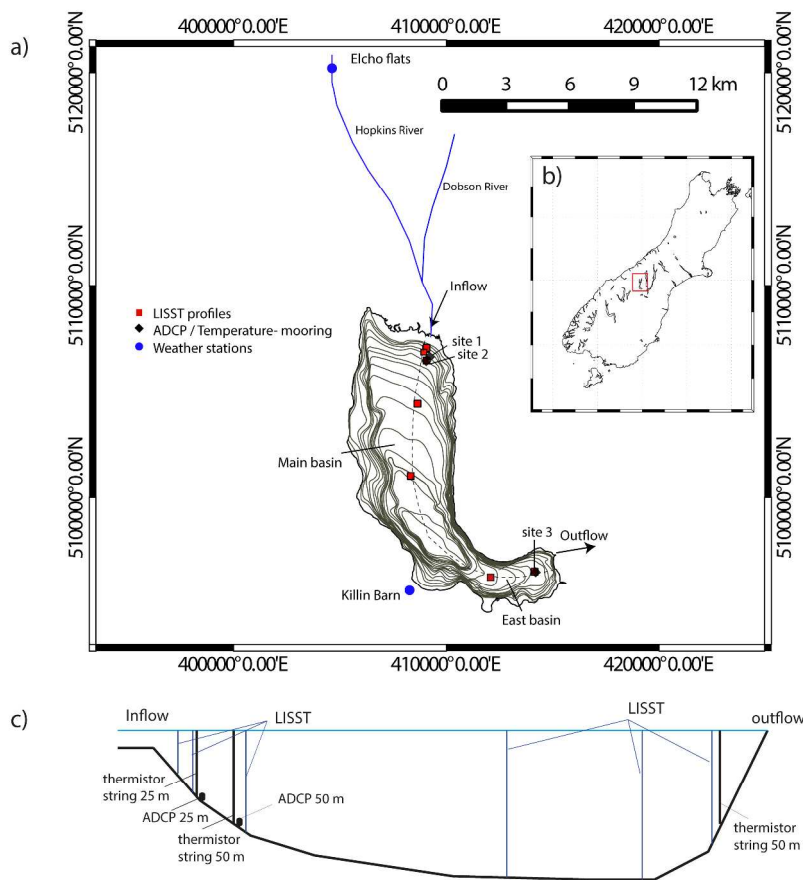
This work was financially supported by the GNS Science Global Change through Time program, the Sarah Beanland Memorial Scholarship, and the ANZICE program (V ICX0704), PMEL Contribution Number 4122, and the Eggers fund. We would like to thank Gary Wilson and the Marine Sciences Department, University of Otago for logistical support. The National Science Foundation East Asia and Pacific Summer Institute supported Paul Stumpner. In addition, we thank Chris and Rae Spiers for their hospitality and large workspace at the Killin Barn, and the Inkersell family at Lake Ohau Station for land access and ongoing support. In addition, we thank three anonymous reviewers for their comments and suggestions which helped to improve the manuscript.

References

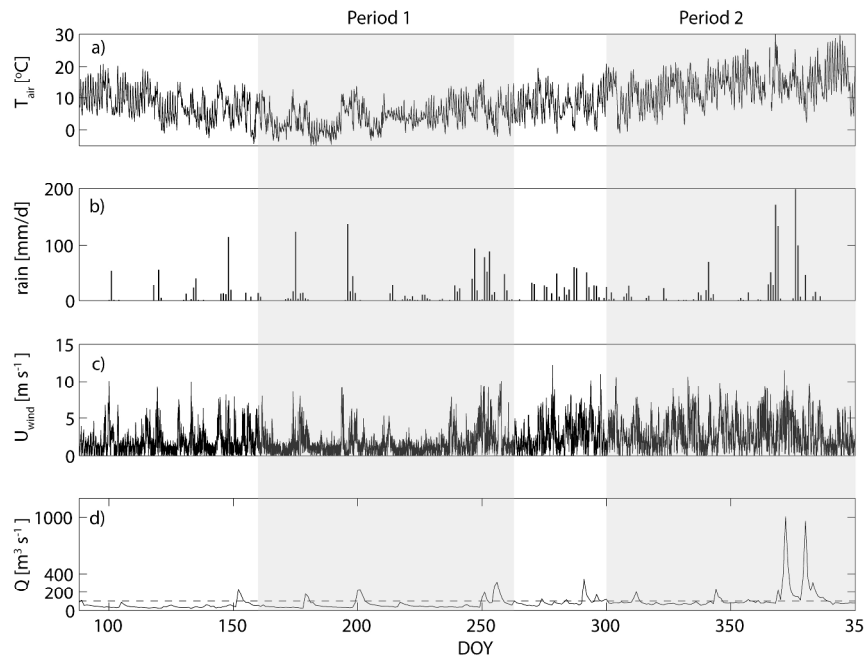
- Alavian, V., Gerhard, H., Jirka, R., Denton, A., Johnson, M. C., and Stefan, H. G. (1992). Density currents entering lakes and reservoirs. *Journal of Hydraulic Engineering* **118**, 1464–1489.
- Amann, B., Mauchle, F., and Grosjean, M. (2014). Quantitative high-resolution warm season rainfall recorded in varved sediments of Lake Oeschinen, northern Swiss Alps: calibration and validation AD 1901–2008. *Journal of Paleolimnology* **51**, 375–391.
- Baringer, M. O., and Price, J. F. (1997). Mixing and spreading of the Mediterranean outflow. *Journal of Physical Oceanography* **27**, 1654–1677.
- Best J.L., Kostaschuk, R.A., Peakall, J., Villard, P.V., Franklin, M. (2005). Whole flow field dynamics and velocity pulsing within natural sediment-laden underflows. *Geology* **33**, 765–68.
- Cenedese, C., Whitehead, J. A., Ascarelli, T. A. and Ohiwa, M. (2004). A dense current flowing down a sloping bottom in a rotating fluid. *Journal of Physical Oceanography* **34**, 188–203
- Chen, C.T., and Millero, F.J. (1986). Precise thermodynamic properties for natural waters covering only the limnological range. *Limnology and Oceanography* **31**, 657–662.
- Dallimore, C. J., Imberger, J. and Ishikawa, T. (2001). Entrainment and turbulence in saline underflow in Lake Ogawara. *Journal of Hydraulic Engineering* **127**, 937–948.
- Desloges, J.R. (1994). Varve deposition and the sediment yield record at three small lakes of the southern Canadian Cordillera. *Arctic and Alpine Research* **26**, 130–140.
- Desloges, J.R. and Gilbert, R. (1994). Sediment source and hydroclimatic inferences from glacial lake sediments: the postglacial sedimentary record of Lillooet Lake, British Columbia. *Journal of Hydrology* **159**, 375–393.
- De Cesare, G., Boillat, J.-L., and Schleiss, A.J. (2006). Circulation in Stratified Lakes due to Flood-Induced Turbidity Currents. *Journal of Environmental Engineering* **132**, 1508–1517.
- Fer, I., Lemmin, U., Thorpe, S.A. (2002). Contribution of entrainment and vertical plumes to the winter cascading of cold shelf waters in a deep lake. *Limnology and Oceanography* **47**, 576–580
- Fischer, H.B, List, E.J., Koh, R.C.Y., Imberger, J. and Brooks, N.H. (1979) Mixing in inland and coastal waters. Academic Press, New York.
- Forrest, A.L., Laval, B.E., Pieters, R., and Lim, D.S.S. (2008). Convectively driven transport in temperate lakes, *Limnology and Oceanography* **53**, 2321–2332.
- Gilbert, R. (1975). Sedimentation in Lillooet Lake, British Columbia. *Canadian Journal of Earth Sciences* **12**, 1697–1711.
- Gilbert R, and Shaw, J. (1981). Sedimentation in proglacial Sunwapta Lake, Alberta. *Canadian Journal of Earth Sciences* **18**, 81–93
- Gilbert, R. and Butler, R.D. (2004). The physical limnology and sedimentology of Meziadin Lake, northern British Columbia, Canada. *Arctic, Antarctic, and Alpine Research* **36**, 33–41.
- Gilbert, R., and Crookshanks, S. (2008). Sediment waves in a modern high-energy glacialacustrine environment. *Sedimentology* **56**, 645–659. doi: 10.1111/j.1365-3091.2008.00990.x

- Gilbert R., Crookshanks, S., Hodder, K.R., Spagnol, J., Stull, R.B. (2006). The record of an extreme flood in the sediments of montane Lillooet Lake, British Columbia: implications for paleoenvironmental assessment. *Journal of Paleolimnology* **35**, 737–745
- Hardy, D.R. (1996). Climatic influences on streamflow and sediment flux into Lake C2, northern Ellesmere Island, Canada. *Journal of Paleolimnology* **16**, 133–149.
- Hamblin, P.F., and Carmack, C. (1978). River-induced currents in a fjord lake. *Journal of Geophysical Research* **83**, 885-899.
- Jonas, T., Stips, A., Eugster, W., and Wüest, A. (2003). Observations of a quasishear-free lacustrine convective boundary layer: Stratification and its implications on turbulence. *Journal of Geophysical Research* **108**, 3328, doi:10.1029/2002JC001440.
- Kerr, T. (2013) The contribution of snowmelt to the rivers of the South Island, New Zealand. *Journal of Hydrology (New Zealand)* **52**, 61.
- Kim, Y.H, and Voulgaris, G. (2003). Estimation of Suspended Sediment Concentration in Estuarine Environments using Acoustic Backscatter from an ADCP., Proceedings of the Coastal Sediment 03, (in CD) Clearwater Florida.sd
- Lambert, A. M., and Giovanoli, F. (1988). Records of riverborne turbidity currents and indications of slope failures in the Rhone delta of Lake Geneva. *Limnology and Oceanography* **33**, 458–468.
- Leeman, A., and Niessen, F. (1994). Varve Formation and the Climatic Record in an Alpine Proglacial Lake; Calibrating Annually-Laminated Sediments against Hydrological and Meteorological data. *The Holocene* **4**, 1-8.
- Lemmin, U., Mortimer, C. H, and Bäuerle, E. (2005). Internal Seiche Dynamics in Lake Geneva *Limnology and Oceanography*, **50**, 207-216
- Middleton, G.V. (1993). Sediment deposition from turbidity currents. *Annual Review of Earth and Planetary Sciences* **21**, 89-114.
- Mulder, T., and Syvitski, J. P. M. (1995). Turbidity currents generated at river mouths during exceptional discharges to the world oceans. *Journal of Geology* **103**, 285–299.
- Ojala, A.E.K., Francus, P., Zolitschka, B., Besonen, M. and Lamoureux, S.F. (2012). Characteristics of sedimentary varve chronologies: A review. *Quaternary Science Reviews* **43**, 45-60.
- Patterson, J.C., Hamblinet, P.F., and Imberger, J. (1984). Classification and dynamic simulation of the vertical density structure of lake. *Limnology and Oceanography* **29**, 845-861.
- Pharo, C.H. and Carmack, E. C. (1979) Sedimentation processes in a short residence-time intermontane lake, Kamloops Lake, British Columbia. *Sedimentology* **26**, 523-541.
- Peeters, F. and Kipfer, R. (2009) Currents in Stratified Water Bodies 1: *Density-Driven Flows Encyclopedia of Inland Waters* **1**, 530-538.
- Putnam, A.E., Schaefer, J.M., Denton, G.H., Barrell, D.J., Birkel, S.D., Andersen, B.r.G., Kaplan, M.R., Finkel, R.C., Schwartz, R. and Doughty, A.M. (2013). The Last Glacial Maximum at 44°S documented by a ¹⁰Be moraine chronology at Lake Ohau, Southern Alps of New Zealand. *Quaternary Science Reviews* **62**, 114-141.

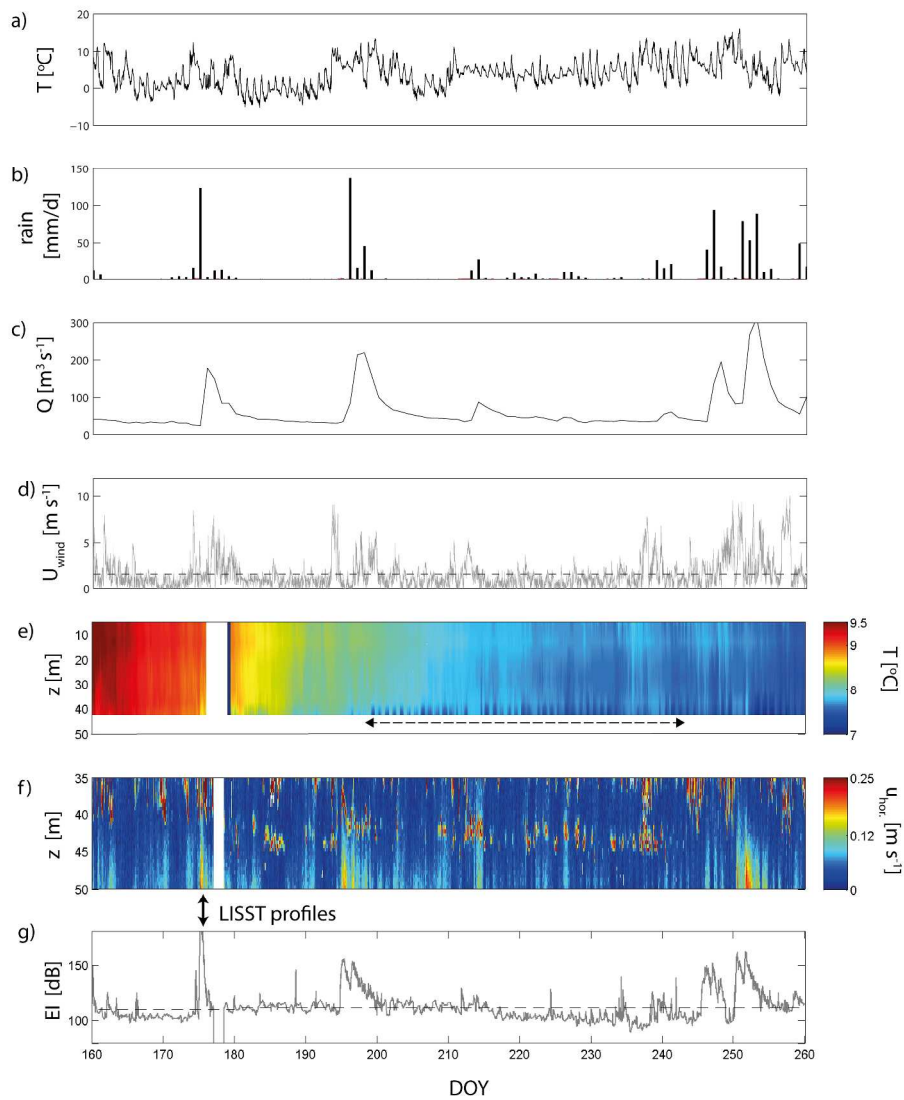
- Reardon, K. E., Bombardelli, F. A., Moreno-Casas, P. A., Rueda, F. J., and Schladow, S. G. (2014). Wind-driven nearshore sediment resuspension in a deep lake during winter, *Water Resources Research* **50**, doi:10.1002/2014WR015396.
- Roop, H. A., Dunbar, G. B.; Levy, R., Vandergoes, M. J., Forrest, A. L., Walker, S. L., Purdie, J., Upton, P. and Whinney, J. (2015). Seasonal controls on sediment transport and deposition in Lake Ohau, South Island, New Zealand: Implications for a high-resolution Holocene palaeoclimate reconstruction. *Sedimentology*. doi.org/10.1111/sed.12162
- Thompson, D.W.J., and Solomon, S. (2002). Interpretation of Recent Southern Hemisphere Climate Change. *Science* **296**, 895-899.
- Thorpe, S. A., Lemmin, U., Perrinjaquet, C., and Fer, I. (1999). Observations of the thermal structure of a lake using a submarine. *Limnology and Oceanography* **44**, 1575– 1582.
- Ummenhofer, C.C., Gupta, S. and England, M.H. (2009). Causes of Late Twentieth-Century Trends in New Zealand Precipitation. *Journal of Climate* **22**, 3-19.
- Tylmann, W., Szpakowska, K. , Ohlendorf, C. , Woszczyk, M., and Zolitschka, B. (2012). Conditions for deposition of annually laminated sediments in small meromictic lakes: a case study of Lake Suminko (northern Poland). *Journal of Paleolimnology* **47**, 55-70
- Weirich, F. (1986). The record of density-induced underflows in a glacial lake. *Sedimentology* **33**, 261-277.
- Wells, M.G., Cenedese, C. and Caulfield, C.P. (2010). The relationship between flux coefficient and entrainment ratio in density currents. *Journal of Physical Oceanography* **40**, 2713–2727. doi: 10.1175/2010JPO4225.1
- Woods, R., Hendrikx, J., Henderson, R., and Tait, A.(2006). Estimating mean flow of New Zealand rivers, *Journal of Hydrology (New Zealand)* **45**, 95.



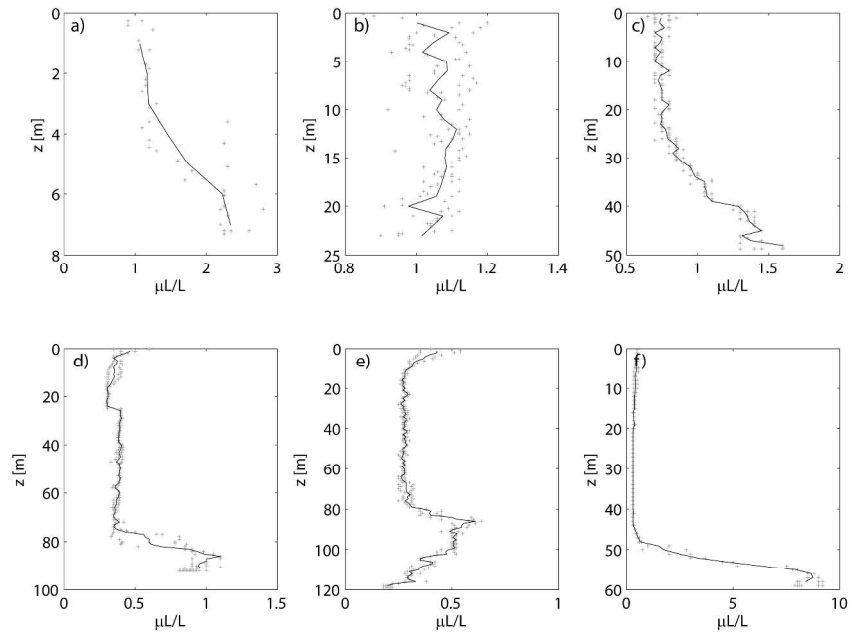
a) Map of Lake Ohau and locations of the moorings, LISST profiles and weather stations. The dashed line depicts the longitudinal profile shown in Figure c; b) Location of Lake Ohau in South Island, New Zealand; and c) Longitudinal profile of Lake Ohau (vertical exaggeration) with position of instruments. Two thermistor chains were arranged in depths of 25 m and 50 m near the head of the lake (site 1 & 2) and one thermistor chain near the outflow in the southeast (site 3). Two ADCPs were located next to the moorings near the inflow at similar depths of 25 m and 50 m (site 1 & 2). LISST profiles were taken along the lake axis as shown in Figure 1a.



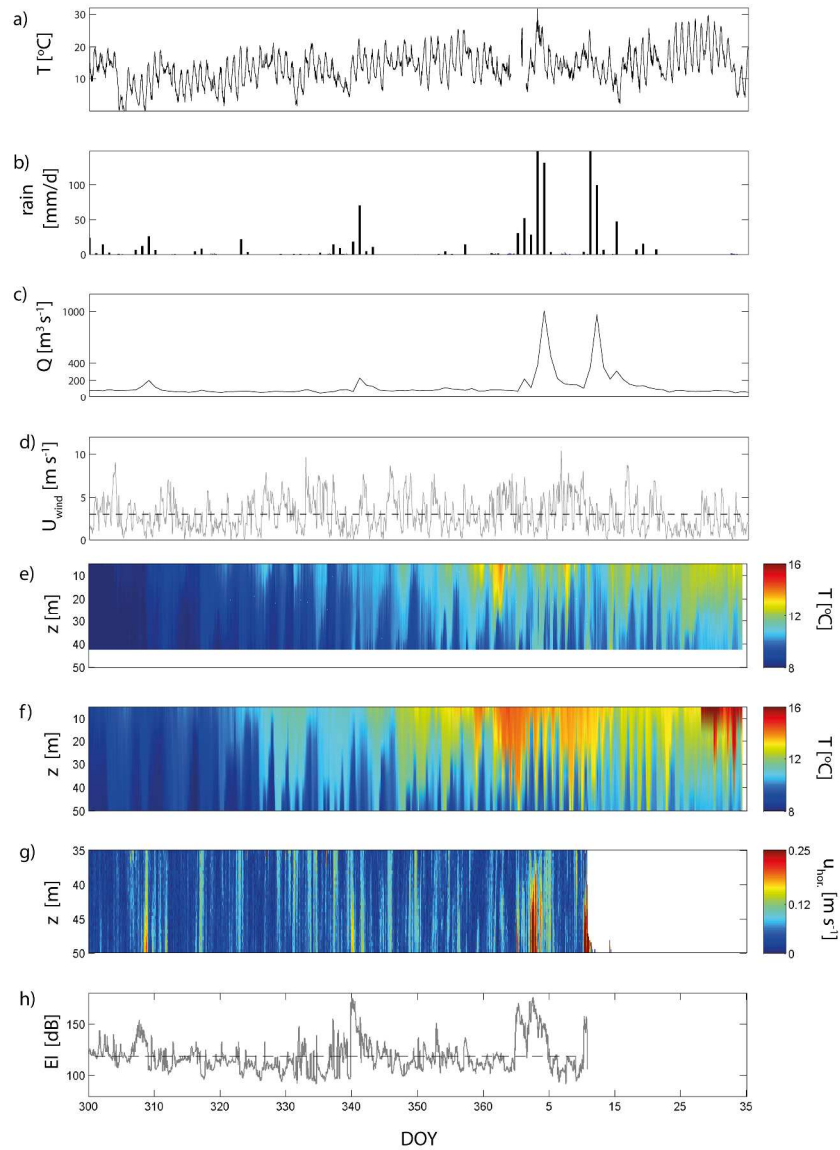
Recorded weather data for Lake Ohau during the experiment. a) Air temperature measured at Killin Barn; b) Precipitation measured at Elcho Flats station upstream of Lake Ohau; c) Observed wind velocity for Killin Barn; and d) Estimated inflow (Q) into Lake Ohau during the experiment. Dashed line represents a discharge of $Q = 100 \text{ m}^3 \text{ s}^{-1}$.



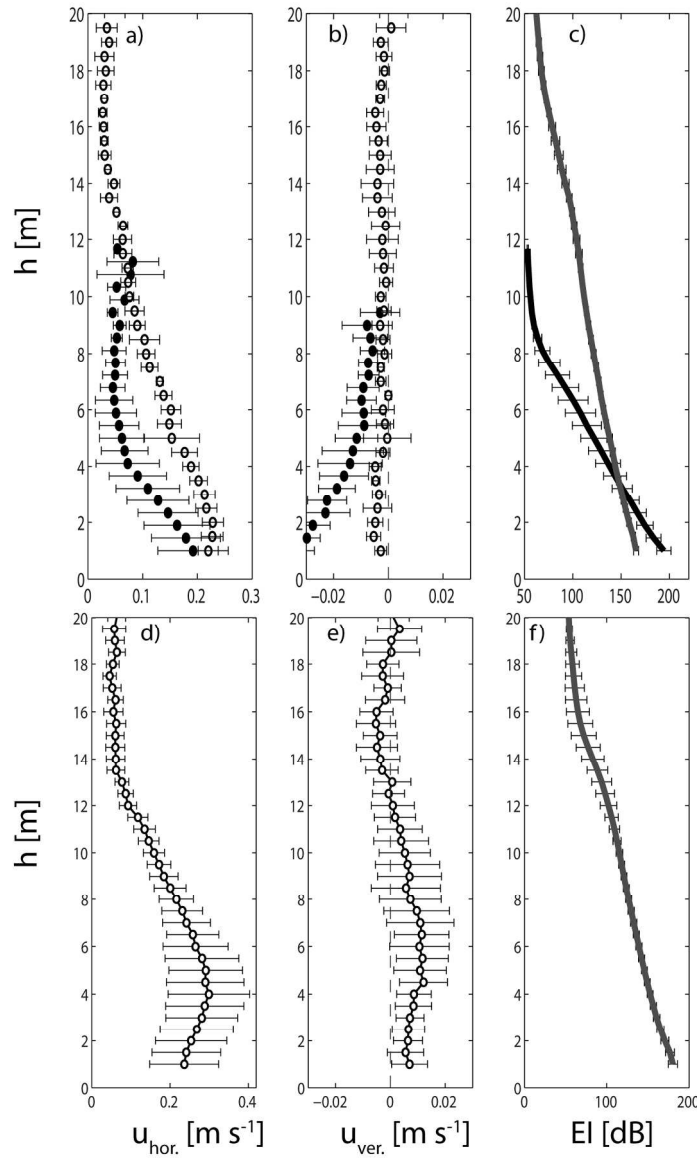
Observed weather and limnological parameters in the water column during Period 1. a) Recorded temperature at Killin Barn; b) Measured rainfall at Elcho Flats; c) Estimated inflow for Lake Ohau; d) Observed wind speed at Killin Barn. Mean wind speed is marked by the dashed line; e) Temperature observed at the 50 m mooring near the inflow; the horizontal arrow indicates the time when periodic temperature fluctuations near the bottom were observed; f) Horizontal ADCP velocities at the 50 m mooring; and g) ADCP echo intensities (EI) measured 5 m above the bottom. The average EI is shown by the dashed black line.



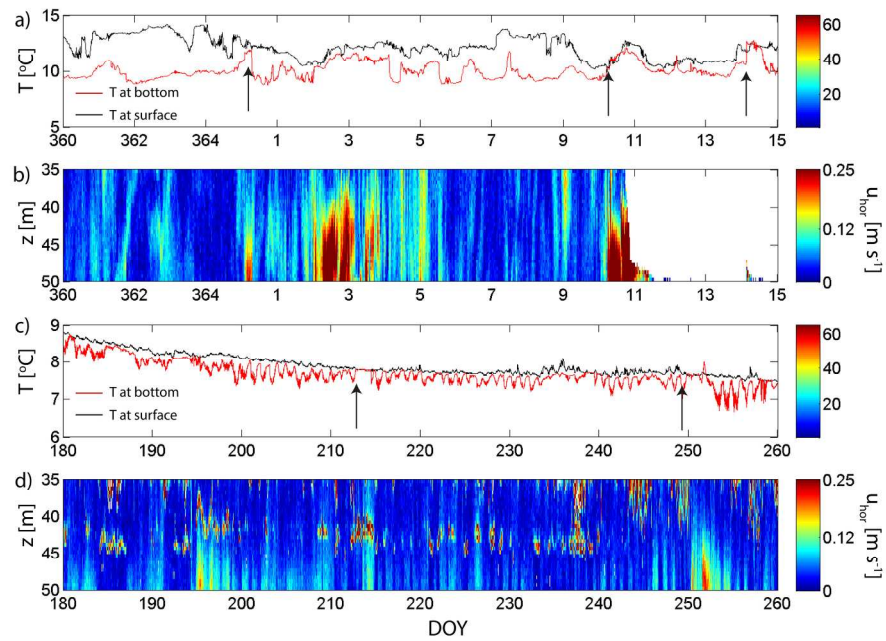
Vertical sediment concentration profiles (LISST) measured at DOY 175 2012 between 11 am and 1 pm in Lake Ohau. Panels a) to f) depict the sediment particle distribution ($\mu\text{L/L}$) at locations shown in Figure 1c, respectively. Solid lines represent averaged values of 1 m bins.



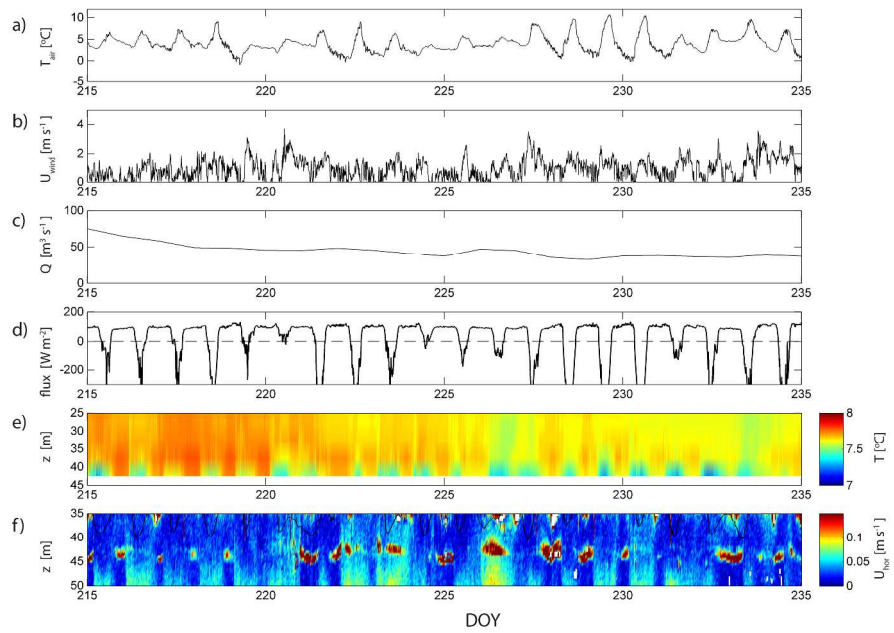
Observed weather and parameters in the water column during Period 2. a) Recorded temperature at Killin Barn; b) Measured rainfall at Elcho Flats; c) Estimated inflow for Lake Ohau; d) Observed wind speed at Killin Barn. Mean wind speed is marked by the dashed line; e) Temperature observed at the 50 m mooring near the inflow (site 2); f) Temperature observed at the 50 m mooring near the outflow (site3); g) Horizontal ADCP velocities at the 50 m mooring; and h) ADCP echo intensities (EI) measured 5 m above the bottom. The average EI is shown by the dashed black line.



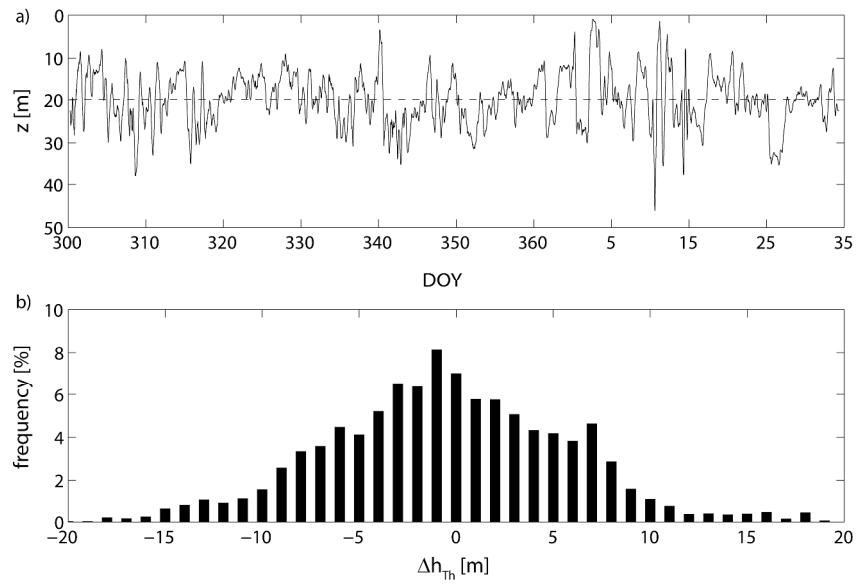
Vertical profiles of observed turbidity currents near the inflow. a) Horizontal velocity; and b) Vertical velocities during a flood event at DOY 250 in Period 1. Solid circles reflect measurements at the 25 m site and open circles reflect data from the 50 m site respectively; c) EI during the same event. Black curve refers to the 25 m site and the grey curve to the 50 m site; d) Horizontal velocity; and e) Vertical velocity profile during the large flood event in Period 2 at the 50 m site; f) Observed EI during this event. Error bars in panels indicate standard deviation of the measured data during a 3h period.



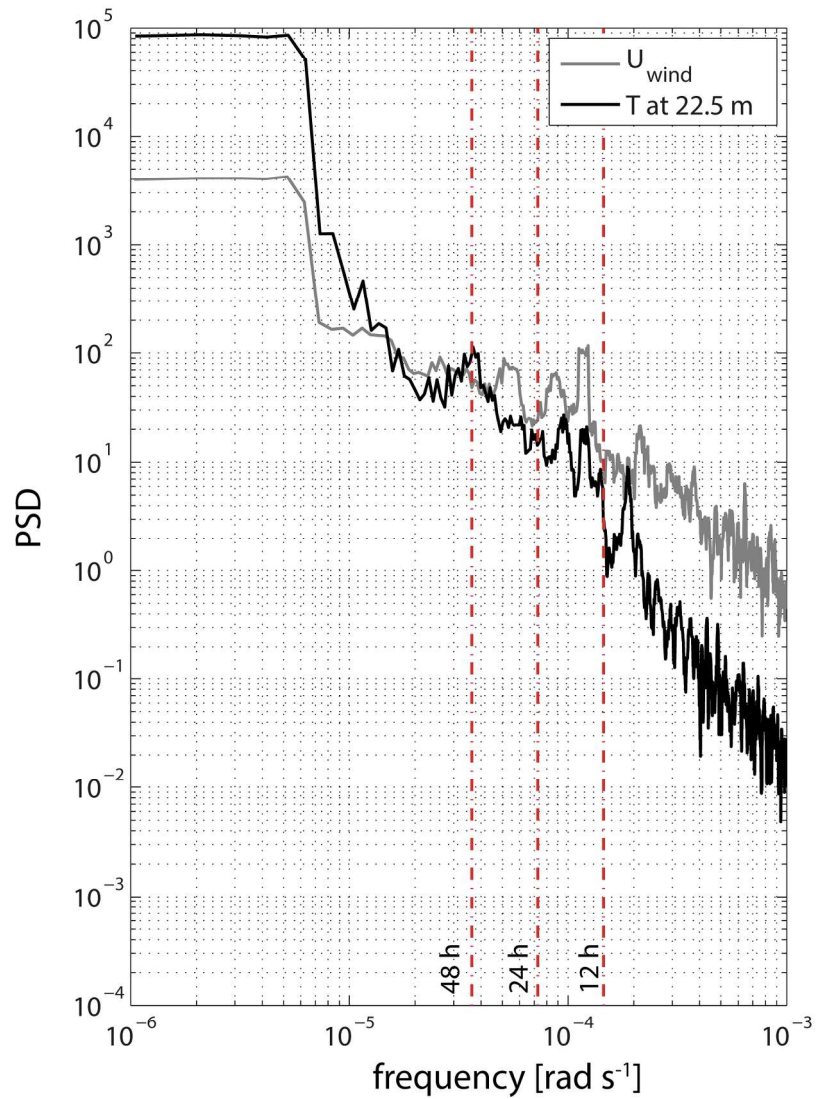
Close-up of temperatures and velocities in the water column during turbidity currents. a) Temperatures of the top thermistor ($z = 5\text{ m}$, black) and the bottom thermistor ($z = 42.5\text{ m}$, red); b) Horizontal velocities in the water column at the 50 m site; c) Temperatures of the top thermistor ($z = 5\text{ m}$, black) and the bottom thermistor ($z = 42.5\text{ m}$, red) in Period 1; and d) Horizontal velocities in the water column at the 50 m site in Period 1. The arrows indicate the onset of temperature inversions, when water temperatures at the bottom were warmer than at the top.



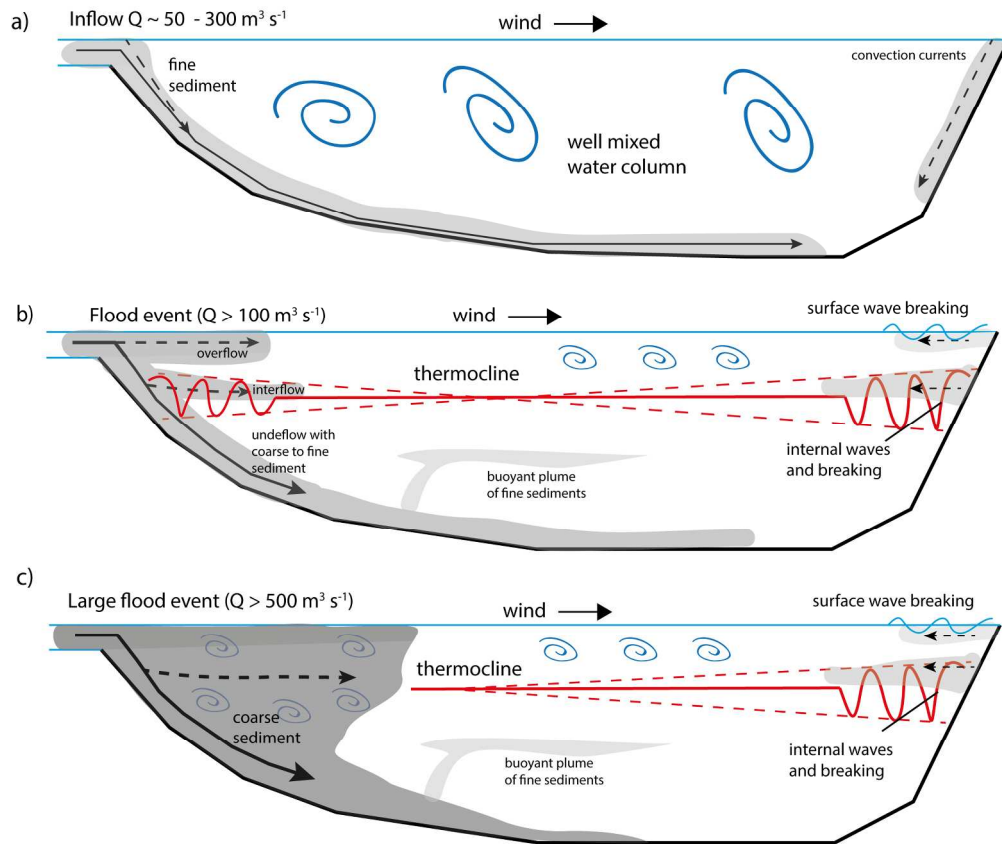
Meteorological and limnological observations made between DOY 215 and 235 the Period 1. a) Air temperature; b) Wind speed; c) Inflow into Lake Ohau; d) Estimated net heat flux. Positive values represent heat gained by the lake; e) Temperature observed at the 50 m mooring near the inflow; and f) Horizontal ADCP velocities at the 50 m mooring.



Frequency distributions of thermocline excursions at the 50 m mooring near the inflow. a) Calculated height of the thermocline. The mean depth is shown by the dashed line; and b) Frequency distribution of the magnitude of the thermocline excursion (Δz_{Th}).



Power spectra densities of the wind velocities at Killin Barn (grey) and the temperatures measured at $z = 22.5$ m near the outflow at site 3 (black line). The vertical dashed lines depict 48h, 24h and 12h periods.



Conceptual model of important processes in Lake Ohau in interannual sedimentation; a) Winter period when the lake is isothermal; b) Summer period during flood events when the lake exhibits a strong thermal gradient; and c) Large flood event during Period 2 where the stratification is eroded near the inflow.

Appendix B

Appendix B is available on the CD-ROM attached to the back cover. This disk contains the hydrometeorological datasets used in Chapter 2 in addition to the X-radiograph images, layer counts, varve motifs, and the Western South Island climate index reconstruction used in Chapters 3 and 4. Inflow and headwater precipitation data are the property of Meridian Energy Ltd. and are not publically available.

